NUCLEAR DAYS

# STUDENT POSTERS

## NUCLEAR DAYS 2025

**Pilsen, Czech Republic**

www.jadernedny.cz

UNIVERSITY OF WEST BOHEMIA IN PILSEN

ŠKODA JS

CENEN
CZECH NUCLEAR EDUCATION NETWORK

# Poster Scientific Committee

| | |
|---|---|
| Ing. Karel BÍŽA | ÚJV Řež |
| doc. Ing. Petr ERET, Ph.D. | University of West Bohemia |
| Ing. Josef KRÁLOVEC, CSc. | Czech Nuclear Veterans |

# Organizing Committee

| | |
|---|---|
| Ing. Pavel BROULÍM, Ph.D. | University of West Bohemia |
| Bára DUBOVÁ | University of West Bohemia |
| Bc. Lucie GRUSOVÁ | ŠKODA JS a.s. |
| Ing. Eva KOZÁKOVÁ KRAUZOVÁ | University of West Bohemia |
| Bc. Martin KOLEČKO | University of West Bohemia |
| Ing. Jana JIŘIČKOVÁ, Ph.D. | University of West Bohemia |
| Ing. David MAŠATA | University of West Bohemia |
| Ing. Jan POSPÍCHAL | University of West Bohemia |
| Dr. Ing. Jaroslav SYNÁČ | University of West Bohemia |
| Ing. Jan ULLMANN | University of West Bohemia |
| Ing. Anna MRÁZOVÁ | University of West Bohemia |
| Ing. Jan ZDEBOR, CSc. | University of West Bohemia |
| Ing. Pavel ŽITEK, Ph.D. | University of West Bohemia |

*The event is organized with the support of the Student Activity Grant (GRAS) and the Student Scientific Conference (SVK – held within the framework of Specific University Research), both provided by the University of West Bohemia in Pilsen.*

UNIVERSITY
OF WEST BOHEMIA
IN PILSEN

## BACHELOR STUDENTS 6

**ISOTHERMAL FLOW BEHAVIOR PAST VORTEX-INDUCING SWIRLER GRID** 7
Matěj DOLEJŠ

**CORE CHARACTERISTICS OF THE SELECTED SMR** 9
Jan HEŘMAN

**ANALYSIS OF SEVERE ACCIDENTS OF VVER 440 REACTORS** 11
Filip Janíček

**OPTIMIZATION OF THE WORKPLACE FOR NON-DESTRUCTIVE CHARACTERIZATION OF CONTAINERS FOR RADIOACTIVE WASTES** 13
Karolína NEJEDLÁ

**ACCIDENT TOLERANT FUELS** 15
Jiří PFEIFFER

**BEHAVIOUR OF NUCLEAR FUEL WITH 10% ENRICHMENT URANIUM-235 AND VARIOUS BURNABLE ABSORBERS** 17
Miloš ZACHAR

## MASTER STUDENTS 19

**EXCLUSION PROTECTION ZONE OF SMR'S** 20
George Alexandru BOCA

**BENDING-INDUCED CHANGES IN CRITICAL HEAT FLUX OF NUCLEAR FUEL ROD IN LOW-PRESSURE SYSTEM** 22
Tomáš KADAVÝ

**DEVELOPMENT OF FULL-CORE VVER-1000 MODEL IN DETERMINISTIC CODE PARCS: VALIDATION OF DATA PREPARATION PROCESS ON HZP CALCULATIONS** 24
Ondřej LACHOUT

**DEBRIS BLOCKAGE OF FLOW THROUGH ROD BUNDLE** 26
Florin MISTRE

**NEUTRONIC ANALYSIS OF A WESTINGHOUSE SMALL MODULAR REACTOR USING OPENMC MONTE CARLO CODE** 28
Sarra MOUMMI

**THE EFFECT OF CLOGGING OF THE SPACER GRID ON THE CRITICAL HEAT FLUX OF A PRESSURELESS FUEL ROD SIMULATOR** 30
Anna MRÁZOVÁ

**CHARACTERIZATION OF THE PERFORMANCE OF A HYBRID SMALL MODULAR REACTOR AND ITS INTERACTION WITH THE POWER GRID** 32
Silvia PICCHI

**LIQUID METAL FLOW IN A MAGNETIC FIELD ENVIRONMENT** 34
Aleš PROCHÁZKA

**EXPERIMENTAL AND COMPUTATIONAL MODELING OF FUEL CLADDING UNDER LOSS OF COOLANT ACCIDENT CONDITIONS** **36**
Michaela SVATOŠOVÁ

**THERMODYNAMIC CONDITIONS IN THE SAFETY DEPRESSURIZATION SYSTEM AT THE TEMELÍN NUCLEAR POWER PLANT** **38**
Petr VASTL

**CONDUCTING TECHNOLOGICAL TESTS DURING THE POWER STARTUP OF THE DUKOVANY POWER PLANT** **40**
Vít VESELÝ

**SIMULATION OF TEMPERATURE EVOLUTION DURING DEPARTURE FROM NUCLEATE BOILING INDUCED BY ELECTRIC ARC HEATING** **42**
Petr VNENK

## DOCTORAL STUDENTS **44**

**MASS SPECTRA ANALYSIS OF IONS PRODUCED FROM NI, CA, SE AND PD OXIDE OR FLUORIDE TARGET MATERIALS BY CAESIUM SPUTTERING** **45**
Filip BABČICKÝ

**ELECTRO- & CURRENT-LESS DEPOSITION OF NICKEL FROM LOW-CONCENTRATION AQUEOUS SOLUTIONS** **47**
Filip BABČICKÝ

**BALANCE OF PLANT DESIGN AND OPTIMIZATION FOR TOKAMAK FUSION POWER PLANTS: APPLICATIONS TO ARC-LIKE AND EU-DEMO REACTORS** **49**
Francesco COLLIVA

**BROOMSTICK EXPERIMENT FOR NUCLEAR DATA VALIDATION AT THE VR-1 REACTOR** **51**
Tomáš CZAKOJ

**MULTISCALE THERMAL-HYDRAULIC ANALYSIS OF EXPERIMENTAL FACILITIES IN SUPPORT OF THE LEAD-COOLED FAST REACTORS DEVELOPMENT** **53**
Tommaso DEL MORO

**UNDERGROUND STORAGE OF SPENT NUCLEAR FUEL: TECHNOLOGIES AND PROSPECTS** **55**
Yuliia HADAIEVA

**ISOTHERMAL FLOW PAST MIXING GRID WITH PARABOLIC VANES** **57**
Vojtěch JÁNSKÝ

**MEASUREMENT OF SPECTRUM AVERAGED CROSS SECTIONS IN THE BENCHMARK LR-0 REFERENCE FIELD** **59**
Alena KRECHLEROVÁ

**CHARACTERIZATION AND DEVELOPMENT OF CEMENTITIOUS MATERIALS USED IN STORAGE FACILITIES FOR IMMOBILIZATION OF ILW RADIOACTIVE WASTE** **61**
Francesco RIZZO

**PHYSICS-INFORMED NUCLEAR IMAGING FOR GLIOMA LOCALIZATION AND RECURRENCE PREDICTION** **63**
Carlos Andres SEPULVEDA LEON

**NEURAL NETWORKS FOR PREDICTIVE CONTROL OF SMRS IN INDUSTRIAL ENERGY SYSTEMS** **65**
Jan ULLMANN

**THERMAL-HYDRAULIC DESIGN AND ANALYSIS OF THE STEAM AND WATER LOOP FACILITIES TO SUPPORT THE DEVELOPMENT OF THE EU-DEMO TOKAMAK FUSION REACTOR** **67**
Alessandra VANNONI

# BACHELOR STUDENTS

# ISOTHERMAL FLOW BEHAVIOR PAST VORTEX-INDUCING SWIRLER GRID

Matěj DOLEJŠ

*University of West Bohemia in Pilsen, Czech Republic*

In this work, airflow through the model of a nuclear reactor fuel assembly has been studied at the University of West Bohemia in Pilsen, specifically flow through and around spacer grids for fuel rods and the influences different shapes and placements have on the airflow.

ZÁPADOČESKÁ UNIVERZITA V PLZNI

# ISOTHERMAL FLOW BEHAVIOR PAST VORTEX-INDUCING SWIRLER GRID

NUCLEAR DAYS

Matěj Dolejš, Daniel Duda, Vitalii Yanovych, Vojtěch Janský, Anna Mrázová & Václav Uruba

## Nuclear fuel assembly model for isothermal wind tunnel experiments

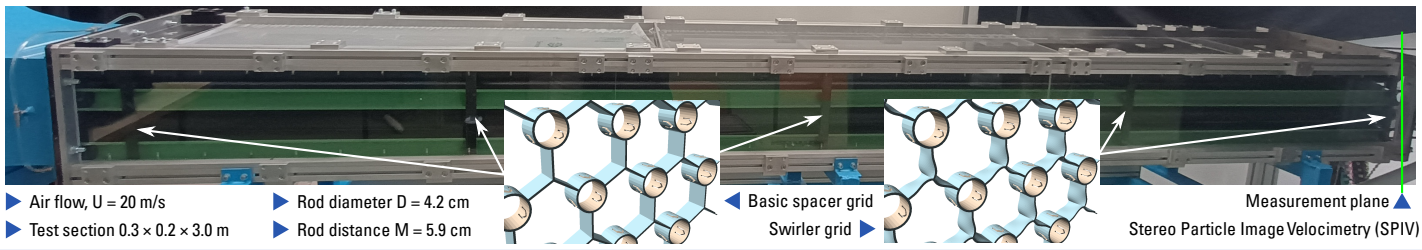


## Abstract & introduction


- Nuclear energy offers stable, large-scale energy source with very low environmental impact
- A facility for physical modeling of flow inside a fuel assembly has been constructed at UWB in Pilsen
- Swirler grid produces longitudinal vortices whose meandering enhances mixing within the inter-rod channel; such vortices decay slower than standard turbulence
- 3 configurations are tested:
  - basic spacer grids only, 5 pieces in total
  - single swirler grid (SG), i.e. 4 basic and 1 SG
  - two counter-rotating SGs, i.e. 3 basic and 2 SG
- Vortices produced at upstream grid are observable even past the next one at distance over 12.7 × M
- Correlation analysis of vortex meandering does not suggest coherent motion of vortex bundle
- Vortices from upstream grid slightly enhance vortex meandering of next vortices


## Mean streamwise velocity

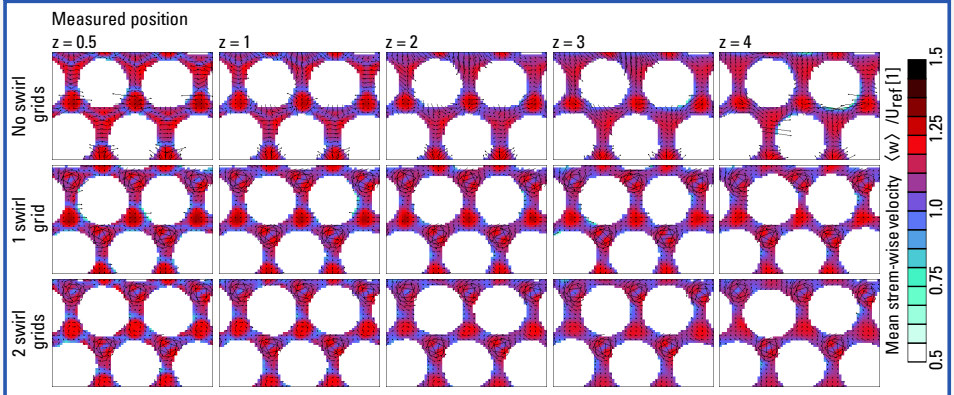


## Turbulent kinetic energy

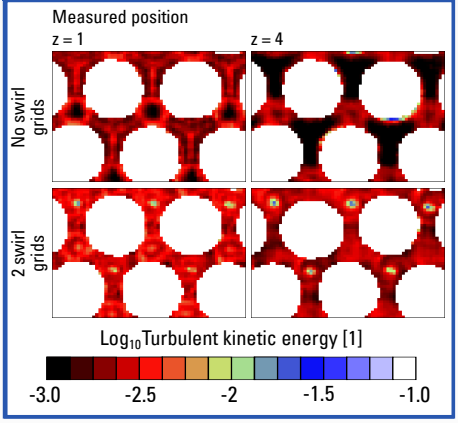


## Vortex tangential velocity and meandering amplitude

- Individual vortices are detected in the instantaneous snaphots via direct fitting of in-plane velocity field

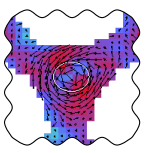

- Taylor vortex model is used:

$$u_\vartheta(r) = \frac{Gr}{R} \cdot e^{-\frac{1}{2}\left(\frac{r}{R}\right)^2}$$

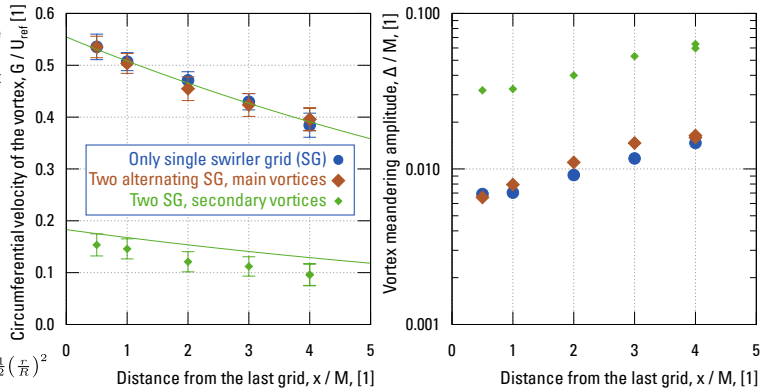


## Fluctuation anisotropy

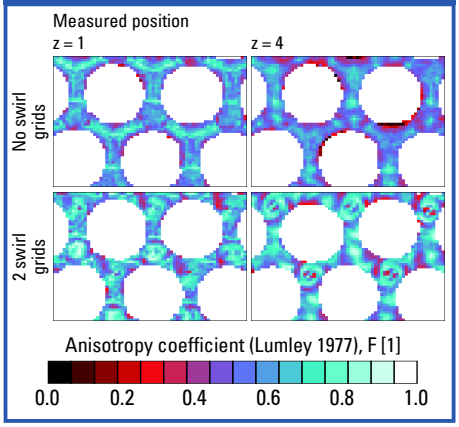


## Correlation of neighboring individual vortices

- Correlation of instantaneous neighboring vortices

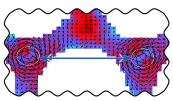

- Vortices past a single swirler grid

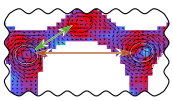

- Main vortices at two counterrotating SGs
- Main and secondary vortex

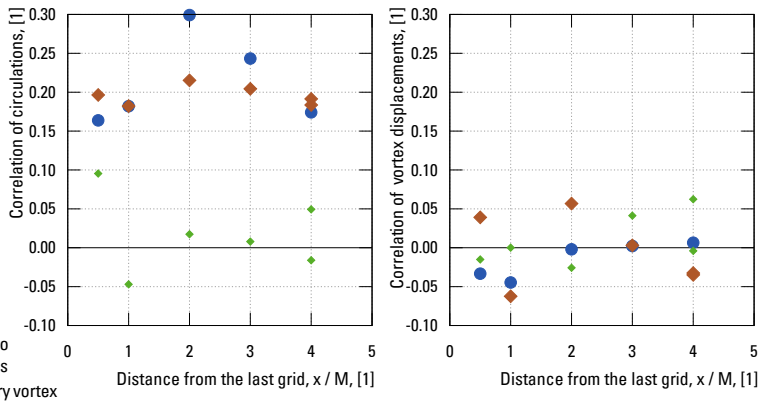

# CORE CHARACTERISTICS OF THE SELECTED SMR

Jan HEŘMAN

*University of West Bohemia in Pilsen, Czech Republic*

This work focuses on small modular reactors, with particular attention given to the Finnish LDR-50 modular reactor designed for centralized district heating. The Serpent 2 calculation code was used to create a 2D model and to calculate the multiplication factor and the power distribution of fuel assemblies. The model results are compared to a reference case and visualized using the NuclearVisualizer tool.

# Core characteristics of the selected SMR

Author: Bc. Jan Heřman Supervisor: Ing. Jiří Závorka Ph.D.

Contact: hermanja@email.cz

FACULTY OF ELECTRICAL ENGINEERING
UNIVERSITY OF WEST BOHEMIA
IN PILSEN

NUCLEAR DAYS

## Introduction

The aim of this work was to create a 2D model of the core of a selected modular reactor in the neutron physics calculation code Serpent 2, calculate the effective multiplication factor k-eff, the power distribution at the level of fuel assemblies (kq), and subsequently compare the results with those of a reference model.

Small Modular Reactors (SMRs) are reactors with an output of up to 300 MWe that are manufactured in series in production facilities and delivered as modules instead of being constructed on-site. SMRs offer the possibility of using nuclear energy for combined heat and power generation, or solely for centralized heat supply. Centralized heat supply (CZT) is an efficient system for the production and distribution of heat, utilizing combined heat and power generation or heat-only supply to reduce primary energy consumption and emissions. Thanks to centralization, individual sources of pollution, such as local boiler plants and domestic coal burning, are reduced. The small modular reactor LDR-50 (Low-temperature District heating Reactor) is one of the few reactors specifically designed for this purpose. The SMR is being developed by the Technical Research Centre of Finland VTT and the company Steady Energy, and it is one of the most advanced projects in this field. Many European countries have extensive district heating networks, and the use of CZT is essential for them. A reactor dedicated to heat production therefore represents significant potential for Europe, especially for the Czech Republic.

## LDR-50

As a result of operation at low temperatures, while a typical CZT system operates at 65–120 °C, the reactor has a lower operating pressure in the range of 0,5–0,8 MPa, which is approximately 20 times lower compared to pressurized water reactors, making it more economical to manufacture and safer. The reactor has an operational thermal power of 50 MWt, with a fuel cycle duration of 24 months. The core is moderated and cooled by light water, which circulates naturally through the primary circuit without the need for pumps. The reactor consists of two nested pressure vessels. The coolant is heated in the reactor core, creating upward flow. At the top of the vessel, the flow is directed into heat exchangers placed around the inner cylinder. Thermal energy is transferred to the secondary circuit, and the cooled water exiting the heat exchangers flows through a downcomer channel to the bottom of the reactor vessel and back into the core. If a failure occurs in the heat exchanger, the temperature in the reactor begins to rise, activating passive heat removal. Heat will be transferred through the containment into a cooling pool, which is designed to maintain natural circulation of the primary circuit for several weeks without operator intervention.

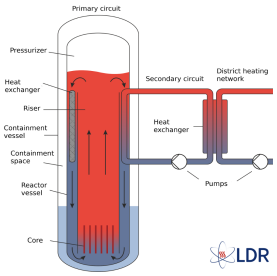


Figure 1. A schematic figure of the LDR module.

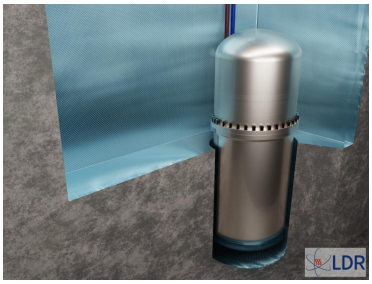


Figure 2. Realistic 3D model of the LDR module.

## Reactor modeling

The reactor core consists of 37 square fuel assemblies surrounded by a stainless-steel reflector and a water cylinder that serves as a downcomer channel for the coolant. The fuel assemblies contain fuel rods with uranium dioxide ($UO_2$) of varying enrichment and guide tubes for control rod clusters. Some rods also contain gadolinium oxide ($Gd_2O_3$) as a burnable absorber to reduce reactivity. The LDR-50 reactor uses six types of fuel assemblies, which differ in composition or profiling. The correctness of the power distribution is verified using the kq coefficient, which indicates the symmetry of the power relative to the center of the core.

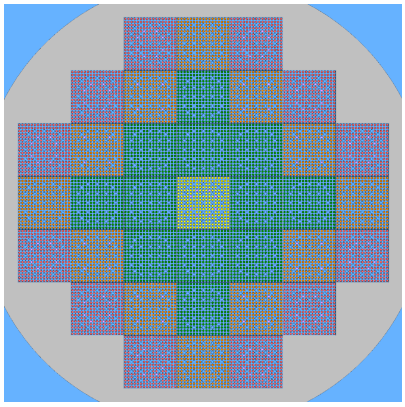

Figure 3. Radial geometry of the reactor core model.

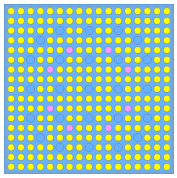

Figure 4. Layout of the fuel assembly types 1, 4 and 5 with fuel containing gadolinium shown in green.

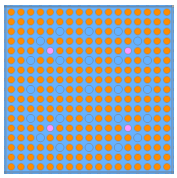

Figure 5. Layout of the fuel assembly type 3 with fuel containing gadolinium shown in green.

## Calculation results

Multiplication factor k-eff

- 2D model k-eff = 1,11220
- reference model k-eff = 1,09395
- relative deviation Δ = 1,8%

Power distribution of fuel assemblies kq

- relative deviation |Δ| < 2,5%

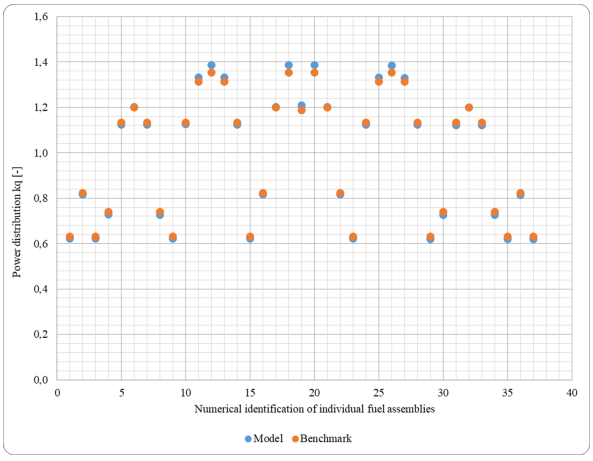


Figure 6. Graphical representation of the normalized power distribution of individual fuel assemblies in the model.

## Choropleth map of power distribution kq

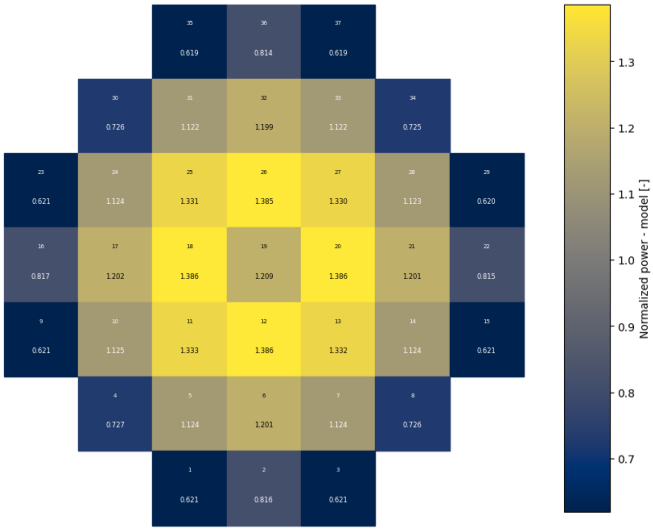


Figure 7. Power distribution of fuel assemblies in the 2D model of LDR-50.

## Conclusions

The main objective of this work was to create a radial 2D model of the Finnish LDR-50 reactor intended for heating using CZT, calculate the effective multiplication factor k-eff, and determine the power distribution of fuel assemblies kq. The calculations were carried out in the cold ARO (All Rods Out) state using the ENDF/B-VII.1 nuclear data library.

The effective multiplication factor k-eff is a dimensionless quantity that expresses the ratio of the number of neutrons produced in one generation of a fission chain reaction to the number of neutrons in the previous generation. It determines whether the reactor is in a critical, supercritical, or subcritical state. The k-eff of the 2D model is 1.8% higher than that of the reference model. This is caused by the fact that the reference model is 3D and therefore includes both axial and radial profiles. Since the 2D model includes only the radial profile, it has higher reactivity, as it does not account for axial neutron leakage and certain structural details of the fuel assemblies that are captured in a full 3D model.

The power distribution of fuel assemblies kq describes the relative power values of individual fuel assemblies in the reactor core. The kq coefficient is defined as the non-uniformity coefficient of the power distribution of fuel assemblies. The power values calculated using the 2D model differ numerically from those of the reference 3D model, but they preserve symmetry with respect to the center of the reactor core. Relative deviations reach up to 2.5%, with the largest differences occurring in fuel assemblies located at the edges and in the central region. These deviations are related to the absence of the axial profile in the 2D model, which is included in the reference 3D model.

The model created in this final project serves as a foundation for further extensions and studies, such as the addition of an axial view in a 3D model. Another possible study, given the importance of CZT, is to calculate the fuel costs for reactor operation using fuel burnup simulations.

## References

R. Komu. and R. Tuominen. "LDR lite benchmark specifications." LDR design document, LDR-PUB-VTT-10002-R2, VTT Technical Research Centre of Finland, 2023.

# ANALYSIS OF SEVERE ACCIDENTS OF VVER 440 REACTORS

Filip Janíček

*Slovak University of Technology in Bratislava, Slovakia*

The thesis presents a simulation of a combined severe accident scenario involving a large-break loss-of-coolant accident (LOCA 2×500 mm) and station blackout in a VVER 440/V-213 power plant under nominal operating conditions. The analysis focuses on the in-vessel phase, assessing core degradation, hydrogen production, and the delayed activation of severe accident management systems. Simulations were performed using MELCOR 2.2 and APROS–SA, with thermal-hydraulic behavior compared under identical boundary conditions. Results confirm the importance of in-vessel retention and validate the role of post-Fukushima safety upgrades.

STU FEI
FACULTY OF ELECTRICAL ENGINEERING AND INFORMATION TECHNOLOGY
INSTITUTE OF NUCLEAR AND PHYSICAL ENGINEERING

# Analysis of severe accidents of VVER 440 reactors

**Author: Bc. Filip Janíček** **Supervisor: Prof. Ing. Vladimír Slugeň, DrSc.**

## Introduction

Nuclear energy remains a key part of global electricity production. However, past severe accidents such as Three Mile Island (1979), Chernobyl (1986), and Fukushima (2011) have highlighted the importance of advanced safety systems and accident prevention strategies.
This work focuses on the VVER 440/V–213 pressurized water reactor design, widely used in Central and Eastern Europe. The study examines nuclear safety principles, particularly **defense-in-depth**, and presents a simulation of a hypothetical severe accident to assess the reactor's safety response capabilities.
By modeling a large break LOCA scenario and analyzing it using advanced computational tools, the goal is to evaluate the **effectiveness of emergency cooling systems**, **containment integrity**, and **hydrogen management** under extreme conditions.

## LOCA 2x500 accident phenomenology

The chosen scenario involves a **guillotine break** of the primary loop piping – a **double-ended break with 2×500 mm diameter**, representing the **maximum design-basis accident** for VVER 440/V–213 reactors [1].
The rupture causes rapid depressurization and loss of coolant inventory from the primary circuit, resulting in:
Rapid drop in core coolant levels
Onset of **core heat-up** and potential damage to **fuel cladding**
**Zirconium-steam reaction** producing hydrogen
Risk of **core melt** if no mitigation occurs
Need for proper functioning of **passive and active emergency systems**
The scenario assumes a **station blackout** (SBO) initially preventing emergency systems activation, with recovery occurring later via **DG-SAM** (severe accident diesel generator). The goal is to simulate containment and reactor vessel integrity preservation during the **in-vessel phase** of the event.

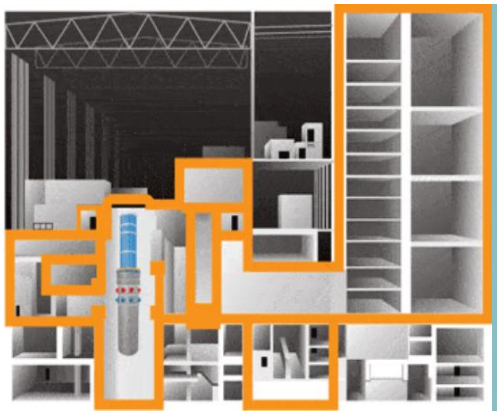

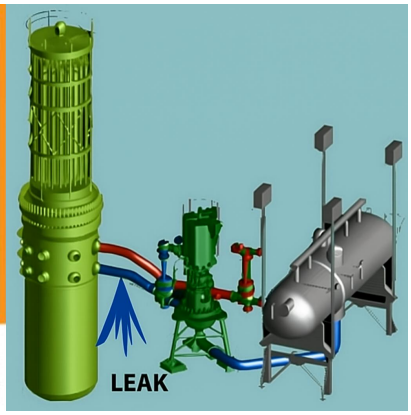


## Calculus of accident scenario

The accident progression was simulated using two deterministic codes: **MELCOR 2.2** and **APROS–SA**, both validated tools for reactor safety analysis.
The model used input parameters based on the Bohunice V2 NPP (Unit 3), under nominal operating conditions. Identical boundary and initial conditions were set for both codes to compare results objectively.
**Key time-dependent outcomes from the simulations include:**
**Core exposure with onset of steam-induced zirconium oxidation :** 310 s (MELCOR), 1369 s (APROS).
**Max. fuel cladding temperature**: Over 1200°C (oxidation and degradation start).
**Hydrogen production**: Peaks after cladding oxidation initiates
**Reactor cavity flooding**: Initiated at 4947 s using TI system and external RPV cooling.
**Residual decay heat**: Drops to 12.7 MW at the end of simulation (9350 s).
Graphs showed strong correlation between both codes in pressure drops, core temperatures, and coolant mass loss. Some delay differences were observed due to variations in the internal solver algorithms.

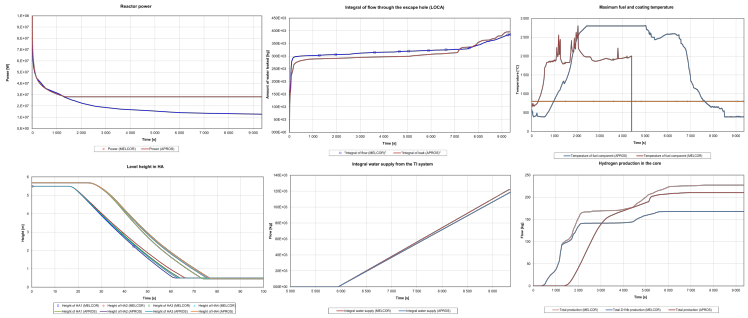


Apros MELCOR

## Conclusion and discus

The simulation results confirm that the **safety concept of VVER 440/V–213** reactors, including both **legacy** and **post-Fukushima upgrades**, is capable of managing a large LOCA event under realistic severe accident conditions.
Particularly effective are:
**Passive safety systems**: hydroaccumulators (HA), containment barbotage (HZ–XL).
**Active systems**: TI system for severe accident water delivery.
**External RPV cooling**: proved essential for maintaining vessel integrity and avoiding ex-vessel progression.
Even with delayed power restoration, **fuel degradation was contained** within the vessel.
The MELCOR and APROS tools proved consistent and complementary, making them reliable instruments for severe accident analysis, emergency planning, and SAM validation.
This study supports continued reliance on VVER technology while stressing the importance of robust simulation, operator training, and system redundancy in safety-critical environments.

## References

[1] SLUGEŇ, Vladimír. *Safety of VVER-440 Reactors: Barriers Against Fission Products Release*. 1st ed. London: Springer, 2011. 178 p. ISBN 978-1-84996-420-3.

## Acknowledgment

vuje SLOVENSKÉ ELEKTRÁRNE NUCLEAR DAYS

# OPTIMIZATION OF THE WORKPLACE FOR NON-DESTRUCTIVE CHARACTERIZATION OF CONTAINERS FOR RADIOACTIVE WASTES

Karolína NEJEDLÁ

*Czech Technical University in Prague, Czech Republic*

Non-destructive characterization is crucial for the future safe disposal of radioactive waste. To analyze both quantitative and qualitative features of a waste drum, techniques such as gamma spectrometry and radiographic imaging are used. For industrial applications, a graphical user interface (GUI) was developed at the Nuclear Research Institute (ÚJV Řež) to optimize the characterization process, verify the homogeneity and structure of processed waste. The application displays the distribution of intensities and detected gamma energies corresponding to individual radionuclides, enabling a deeper understanding of the drum's contents. The outcome includes a graphical comparison of the spatial distribution of activity with the internal structure of the drum.

# Optimization of the Workplace for Non-destructive Characterization of Containers for Radioactive Waste

FACULTY OF NUCLEAR SCIENCES AND PHYSICAL ENGINEERING CTU IN PRAGUE

NUCLEAR RESEARCH INSTITUTE

**Author: Karolína Nejedlá, Bachelor's thesis, 2025** nejedka1@cvut.cz

Supervisor: Ing. Pavel Novotný, Ph.D. Co-supervisor: Bc. Jakub Záruba

## Introduction

**Non-destructive characterization** is crucial for the future safe disposal of **radioactive waste**. To analyze both quantitative and qualitative features of a waste drum, techniques such as **gamma spectrometry** and **radiographic imaging** are used.

For industrial applications, a **graphical user interface (GUI)** was developed at the Nuclear Research Institute (ÚJV Řež) to optimize the characterization process, verify the homogeneity and structure of processed waste. The application displays the distribution of intensities and detected gamma energies corresponding to individual radionuclides, enabling a deeper understanding of the drum's contents. The outcome includes a graphical **comparison of the spatial distribution of activity with the internal structure of the drum.**

## Objectives

1. To propose a suitable **measurement procedure** that allows **the integration of data from radiographic and spectrometric analysis**
2. To develop a **method for processing the measured data** and create a **software tool** for the combined visualization of the results obtained from both techniques

## Measurement system

This system combines gamma spectrometry and radiography to characterize radioactive waste drums non-destructively.

The system is configured to allow direct spatial comparison of radiographic and spectrometric data. The waste drum is divided into a **6×6 measurement grid**, with **60° rotational steps and six vertical levels**. This configuration ensures full-volume coverage and enables **detailed 3D activity and density mapping**.

Both measurements start from the same manually aligned reference position to ensure consistent data registration.

## Gamma Spectrometry

**The segmented gamma scanner** (SGS) is a complex measuring system equipped with a high-resolution **HPGe detector**. It performs vertical and angular scanning, including rotational scans at up to 12 angular positions, allowing for spatially resolved measurement of gamma radiation emitted from the radioactive contents of the waste drum.

Spectral data are processed using an **8192-channel multichannel analyzer** (MCA), enabling detailed gamma-ray spectroscopy.

**Genie 2000** software is used for peak analysis and radionuclide identification based on the acquired spectra.

## Radiographic Imaging

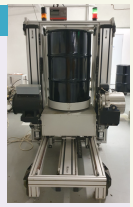

**Transmission radiography** is performed using a **Co-60** source and the **MOS-100** device, custom-built by VF Černá Hora. This setup reveals the internal structure of the radioactive waste drum.

Cobalt-60 emits high-energy photons (1173 and 1332 keV), making it ideal for penetrating dense waste materials. The system uses a **CsI(Tl) scintillation detector**, which is less hygroscopic and more robust than traditional NaI(Tl) detectors.

The MOS-100 enables **scanning** in **vertical, horizontal, and angular directions**.
The system operates in both passive mode (detection only) and active mode (with source irradiation).

## Radioactive Waste Management

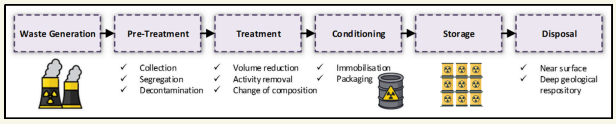


## Waste Disposal

**Low Level & Intermediate Level Waste**
Near-surface disposal at repositories

**High Level Waste & Spent Nuclear Fuel**
Deep geological disposal
Four candidate sites
Bukov underground research facility

## Waste Package

has to meet

**Waste Acceptance Criteria (WAC)**
- Physical & chemical properties
- Radiological properties
- Packaging & transport

has to pass

**Waste package integrity tests**
Drop test
Leak tightness test
Thermal test

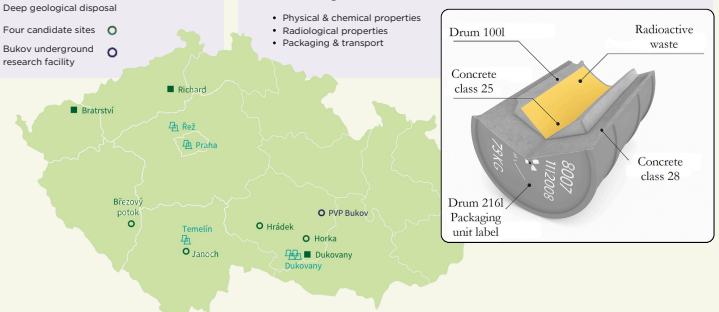





## Graphical User Interface

**Python-based graphical user interface** (GUI) tool designed to efficiently analyse the measurement results in accordance with the proposed methodology.

It uses ttkbootstrap and Tkinter libraries, making the interface **intuitive** and **user-friendly**. The structure includes multiple widgets for:
- data input,
- image visualization and adjustment,
- output export,
- gamma energy and angle selection,
- colormap and post-processing filter selection,
- help display and database viewing.

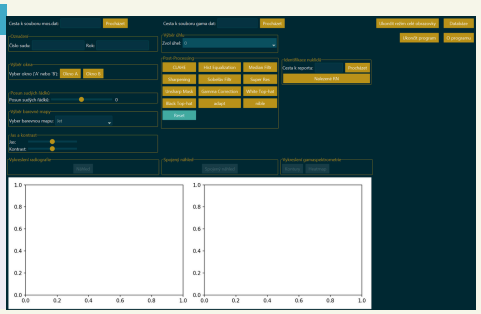

## Visualisation of spectrometric data

For processing the data from the Genie 2000 report, **Counts Per Second** (CPS) must be calculated by dividing the measured pulse count by the live measurement time. A **correction for dead time** is also applied. The processed data are then imported into the Python program, where they can be displayed either as a **gamma intensity heatmap** (a 2D image with color-coded radiation intensity in a 6 × 6 grid) or as **gamma intensity contours** – with each contour line representing a specific level of relative radiation intensity.

Additionally, using **Nuclide Identification Analysis** in Genie 2000, certain radionuclides can be identified, and their activity and associated uncertainty can be calculated.

**Visualization of the spatial distribution of relative gamma intensity for selected energies in the waste drum**

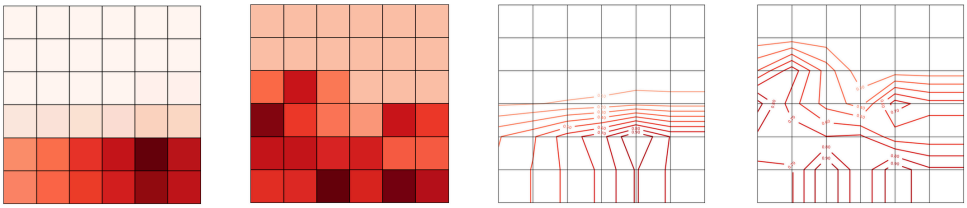

Heatmap for 661,7 keV energy (Cs-137) | Heatmap for 1332,5 keV energy (Co-60) | Contours for 661,7 keV energy (Cs-137) | Contours for 1332,5 keV energy (Co-60)

## Visualisation of radiographic data

The acquired data are in .txt format (originally mos.dat) and structured as an **n × n matrix**. The values are grouped by measuring angle (1–6) and **normalized to a 0–1 range**.

Visualization is performed using the **matplotlib** library and various **colormaps** (Jet, Flag, Viridis, Binary, Seismic, PuOr, Spectral, etc.). Different colormaps help visually emphasize the **density distribution** inside the drum, and selecting an appropriate scale is essential for correct interpretation of results.

Additionally, **post-processing filters** (Histogram Equalization, Median Filtering, Sharpening, Sobel Filter, Adapt, Super Resolution, etc.) are applied to reduce noise, smooth contours, and enhance internal structures within the drum.

**Radiographic imaging of the internal structure of the waste drum using various colormaps and post-process filters**

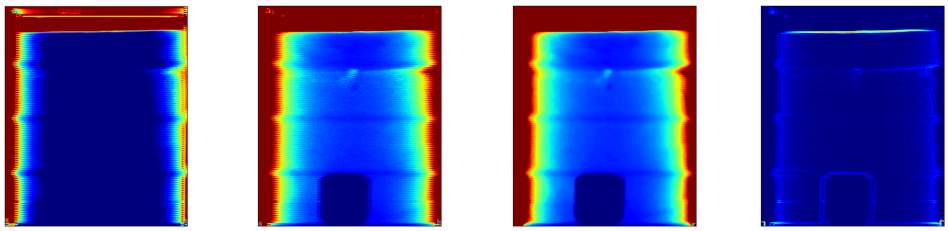

Colormap: Jet, no processing | Colormap: Jet, max brightness, no filtering | Colormap: Jet, max brightness, Median filtering | Colormap: Jet, Sobel filter

## Graphical comparison

The integration of radiographic and gamma-spectrometric data enables spatial **comparison** between **morphological structures** and **areas of elevated gamma activity.**

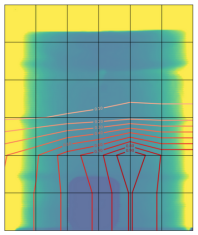

Combined visualization of the radiographic image (viridis colormap, median filtering) with gamma activity contours for 661,7 keV

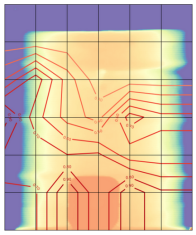

Combined visualization of the radiographic image (spectral colormap, median filtering) with gamma activity contours for 1332,5 keV

## Conclusion

This work proposed and described a methodology for **non-destructive characterization** of waste drums using gamma **spectrometric analysis** and **transmission radiography**.

The outcome is a **software application** suitable for industrial use, enabling **visualization of the internal structure of the drum** as well as the **spatial distribution of activity**. A key advantage of the developed tool is its **intuitive control** and broad range of **graphical adjustments** – including brightness and contrast settings, colormap selection, and post-processing filters.

Moreover, relative gamma intensity can be overlaid on the radiographic image, making the application a powerful tool for visualizing the drum's interior, verifying its **homogeneity**, and identifying the presence of **radioactive materials**.

**REFERENCES**

SÚRAO (2024). *Zpráva o činnosti Správy úložišť radioaktivních odpadů v roce 2023.* Accessed July 27, 2025.

Monitor obsahu sudů MOS-100. *Návod k obsluze a údržbě.* Černá Hora: VF a. s. Technical report, VF K0237-B-N01.

Ministerstvo průmyslu a obchodu ČR (2025). *Koncepce nakládání s radioaktivním odpadem a vyhořelým jaderným palivem: aktualizace pro období 2025 až 2035 s výhledem po roce 2050* [online]. Accessed July 27, 2025.

# ACCIDENT TOLERANT FUELS

Jiří PFEIFFER

*University of West Bohemia in Pilsen, Czech Republic*

The final project focuses on comparing available modifications in the form of cladding of fuel rods and adding impurities to the uranium dioxide compound. Their influence on the value of the multiplication factor at certain burnup values is investigated. The aim of the work is to compare the modifications with the most used combination of cladding and fuel using the computational code $U_WB_1$.

# Accident tolerant fuels

FACULTY OF ELECTRICAL ENGINEERING
UNIVERSITY OF WEST BOHEMIA

Author: Jiří Pfeiffer
Supervisor: Ing. David Mašata

## Introduction

The aim of this study is to build on the commonly used combination of zirconium-clad fuel rods and uranium dioxide fuel by **adding additional components** that enhance safety. However, it is important to consider that introducing other materials **may increase neutron absorption,** therefore, the study also focuses on modifications that **improve overall fuel burnup**.

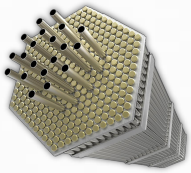

*Fig. 1: Fuel assembly [1]*

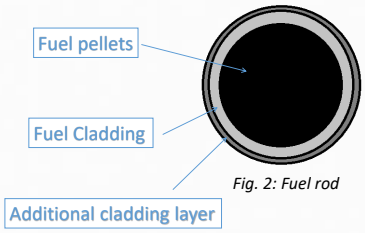


*Fig. 2: Fuel rod*

## Calculations

A calculation was performed for the material using the **UWB1** computational code to assess its impact on the neutron balance.

### Two approaches were investigated:

Adding an **additional layer (1)** to the base layer of cladding to either improve the overall multiplication factor or enhance the fuel rod's properties in case of a failure, and the **incorporation of compounds (2)** into the original uranium dioxide composition to achieve similar improvements.

## (1) Cladding

The main goal of implementing various types of fuel rod cladding is to protect the coolant from the **release of radioactive products** from the fuel rods, which would result in contamination of the coolant. This serves as one of the passive safety measures.

Each type of fuel rod cladding is characterized primarily by its overall **mechanical properties**, which are continuously being improved to **enhance fuel performance** (e.g., adding cladding layers), however, they differ in their neutron absorption properties.

### Sellected cladding layers:

- Chrome (Cr)
- Metal alloys (FeCrAl)
- SiC - composite (SiC)
- Diamond (C)

*Fig. 3: Zircalloy-4 tubes [2]*

## (2) Improved fuel

**Uranium dioxide** is a solid black substance with very low thermal conductivity and a high melting point. This material is compressed into pellets, which are inserted into a cylindrical casing.

In terms of improvements, the designs are divided into two groups: **additives**, and **substitution of a specific element** in the original uranium dioxide compound.

### Sellected fuel materials:

- $UO_2 + Cr_3O_3 + Al_3O_3$
- $UO_2$ + Beryllium
- Silicide fuel ($UO_2$ -> $U_3Si_2$)

*Fig. 4: Fuel pellets [3]*

**Results:** Comparison of $k_{inf}$ values for the **fuel additives**

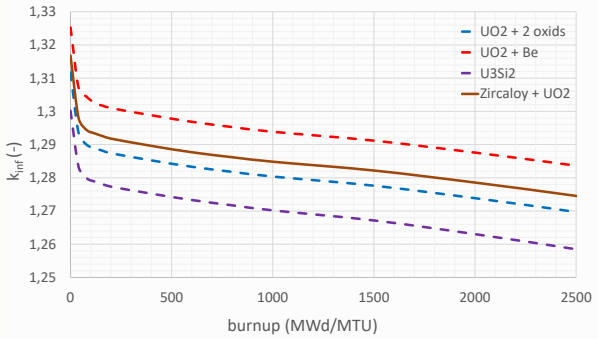


**Results:** Comparison of $k_{inf}$ values for the **fuel cladding**

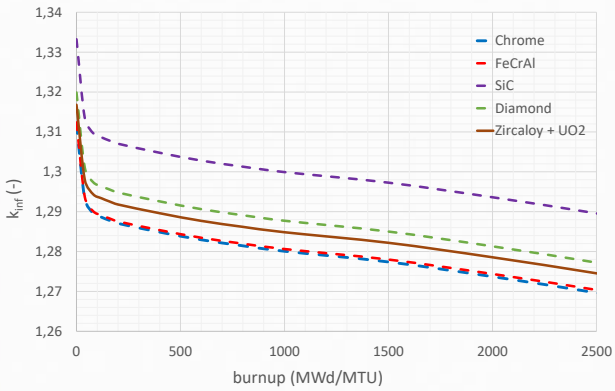


## Conclusion

- From a safety perspective, zirconium with a **diamond coating is the best cladding option**, offering significant safety improvements and a positive impact on overall fuel burnup. This fuel type is currently undergoing testing and further investigation, and it has the potential to replace the most used cladding material (Zircaloy – 4).
- Among fuel additives, uranium dioxide **with beryllium** shows the **best burnup performance**, mainly due to the favorable properties of beryllium itself. However, despite these promising results, **beryllium can introduce reactor instability**. The other two cases are primarily designed to enhance fuel behavior during accident conditions.
- Improved technology may allow combining cladding and additives to achieve better overall reactor efficiency and safety.

[1] Energy Encyclopedia, https://www.energyencyclopedia.com/en/nuclear-energy/nuclear-fuel/fuel-assembly
[2] SuperiorTube, https://www.superiortube.com/products/materials/zirconium-alloys
[3] Deep isolation, https://www.deepisolation.com/about-nuclear-waste/what-is-nuclear-waste/

# BEHAVIOUR OF NUCLEAR FUEL WITH 10% ENRICHMENT URANIUM-235 AND VARIOUS BURNABLE ABSORBERS

Miloš ZACHAR

*Brno University of Technology, Czech Republic*

Bachelor's thesis deals with four types of burnup absorbers that reduce the reactivity of freshly loaded fuel with the aim of using it at higher enrichment than is currently commercially available. The burnable absorbers are simulated using fuels enriched to 7 and 10%, and the simulation results are presented graphically. An enrichment of 10% was chosen for the page.

# BEHAVIOUR OF NUCLEAR FUEL WITH 10 % ENRICHMENT URANIUM-235 AND VARIOUS BURNABLE ABSORBERS

## 1 GADOLINIUM

Short-term subcriticality with gadolinium and subsequent massive increase in the multiplication factor. Depending on the boric acid concentration, the fuel in the reactor is supercritical until burnup is 60 to 80 GWd/tU.

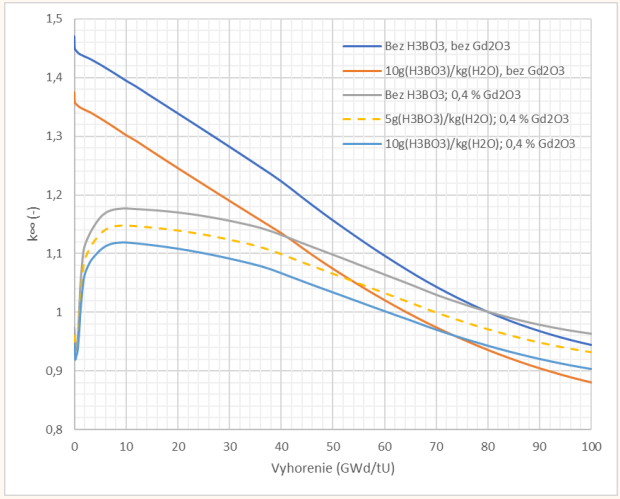


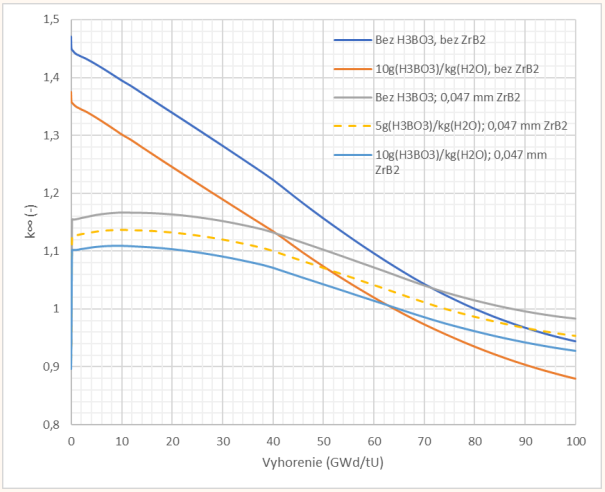


## 2 BORON

The fuel is initially subcritical, the subsequent increase in criticality is faster than with gadolinium. Further burnup is gradual and the multiplication factor is almost stable.

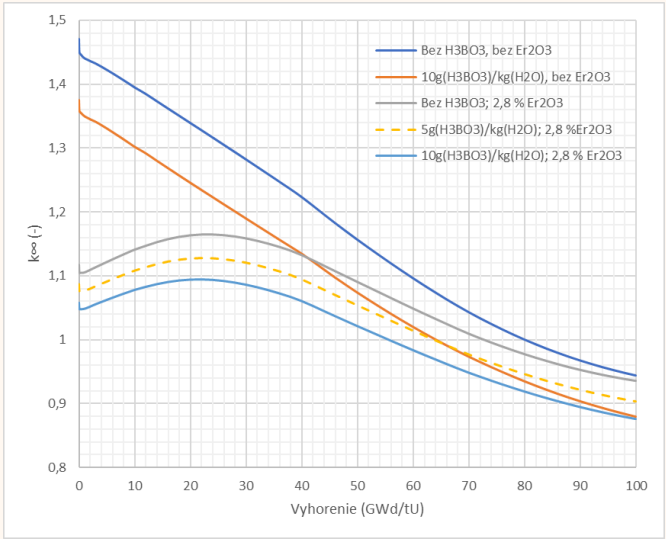


## 3 ERBIUM

The increase and decrease of the multiplication coefficient is gradual, the effect of erbium is long-term and the course is favorable for regulation.

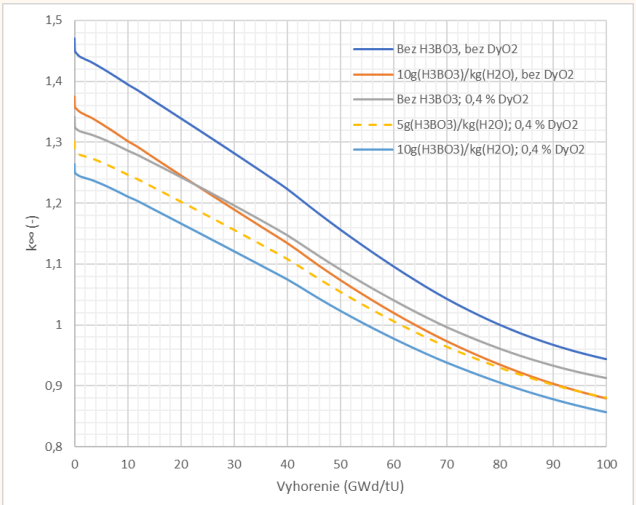


## 4 DYSPROSIUM

The effect of the dysprosium burnable absorber is initially insufficient, but it is too long-term. This process is insufficient from a regulatory point of view.

SIMULATIONS WERE EVALUATED FOR THREE-CAMPAIGN FUEL OPERATION WITH A TOTAL BURNUP OF 96 GWD/TU.

# MASTER STUDENTS

# EXCLUSION PROTECTION ZONE OF SMR'S

George Alexandru BOCA

*University of Bucharest, Romania*

This poster presents an analysis of the differences between the size of exclusion zones for SMRs, the differences between SMR EPZs and classic ones, and how these can impact site selection.

# EPZ of SMR's

Boca George Alexandru (+40 748 381 453, george.boca@ropower.com)
ROPOWER NUCLEAR SA

## Abstract

**What is an EPZ?**

EPZ stands for Exclusion Protection Zone, which represents the final safety barrier for nuclear safety. It is essentially a radius around the reactor within which no humans can reside, with the purpose of containing and reducing radiation emissions in case of an accident.

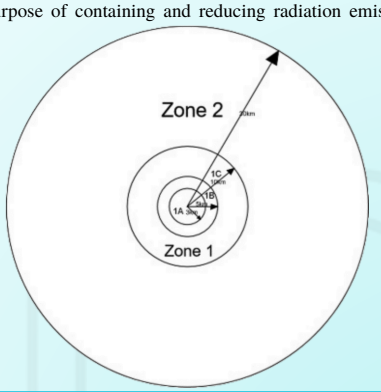


## Methotology

The EPZ is an integral siting criterion, and we calculate it in the following ways.

First, we need something called a source term – a realistic and conservative estimate of the amount of radiation (radionuclides) that would be released in the event of an accident.
Second, we use a software program (such as RODOS) to simulate the spread of radiation and determine where the radiation dose levels fall below the legal limit for the EPZ. This is how we establish the radius.

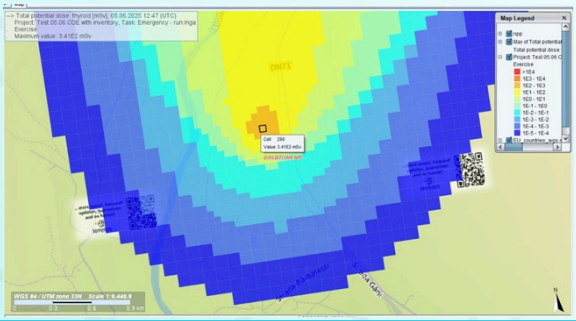

## How does the EPZ for an SMR differ from that of a "classical" reactor?

The main difference is the size, which is directly influenced by the source term. As expected, a smaller reactor has a smaller source term (because it contains less fuel), leading to a smaller EPZ. However, there is no linear correlation between a reactor's power and its EPZ, as we must also consider the capacity factor and the intrinsic neutronics of the reactor (for example, SMRs generally have a lower burn-up rate due to the smaller neutron flux caused by their reduced core dimensions).

## What are the implications of this?

The main implications of the EPZ are related to site selection and nuclear safety.

**Site selection**

A smaller EPZ opens up a wider range of possible sites, particularly the locations of old thermal power plants (coal or gas). This is a significant advantage because an SMR plant is often designed to provide a similar power output to the plant it replaces, meaning it can take advantage of the existing power grid infrastructure.

**Nuclear safety**

A smaller EPZ inherently improves safety expectations. This is due to the smaller potential radiation release, as well as the advanced safety features (both active and passive) that are characteristic of next-generation SMRs.

## Conclusion

The main difference is the size, which is directly influenced by the source term. As expected, a smaller reactor has a smaller source term (because it contains less fuel), leading to a smaller EPZ. However, there is no linear correlation between a reactor's power and its EPZ, as we must also consider the capacity factor and the intrinsic neutronics of the reactor (for example, SMRs generally have a lower burn-up rate due to the smaller neutron flux caused by their reduced core dimensions).

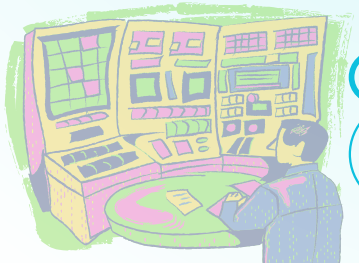

**Acknowledgement**

1. https://www.sciencedirect.com/science/article/pii/S209044792200140X
2. https://nuclearforclimate.com.au/site-selection/

# BENDING-INDUCED CHANGES IN CRITICAL HEAT FLUX OF NUCLEAR FUEL ROD IN LOW-PRESSURE SYSTEM

Tomáš KADAVÝ

*University of West Bohemia in Pilsen, Czech Republic*

This poster studies the effect of fuel rod deflection on the critical heat flux (CHF) in a low-pressure water loop. Experiments with various bend deflections and coolant flow rates showed up to a 10% increase in CHF compared to no deflection scenario. Results suggest that bending can delay boiling crisis. Limitations are discussed.

# Bending-Induced Changes in Critical Heat Flux of Nuclear Fuel Rod in Low-Pressure System

Tomáš Kadavý[1]

[1] Department of Power System Engineering, Faculty of Mechanical Engineering, UWB in Pilsen

UNIVERSITY OF WEST BOHEMIA

## Introduction

Spent nuclear fuel is commonly stored in Spent Fuel Pools before final disposal. Ensuring sufficient heat removal from fuel assemblies is a key safety concern. One of the critical phenomena affecting heat transfer in such systems is the Critical Heat Flux (CHF) – the point at which boiling crisis occurs and heat transfer efficiency drops sharply.

This study focuses on how mechanical bending of a nuclear fuel rod affects CHF behavior under low-pressure coolant conditions.

Geometrical deformations such as rod bowing may occur due to handling, irradiation-induced creep, or mechanical stresses, and their influence on boiling crisis has not been fully quantified, especially in simplified systems.

## Objectives

Modify the experimental apparatus to enable controlled bending of the fuel rod imitator.

Investigate and evaluate the effect of rod bending on critical heat flux.

## Methology

The study was conducted using a low-pressure experimental rig equipped with an electrically heated fuel rod imitator with an outer diameter of 9 mm and a heated length of 1476 mm, placed inside a glass tube with an inner diameter of 14.5 mm. The test section was modified to allow rod bending using a custom-machined steel fixture and a 3D-printed reinforcement part to stabilize the glass flow channel.

Four different bending deflections were tested: 0 mm, 1 mm, 1.5 mm, and 2 mm. For each bending value, measurements were performed at four different coolant flow rates, and each measurement was repeated five times to ensure reproducibility.

During testing, the power supplied to the heating element was gradually increased until a critical heat flux (CHF) event occurred, indicated by a sudden temperature spike on one of the thermocouples mounted on the inner surface of the rod imitator. This triggered an automatic shutoff of the power supply. The CHF was evaluated as the critical heat flux density (heat flux per unit heated surface area) normalized by the coolant mass flow rate through the given cross-section.

## Experimental apparatus

1 Coolant tank
2 Coolant pump
3 Inlet valve
4 Test Channel with Heated Rod
5 Vapor outlet
6 Return line
7 Water to Air Cooler

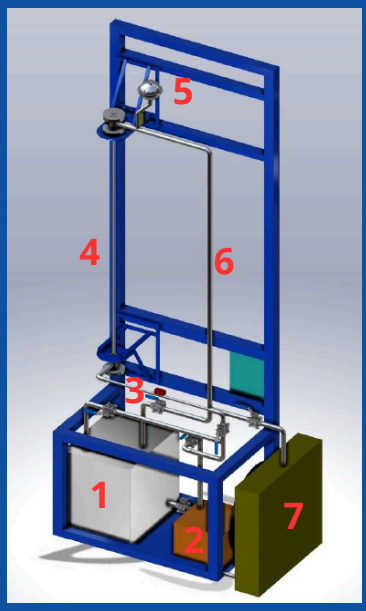


Fig. 1 Experimental stand

## Modifications

Custom-made steel fixture (Fig. 2) allows rod deflection by 3 adjustment screws. Proper sealing is essential – two sets of O-rings are used.

Fig. 2 Steel fixture

Fig. 3 3D-printed fixture

A 3D-printed fixture (Fig.3) made from heat-resistant plastic material ensures coaxial alignment of the steel fixture and the glass tube, and reinforces the entire assembly.

Fig. 4 Bent fuel rod imitator inside the glass flow channel

Fig. 5 Assembled Flow Channel

## Results

The influence of rod bending on critical heat flux (CHF) increases with both higher coolant flow rates and greater deflection values. Compared to the unbent condition, the CHF values increased by up to 10% during maximum deflection. In the context of spent fuel pools, this effect could be considered positive, as boiling crisis occurred at higher power levels when the rod was bent.

These findings contrast with expectations, which generally predict a decrease in CHF with increased bending due to early dryout. However, the specific conditions of this experiment such as a single-rod channel, unheated walls, and outter air-cooled contact surfaces may explain the deviation.

A rational second-order model with five parameters was fitted to the measured data using a Python script, the results are available in the full text of the Thesis (page 75) in the QR code at Fig. 8.

$$Q_{krit} = \frac{p_1 * G^2 + p_2 * G + p_3}{G^2 + q_1 * G + q_2}$$

Qcrit – Critical heat flux [kW/m^2]; G – Mass flux [kg/m^2s]
p1,p2,p3,q1,q2 – Function parameters [–]

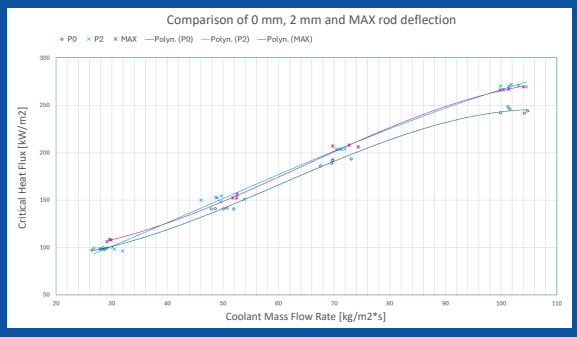


Fig. 6 Comparison of 0 mm, 2 mm and MAX rod deflection

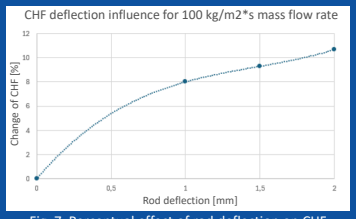


Fig. 7 Percentual effect of rod deflection on CHF

Fig. 8 Full text of the thesis with detailed results

# DEVELOPMENT OF FULL-CORE VVER-1000 MODEL IN DETERMINISTIC CODE PARCS: VALIDATION OF DATA PREPARATION PROCESS ON HZP CALCULATIONS

Ondřej LACHOUT

*Czech Technical University in Prague, Czech Republic*

The accurate prediction of reactor core behavior under various operating conditions is fundamental for ensuring nuclear safety and effective reactor operation. Deterministic reactor physics codes, such as PARCS (Purdue Advanced Reactor Core Simulator), offer efficient tools for full-core simulations. However, their accuracy is strongly influenced by the quality of the macroscopic nuclear data used as input. This study focuses on the development and validation of a full-core VVER-1000 model in PARCS, with emphasis on verifying the macroscopic data preparation process for Hot Zero Power (HZP) conditions. The macroscopic cross-section library was generated using the Monte Carlo code Serpent2, based on infinite lattice models of individual fuel assemblies. Data were parametrized with respect to key reactor state variables, including moderator and fuel temperature, coolant density, and boron concentration. Special attention was given to reflector modeling and the preparation of homogenized macroscopic data using a full-core Serpent model at zero burnup. To evaluate model fidelity, the X2 Khmelnitsky benchmark—containing experimental HZP data—was employed. PARCS calculations were compared with both benchmark measurements and parallel full-core Serpent simulations. The results show strong agreement in key parameters, including critical boron concentration, control rod worth, power distribution, and moderator reactivity coefficient. Notable discrepancies were observed only in the integral characteristics of one control rod bank, likely due to limitations in nodal treatment of control rods in PARCS. The study demonstrates the reliability of the macroscopic data preparation procedure and supports the validity of the deterministic PARCS model under HZP conditions. Future work will extend this approach to Hot Full Power states and evaluate the influence of various data preparation strategies on reactor simulation accuracy.

# Development of Full-Core VVER-1000 Model in Deterministic Code PARCS: Validation of Data Preparation Process on HZP Calculations

Author: **Ondřej Lachout**[1]
Co-author: Pavel Suk[1]
[1]Czech Technical University, Faculty of Nuclear Sciences and Physical Engineering, Department of Nuclear Reactors, Czech republic

CTU IN PRAGUE

## ABSTRACT

**The accurate simulation of reactor core behavior is essential for safe and reliable nuclear power plant operation. Deterministic macrocodes like PARCS are widely used for full-core analyses, but their accuracy depends on the quality of macroscopic input data. This study developed a full-core VVER-1000 model in PARCS, focusing on validating the macroscopic data preparation process using Hot Zero Power (HZP) conditions. Macroscopic cross-section data were generated using the Monte Carlo code Serpent2, based on an infinite lattice model of fuel assemblies. To validate the model, results were compared against the X2 Khmelnitsky benchmark and a separate full-core Serpent model. This dual validation approach allowed a thorough assessment of the data preparation methodology and the reliability of the PARCS model.**

## MACROSCOPIC DATA PREPARATION

The entire process, from the preparation of lattice code input templates to the execution of the full-core calculation in deterministic macrocode, is a very extensive task and requires interaction between a group of computational programmes and scripts, allowing proper communication and data transfer between them. [1]

### Fuel Elements

Macroscopic nuclear data for fuel elements, i.e. fuel assemblies, are prepared on an infinite fuel lattice model with periodic boundary conditions. At the lattice code level (in this case, the code Serpent 2.2.1 [2] was used), the geometry of the fuel assembly (FA) and the composition of the material is modelled in detail. For the purposes of macrocode, the data are spatially homogenised by the lattice code over the whole assembly.

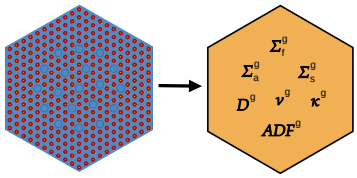


**Figure 1:** *Homogenisation of the fuel assembly lattice model.*

### Reflectors

In this study, for the purposes of generating reflector data, a full-scale model of the VVER-1000 reactor core was created in Serpent, following the benchmark specifications. Radial reflectors were homogenised as hexagonal elements in 1/6 core symmetry, and axial reflectors were constructed from axial regions excluding the active fuel length. The visualisation of the radial and axial reflectors is presented in Figure 2.

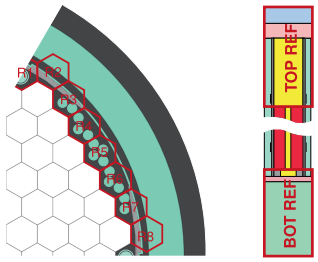


**Figure 2:** *Radial and axial reflectors visualisation. [3] (modified)*

**Table 1:** *Conditions for the preparation of macroscopic data. [4]*

| | $T_f$ (K) | $T_c$ (K) | $\rho_c$ (g cm$^3$) | $C_b$ (ppm) |
|---|---|---|---|---|
| HZP | 554 | 554 | 0.76309 | 1207 |

## FULL-CORE CALCULATIONS

A full-core model of VVER-1000/320 was created following the X2 Khmelnitsky benchmark in the PARCS deterministic macrocode, in version 3.3.6 [5]. Specifications of model geometry, materials, and other operational parameters are presented in [3].

### Critical Boron Concentration

All calculations were performed with ENDF/B-VII.1, however uniquely for this section, multiple nuclear data libraries were analysed to highlight the strong dependence of results on the choice of nuclear data library (calculations with ENDF/B-VII.0 and ENDF/B-VIII.0 are also provided). The results of critical boron concentration ($C_b$) calculations are presented in Table 2

**Table 2:** *Comparison of critical boron calculations.*

| Model | $C_b$ (ppm) | $\Delta C_b$ (ppm) |
|---|---|---|
| Benchmark | $1207 \pm 24$ | – |
| Serpent – E70 | $1204 \pm 1$ | $-3$ |
| Serpent – E71 | $1206 \pm 1$ | $-1$ |
| Serpent – E80 | $1222 \pm 1$ | $+15$ |
| PARCS – E70 | 1212 | $+5$ |
| PARCS – E71 | 1214 | $+7$ |
| PARCS – E80 | 1229 | $+22$ |

$$\Delta C_b = C_b - C_b^{\mathrm{BEN}}. \qquad (1)$$

### Control Rod Banks Worth

Two measurements are provided within the benchmark; the first assumes full reactor SCRAM with the insertion of all control rod banks, and for the second case the control rod bank at position #17 (see Figure 3) is stuck at the top position. The results are presented in Figure 4.

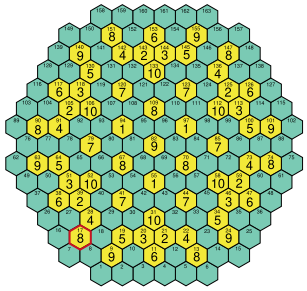

**Figure 3:** *Positions of CR banks in the core. [5] (modified)*

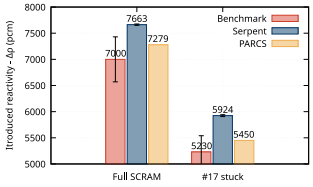


**Figure 4:** *Results of the SCRAM calculations.*

### Power Distribution

The benchmark does not provide data for power distribution at HZP, however PARCS and Serpent results were compared both for radial assembly-wise normalized power distribution (Figure 5) and normalised axial power distribution (Figure 6).

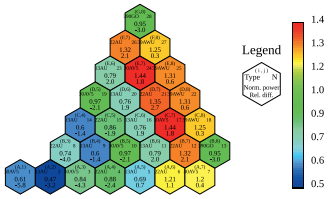


**Figure 5:** *Normalised radial power distribution.*

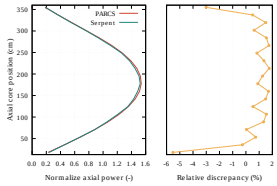


**Figure 6:** *Normalised axial power distribution.*

### Integral Characteristic of CR Bank #10

The integral curve calculated by PARCS is compared to Benchmark's and Serpent's results, which are 15 % lower on average. This could be, among other things, caused by a 1.9 % lower normalised radial power for the FA position with the CR bank #10.

### Moderator Reactivity Coefficient

The moderator reactivity feedback was measured in two reactor states with different concentration of boron in the coolant, see the paper [3]. The results of the calculation are shown in Table 3.

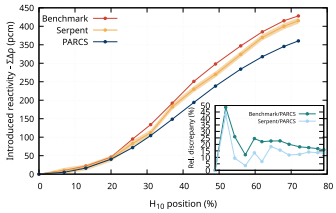


**Table 3:** *Calculation of the moderator reactivity coefficient.*

| | $T_m^{in}$ (°C) | $\Delta\rho/\Delta T$ (pcm/°C) | | |
|---|---|---|---|---|
| | | Benchmark | Serpent | PARCS |
| 1. | 280.7-276.0 | $-4.88 \pm 0.50$ | $-5.41 \pm 1.07$ | -4.98 |
| 2. | 280.3-275.7 | $-13.58 \pm 0.14$ | $-15.13 \pm 1.23$ | -13.96 |

**Figure 7:** *Integral characteristics of the control rod bank #10.*

## CONCLUSION

**The macroscopic cross-section library, generated using the Serpent code, was validated against both experimental measurements and a parallel high-fidelity Serpent full-core simulation, following the X2 Khmelnitsky benchmark specifications. The comparison of critical boron concentration presents discrepancies in the PARCS model reaching up to 22 ppm of boron, depending on the dataset used. The control rod banks worth calculations demonstrated particularly good agreement. Power distribution comparisons showed satisfactory agreement between PARCS and Serpent, with average relative differences within acceptable margins. The only significant deviations were observed in the calculation of the integral characteristics of control rod bank #10, likely due to limitations in the treatment of control rod modeling in PARCS.**

### References

[1] O. Lachout, P. Suk, "Analysis of Operational Characteristics of a Small Modular Reactor With Accident Tolerant Fuel." Proceedings of the 2024 31st International Conference on Nuclear Engineering. Volume 11: Student Paper Competition. Prague, Czech Republic. August 4–8, 2024. V011T15A073. ASME. https://doi.org/10.1115/ICONE31-136104.
[2] J. Leppänen, M. Pusa, et al., "The Serpent Monte Carlo code: Status, development and applications in 2013," Annals of Nuclear Energy, vol. 82, pp. 142–150, Aug. 2015, doi: 10.1016/j.anucene.2014.08.024.
[3] Y. Bilodid, E. Fridman, and T. Lötsch, "X2 VVER-1000 benchmark revision: Fresh HZP core state and the reference Monte Carlo solution," Annals of Nuclear Energy, 2020, doi: 10.1016/j.anucene.2020.107558.
[4] T. Lötsch, V. Khalimonchuk, and A. Kuchin, "Proposal of a benchmark for core burnup calculations for a WWER-1000 reactor core," in Proc. 19th AER Symp. VVER Reactor Physics and Reactor Safety, St. Constantine and Elena Resort, Bulgaria, 2009. Available: https://inis.iaea.org/records/h08fn-2c968.
[5] T. Downar, A. Ward, Y. Xu, and V. Seker, PARCS NRC - v3.3.6 Release: Volume I: Input Manual. University of Michigan and U.S. Nuclear Regulatory Commission, 2021.

# DEBRIS BLOCKAGE OF FLOW THROUGH ROD BUNDLE

Florin MISTRE

*IMT Atlantique, France*

Nuclear fuel is organized in nuclear reactor in a form of fuel rods, there is a coolant flowing in the space between rods. These rods are kept in their position by spacer grids. Blockage of a spacer grid by some piece of debris (metal fragment, corrosion product or other foreign material) can significantly alter the flow, decrease heat transfer and increase risk of local overheating. Isothermal flow through a model nuclear fuel assembly is studied by Particle Image Velocimetry (PIV). Blockage is introduced artificially by using circular plug placed at the "star" or "circle" node of the spacer grid. Results reveal that the blockage location leads to different behavior in in terms of wake strength, wake width, fluctuation amplitudes or length-scales.

ZÁPADOČESKÁ UNIVERZITA V PLZNI

# DEBRIS BLOCKAGE OF FLOW THROUGH ROD BUNDLE

NUCLEAR DAYS

Florin Mistre, Daniel Duda, Anna Mrázová, Vojtěch Janský, Vitalii Yanovych & Václav Uruba

## Wind tunnel measurement of isothermal flow through nuclear fuel assembly model

- Hexagonal rod arrangment
  3 measuring planes

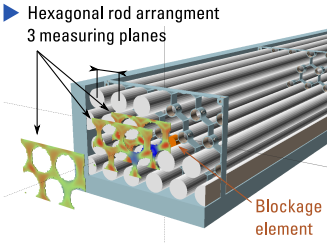


- Test section 0.3 × 0.2 × 3.0 m, spacer grid 4×

- Stereo Particle Image Velocimetry

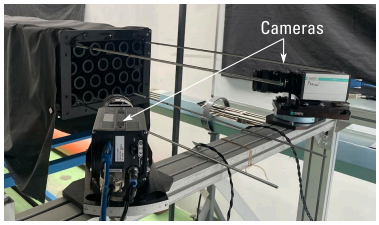


- Tracer particles & laser sheet

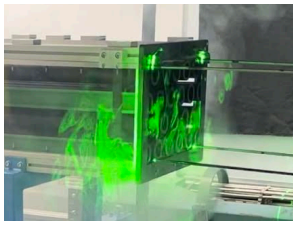

## Abstract & introduction

- Blockage of a spacer grid by some piece of debris (metal fragment, corrosion product or other foreign material) can significantly alter the flow, decrease heat transfer and increase risk of local overheating.
- Isothermal flow through a model nuclear fuel assembly is studied by Particle Image Velocimetry (PIV)
- Blockage is introduced artificially by using circular plug placed at the "star" or "circle" node of the spacer grid:


- Results reveal that the blockage location leads to different behaviour in terms of wake strength, wake width, fluctuation amplitudes or length-scales.

## Mean streamwise velocity

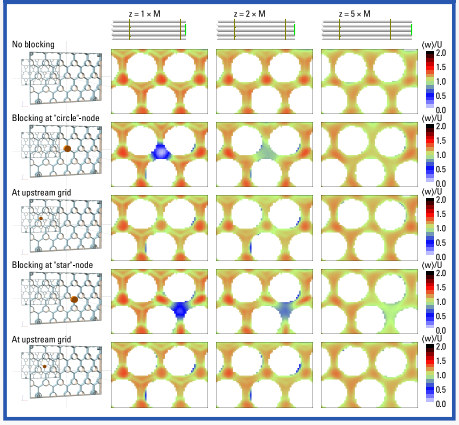


## Turbulent kinetic energy

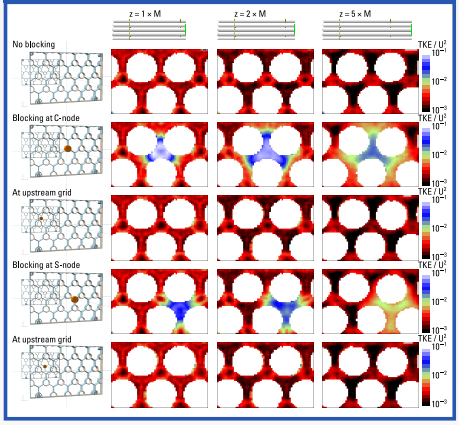


## Velocity histograms at selected points

- Positions of the points of interest within the Field of View:

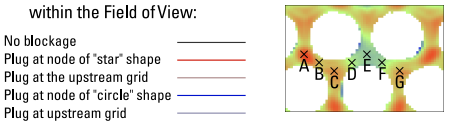


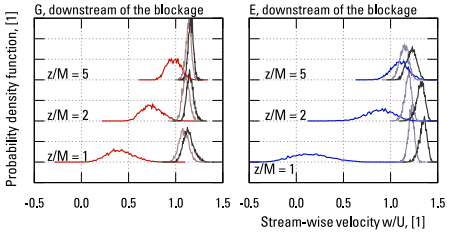


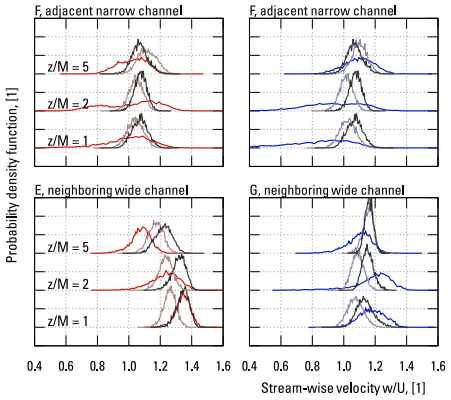


## Flatness of streamwise velocity

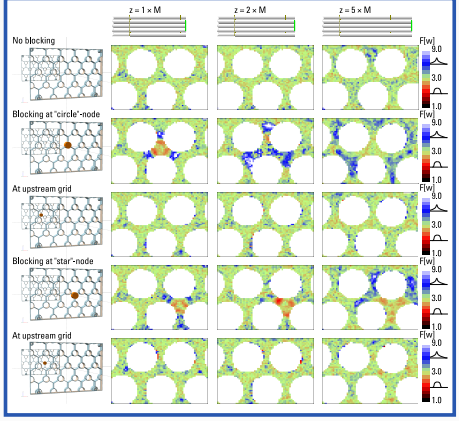


## Estimation of Taylor microscale

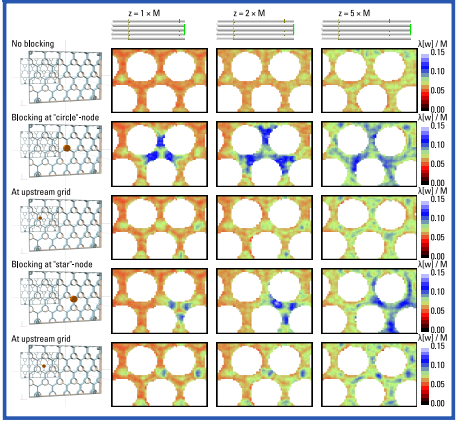


## Autocorrelation function ... with the point F in a narrow channel

- Autocorrelation of streamwise velocity w:

$$R_{ww}(\vec{x},\vec{y}) = \frac{\left\langle \left(w(\vec{x},t_i) - \langle w(\vec{x})\rangle\right)\cdot\left(w(\vec{y},t_i) - \langle w(\vec{y})\rangle\right)\right\rangle}{\sigma[w(\vec{x})]\cdot\sigma[w(\vec{y})]}$$

Reference point

Standard deviation at given point

Correlation with point E (at the wake axis past the plug at C-node)

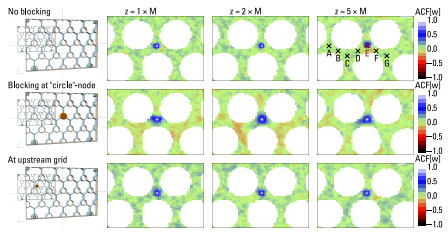


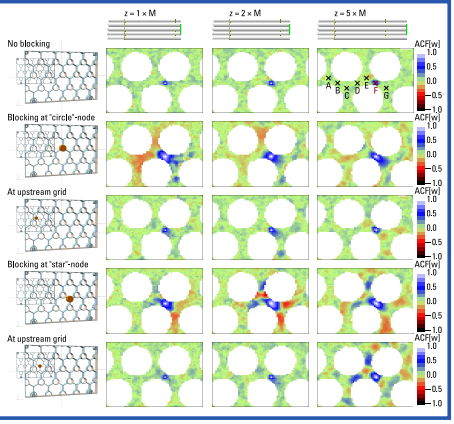

# NEUTRONIC ANALYSIS OF A WESTINGHOUSE SMALL MODULAR REACTOR USING OPENMC MONTE CARLO CODE

Sarra MOUMMI

*Faculty of Sciences of Tunis, Tunisia*

This study investigates pyrex insertion effects on reactor physics parameters in Westinghouse SMR configurations using OpenMC Monte Carlo simulations. Three core configurations were analyzed: reference core, partial pyrex insertion, and full pyrex insertion. Results demonstrate significant reactivity reduction with progressive pyrex implementation. Flux distributions show enhanced flattening and improved power homogenization with pyrex presence. Temperature coefficients became increasingly negative, strengthening inherent safety margins, while control rod effectiveness increased substantially. Spatial neutron flux and fission rate distributions reveal localized absorption effects in pyrex regions with corresponding redistribution of neutron population. OpenMC simulations accurately captured complex neutron-absorber interactions in heterogeneous SMR core geometries. The findings validate pyrex effectiveness as a viable solution for reactivity control and flux optimization in small modular reactor applications requiring precise neutron management and enhanced safety characteristics.

# Neutronic Analysis of a Westinghouse Small Modular Reactor using OpenMC Monte Carlo Code

S.Moumni, W. Dridi
National Center for Nuclear Sciences and Technologies (CNSTN), Tunisia

## BACKGROUND

- Clean and reliable energy is a major global challenge.
- Traditional nuclear reactors are powerful but expensive and complex.
- Small Modular Reactors (SMRs) offer a safer, more flexible, and cost-effective solution.
- Neutronic modeling is essential to design efficient and safe reactor cores.

### Objective

- Model the core of a Small Modular Reactor (SMR).
- Analyze neutronic parameters (keff, flux, reaction rates).
- Study the effect of PYREX absorbers on performance and safety.

## Methodology

### SOFTWARE

OpenMC is an open source Monte Carlo particle transport code.

### Assembly Configurations

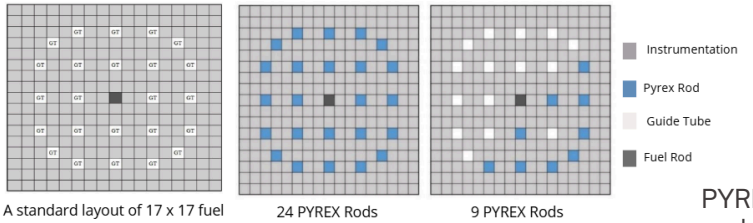


A standard layout of 17 x 17 fuel assembly

24 PYREX Rods

9 PYREX Rods

Pyrex rod configurations for UOX fuel

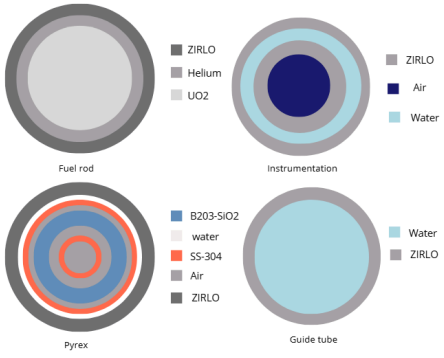


## Results

**Reactor physics parameters**

| Details | Cœur Réf. | Pyrex partiel | Pyrex total |
|---|---|---|---|
| Multiplication Factor | 1.25388 | 1.17365 | 1.04729 |
| Max/Average Flux Ratio | 3.448 | 3.349 | 2.776 |
| Control Rod Worth | — | 0.08023 | 0.20659 |
| Fuel Co-efficient of Reactivity (δk/°C) | -3.57e-5 | -4.58e-5 | -6.22e-5 |
| Moderator Co-efficient of Reactivity (δk/°C) | -4.17e-5 | -6.30e-5 | -8.57e-5 |

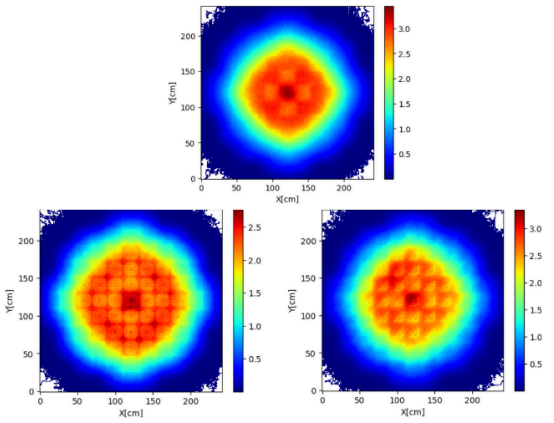


**Normalized flux distribution comparison: reference core, partial Pyrex insertion, and full Pyrex insertion.**

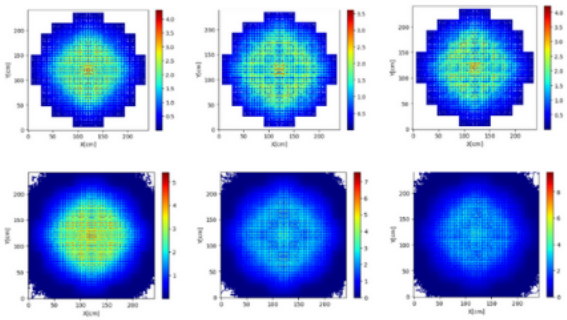

**Absorption/Fission – Ref. vs Pyrex**

## DISCUSSION

PYREX insertion reduces core reactivity by up to 15,734 pcm and improves flux uniformity. Negative temperature coefficients are enhanced, reinforcing inherent safety.

OpenMC results show that absorber insertion flattens the neutron flux and reduces peak reaction rates, particularly in the fission distribution.

### conclusion

OpenMC proved to be a reliable and efficient tool for accurately modeling the SMR core and analyzing the impact of absorber materials on neutronic behavior.

# THE EFFECT OF CLOGGING OF THE SPACER GRID ON THE CRITICAL HEAT FLUX OF A PRESSURELESS FUEL ROD SIMULATOR

Anna MRÁZOVÁ

*University of West Bohemia in Pilsen, Czech Republic*

This poster investigates the influence of partial and complete blockage of the spacer grid on the power required to reach the critical coolant temperature in a vertical unpressurized experimental loop containing a single heated rod simulating a nuclear fuel element. Flow restrictors were designed to obstruct approximately one-third and three-quarters of the flow cross-section, respectively. The experimental setup included a glass channel, a directly heated stainless-steel rod, and advanced data acquisition via thermocouples and ultrasonic flow sensors. Experiments were carried out under various coolant flow rates, and critical heat flux conditions were evaluated. Results show that at higher flow rates, increased power was required to reach the set critical temperature of 180 °C, even in the presence of flow obstruction. Contrary to expectations, the introduced foreign objects (flow restrictors) enhanced local coolant mixing, delaying the onset of critical heat flux compared to the unobstructed case. The presence of the foreign element did not cause local overheating but showed a beneficial thermohydraulic effect under tested conditions. These findings are particularly relevant for understanding post-operational behaviour of impurities in spent fuel pools where flow rates and thermal conditions differ significantly from reactor cores.

FACULTY OF MECHANICAL ENGINEERING
UNIVERSITY OF WEST BOHEMIA

# The effect of clogging of the spacer grid on the critical heat flux of a pressureless fuel rod simulator

NUCLEAR DAYS

Anna Mrázová, Department of Power System Engineering

• Introduction

Foreign object intrusion is a much talked about topic in industrial practice recently. Foreign objects can cause problems ranging from economic loss to loss of safety in the workplace. Indeed, there is a wealth of experience with such foreign object intrusion problems from nuclear power plant operations. For example, the first Czechoslovak nuclear power plant, Jaslovské Bohunice, was shut down after the most recent accident, which was caused by the presence of silica gel in the fuel assembly, where it impeded the cooling of the assembly and caused the fuel rods to melt.

In both plant facilities and manufacturing technologies, this negative factor has been the focus of attention, but is its impact really only negative? It is this consideration that gave rise to this topic.

The research focuses on the thermohydraulics in an experimental pressureless loop containing a single heated rod simulating a fuel rod and the spacers that the rod is fitted with.

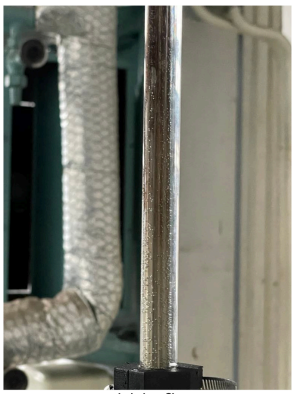

Bubble flow

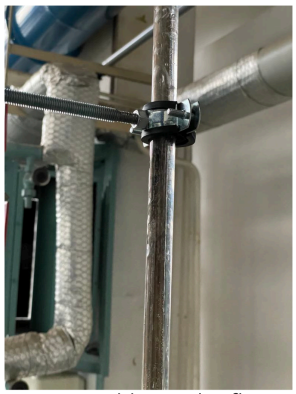

Transition to slug flow

Churn flow

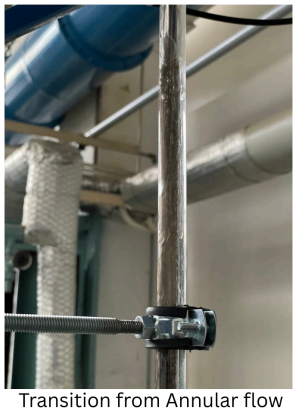

Transition from Annular flow to DRYOUT

• Experimental setup

Measurements take place on a closed loop where distilled water flows through a glass channel with a heated stainless steel fuel rod simulator powered by a SELCO ETG 206 DC source. Flow is limited to 0.2 m³/h, velocity to 0.6 m/s, and inlet temperature to 40 °C. Flow is measured by a KOBOLD DUK meter, cooling is via a water-air exchanger, and control is through NI LabVIEW. Temperature is logged every 0.5 seconds using K-type thermocouples. To simulate channel blockage, a 3D printed metal element was designed. It narrows the flow area by ⅓, ½, or ¾. The element was produced using DMLS from 316L steel for strength and corrosion resistance.

• Results and Conslusion

Measurements were taken for 3 levels of flow blockage (unclogged, ½, ¾) and four pump speeds (30-75 rpm). The figures above show the condition of the fuel rod and the element before and after the measurements. The results showed that higher flow rates required higher power to reach critical temperature, and at lower flow rates, power was slightly higher for the unclogged variant. Surprisingly, the blockage improved heat dissipation instead of causing overheating. It is this effect that should be the next subject of investigation.

# CHARACTERIZATION OF THE PERFORMANCE OF A HYBRID SMALL MODULAR REACTOR AND ITS INTERACTION WITH THE POWER GRID

Silvia PICCHI

*University of Pisa, Italy*

Hybrid energy systems incorporating Small Modular Reactors (SMRs) represent a promising nuclear technology which allows the combined production of heat and power. This increases the flexibility of nuclear plants and opens new possibilities for the decarbonization of energy production. This thesis explores this concept from both a technical and an economic perspective, proposing and evaluating a conceptual design of the balance of plant for a hybrid light-water SMR. The technical analysis focuses on the design and modeling of the plant interaction with power grid disturbances, particularly for primary frequency regulation. The economic assessment proposes a methodology to estimate the overnight capital cost of LW-SMRs at the preliminary design stage and evaluates the economic competitiveness of hybrid designs compared to full-electrical and full-thermal configurations. The results of the simulations demonstrate the potential of cogeneration plants to mitigate the impact of such transients on the primary loop. Using the heat output to bypass the turbines and modulate electrical power, it is possible to reduce disturbances to the steam generator, the interface between the primary and secondary loops. For the economic assessment, the proposed methodology is applied to open-literature data to estimate the overnight capital costs of electrical, thermal and hybrid SMRs. The reactors are then compared using the Levelized Cost of Electricity (LCOE) and Heat (LCOH), which suggest the potential economic advantages of hybrid SMRs, as LCOE and LCOH calculated are in most cases lower for the hybrid reactors.

# Characterization of the performance of a hybrid Small Modular Reactor and its interaction with the power grid

Silvia Picchi[1,3,*], Walter Ambrosini[2], Andrea Pucciarelli[2], Alessandro De Angelis[2], Charly Boudot[3], Lorenzo Longo[3]

[1] Università di Pisa, DESTEC, Largo Lucio Lazzarino, 56122 Pisa, Italy, [2] Università di Pisa, DICI, Largo Lucio Lazzarino, 56122 Pisa, Italy, [3] CEA, DES, IRESNE, DER, 13108 Saint Paul lez Durance, France, * s.picchi12@studenti.unipi.it

## Introduction

Hybrid energy systems incorporating **Small Modular Reactors (SMRs)** represent a promising nuclear technology which allows the combined production of heat and power. This increases the flexibility of nuclear plants and opens new possibilities for the decarbonization of energy production.
This MSc thesis work proposes to assess the **benefits of the hybridization** of a Light-Water SMR during a frequency regulation transient and to evaluate its **economic feasibility**. The division between the electrical and thermal outputs of the power plant is expressed by the **Degree of Hybridization (DOH)**, defined as the ratio between the thermal power output and the thermal power exchanged at the steam generator: $DOH = \dot{Q}_{th}/\dot{Q}_{SG}$.

## Simulations Setup

The hybrid secondary loop of the SMR has been designed based on E-SMR dataset (thermal/electrical outputs: 270 MWth/115 MWe, DOH = 50%) and modeled using Dymola 24x and libraries TANDEM and ThermoPower.

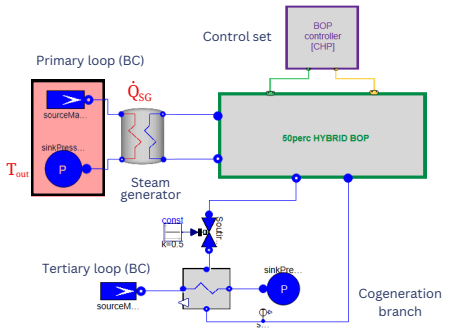


To evaluate the impact of grid disturbances on the plant, two software are used in **chaining**: PowerFactory, to model and simulate electrical systems, and Dymola, for the thermal-hydraulics of the plant.

The study compares DOH = 0% and 50% during a primary frequency regulation transient. The DOH = 50% is analyzed for three **different control scenarios**, differing for the control action on the valve of the cogeneration branch.

## Results of the Technical Analysis

Comparison of the impact of the primary frequency regulation transient for the non-hybrid plant (DOH = 0%) and hybrid plant (DOH = 50%) on the boundary conditions of the steam generator.

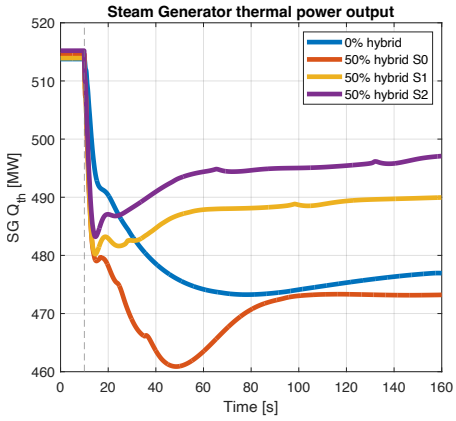


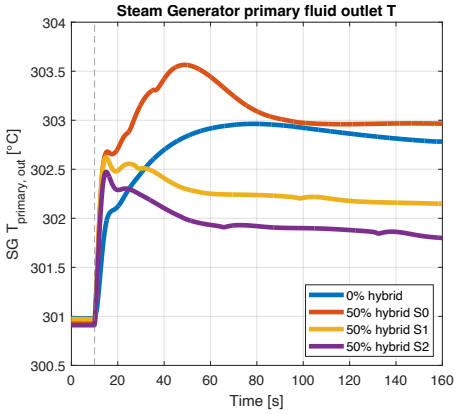


Types of PI control on cogeneration branch:

| | Description | Scheme |
|---|---|---|
| **S0** | No control | PI |
| **S1** | Control of $\dot{Q}_{th}$ | PI |
| **S2** | Contributes to control of $P_m$ | PI |

Overall variation of the primary fluid outlet temperature during the transient:

**SG primary fluid outlet T [°C]**

| Case | | Initial | Final | Δ |
|---|---|---|---|---|
| 0% hybrid | | 301.0 | 302.8 | 1.8 |
| 50% hybrid | S0 | 300.9 | 303.0 | 2.0 |
| | S1 | 301.0 | 302.1 | 1.2 |
| | S2 | 300.9 | 301.8 | 0.9 |

## Results of the Economic Analysis

The economic study proposes a methodology to **estimate** the **Overnight Capital Cost (OCC)** of LW-SMRs at preliminary design stage and evaluates the economic competitiveness of cogenerative designs compared to single-output (full-electrical and full-thermal) configurations.
The proposed approach for OCC estimation is based on equipment and labor costs available in the EEDB, open literature and textbooks. To compare whether it is more convenient to invest in a cogenerative or in a single-output reactor, the Levelized Cost of Electricity (LCOE) and Heat (LCOH) are compared, using the **cost allocation method** with three different approaches.

**Levelized Cost of Electricity**

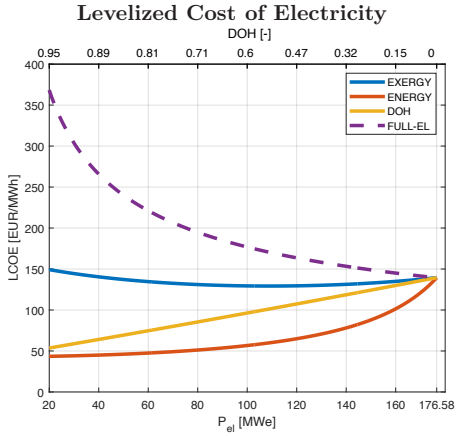


**Levelized Cost of Heat**

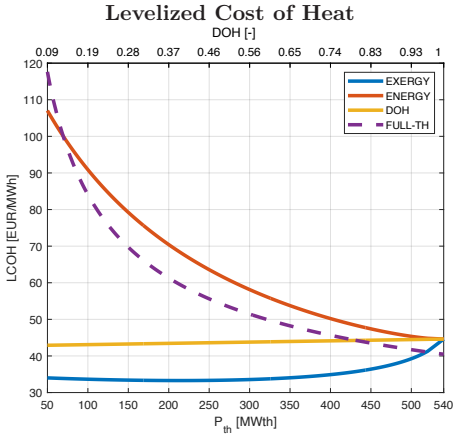


$$Levelized\ Cost\ of\ X = \frac{\sum_{t=0}^{T}(CAPEX_t + OPEX_t + Fuel_t + Decommissioning_t)/(1+r)^t}{\sum_{t=0}^{T} energy_x/(1+r)^t}$$

## Conclusions and Future Work

The technical results show that cogeneration can increase the flexibility of utilization of the plant, contributing to **decrease the impact** on the **primary loop**, when **appropriate control strategies** are implemented. The economic analysis suggests the **convenience of hybrid plants** in most cases investigated.

The simulation setup can be improved by adding a full model of the primary loop. Technoeconomic evaluations should focus first on defining standard datasets and approaches.

## References and Acknowledgements

**References:**

[1] C. Boudot, "*Methodologie d'etude de l'integration de SMR dans des reseaux electriques dans le cadre de la transition energetique*". PhD thesis, Université Grenoble Alpes (2023)
[2] G. Simonini "Modelica models description for the 'TANDEM' Library" (2024)
[3] G. Maronati, "Assessing I2S-LWR economic competitiveness using systematic differential capital cost evaluation methodology" (2020)
[4] Oak Ridge National Laboratory and United Engineers & Constructors Inc. - EEDB Technical Reference Book (1987)
[5] M. Noussan, "Allocation factors in Combined Heat and Power systems – Comparison of different methods in real applications" (2018)

**Acknowledgements:** the work presented has been completed thanks to a collaboration between the University of Pisa and CEA Cadarache.

Co-funded by the European Union

# LIQUID METAL FLOW IN A MAGNETIC FIELD ENVIRONMENT

Aleš PROCHÁZKA

*Czech Technical University in Prague, Czech Republic*

This poster is based on a thesis that investigates the design, construction and experimental validation of a DC magnetohydrodynamic (MHD) pump for liquid metal applications. The work includes: (1) a comprehensive review of liquid metal uses in nuclear energy systems, particularly in fast reactors and fusion devices; (2) theoretical analysis of fundamental MHD phenomena and pumping principles; (3) experimental testing with galinstan (GaInSn alloy) as the working fluid; (4) analytical computation and numerical modeling using ANSYS software suite. The study compares three methodological approaches analytical calculations, numerical simulations, and physical experiments all of which confirm the linear relationship between applied current and generated pressure head. The results demonstrate strong correlation between theoretical predictions and experimental data, with deviations attributable to model simplifications and measurement constraints. The research provides insights into MHD pumping technology and its potential applications in advanced nuclear systems.

# Liquid Metal Flow in a Magnetic Field Environment

Aleš Procházka, Master's Thesis Poster, 2025
Supervisor: doc. Ing. Pavel Zácha, Ph.D.; Ing. Jan Štěpánek, Ph.D.

*Faculty of Mechanical Engineering, Technická 4, 160 00 Prague, Czech Republic*
*Czech Technical University in Prague*
*ales.prochazka@fs.cvut.cz, ales-prochazka@seznam.cz*

CTU CZECH TECHNICAL UNIVERSITY IN PRAGUE

## Introduction

Magnetohydrodynamics (MHD) deals with the behavior of conductive fluid flow in the presence of an electromagnetic field. The conductive medium can typically be plasma, molten salts, or liquid metals. In proposed thermonuclear power plants with tokamaks, a very strong magnetic field will be maintained. Some concepts of fusion energy reactors include the presence of a PbLi liquid alloy blanket, which ensures the production of tritium, an essential component of the fuel for the fusion reaction. The liquid metal, being conductive, interacts with the magnetic field, which can lead to various magnetohydrodynamic (MHD) effects. Therefore, the study of liquid metal flow behavior in a magnetic field environment is part of fusion technology research and development.

Furthermore, MHD effects have also been utilized in operated fast breeder reactors cooled by liquid metals, such as sodium and its alloys, for pumping the coolant. With ongoing research into 4th-generation reactors and the advent of new SMR concepts, MHD pumping continues to be explored and considered as an alternative to traditional mechanical pumps.

## Main Objectives

The main objectives of the work are:

1. **design, construction, and measurements on an experimental device** using the liquid metal galinstan and leveraging MHD effects;
2. **numerical simulation** of the performed experimental measurements;
3. **validation and comparison** of the numerical solution with experimental data and a simplified analytical solution.

The experimental setup was realized as a U-tube with an MHD pump, where the pump's head was measured as the difference in liquid levels in the individual branches of the U-tube. The numerical simulation was performed using computational software from the ANSYS suite.

## Experimental Setup and Methodology

The body of the MHD pump consists of a 3D-printed plastic glued assembly. The side walls of the pump's flow channel are formed by copper electrodes, to which an electric current in the range of 10 – 40 A is supplied in 5 A increments. Permanent magnets are placed above and below the channel, providing a magnetic field with an average magnetic induction of 0.6 T. The pump is then connected to the branches of the U-tube via feedthroughs. The U-tube is composed of silicone hoses and glass tubes The principle of MHD pumping lies in the generation of the Lorentz force (see Figs. 1 and 2). The working fluid is the alloy galinstan.

The magnetic field was simulated after the experiment using ANSYS Electronics Desktop (Maxwell module), and the problem of liquid level motion was defined in ANSYS Fluent. The calculation was run using the ANSYS System Coupling utility, which allows linking separate parts of the computation.

The analytical calculation was performed using the equivalent electrical circuit method, and the difference in liquid levels was obtained from the equality of the pressure generated by the pump and the hydrostatic pressure. Results are summarized in Tab. 1 and Fig 4.

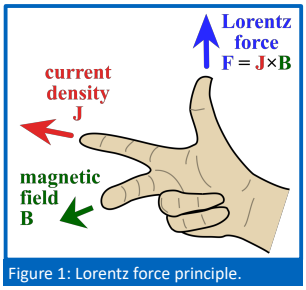

Figure 1: Lorentz force principle.

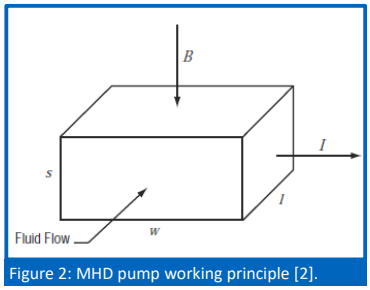

Figure 2: MHD pump working principle [2].

The experimental setup is shown in Fig. 3. While galinstan remains liquid at ambient conditions, its strong tendency to oxidize and adhere to surfaces made measurements particularly challenging. The oxide layer formation and wall wetting effects introduced significant uncertainties in liquid level determination..

**Experiment Components:**

1. MHD pump with copper electrodes and permanent magnets,
2. silicone tube,
3. silicone-glass transition, piece
4. glass tube.

**Galinstan Properties:**

$T_{melt}$ = -19 °C,

$T_{vap}$ > 1300 °C,

ρ = 6440 kg/m$^3$,

σ = 3.46*10$^6$ S/m,

μ = 2.4*10$^{-3}$ Pa·s,

λ = 16.5 W/(m·K).

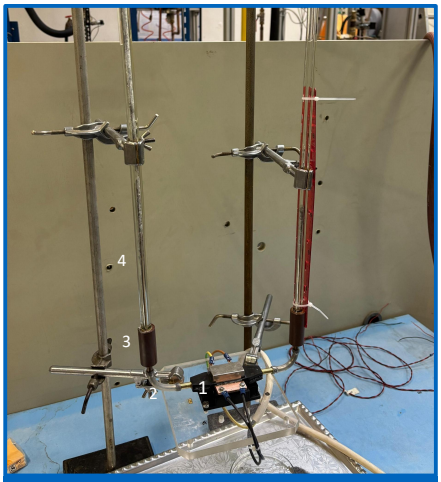

Figure 3: Experimental U-tube

## Results

The experimental measurements, analytical and numerical calculations all demonstrate a consistent increasing trend in level difference with higher electric currents. The experimental values were consistently lower than calculated values.

| Electric current [A] | 10 | 15 | 20 | 25 | 30 | 35 | 40 |
|---|---|---|---|---|---|---|---|
| **Level difference [mm]** | | | | | | | |
| Experiment | 22 | 42 | 50 | 60 | 72 | 86 | 108 |
| Analytical calculation | 28.78 | 43.17 | 57.56 | 71.95 | 86.34 | 100.73 | 115.12 |
| Numerical calculation | 26.62 | 43.02 | 53.87 | 67.55 | 80.68 | 93.99 | 109.07 |

Table 1: Comparison of resulting level differences for various electric current values.

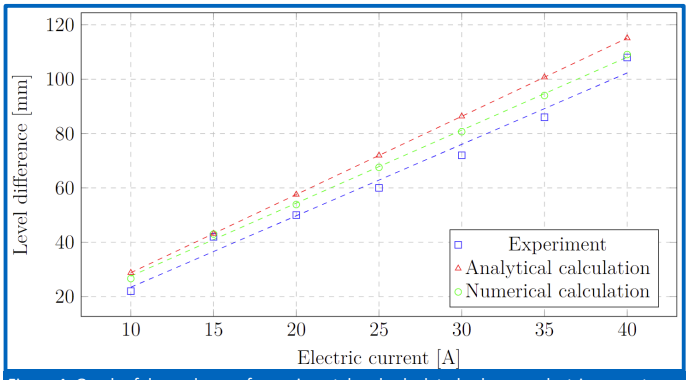

Figure 4: Graph of dependence of experimental and calculated values on electric current.

## Conclusion

The discrepancies between experimental, analytical, and numerical results may arise from:

1. **geometric simplifications** and **field inhomogeneity** (non-uniform B and I distributions);
2. **unaccounted losses** (oxidation, contact resistance, micro-scale imperfections) and **material property variations** (galinstan conductivity, magnet deviations);
3. **numerical limitations** (mesh discretization, solver approximations) that underestimate real-world complexities.

While trends align, quantitative differences highlight the need for refined models that better capture geometric, material, and loss effects in MHD systems. Nevertheless, this study successfully demonstrated magnetohydrodynamic pumping using galinstan in a U-tube configuration, validating the fundamental principles of MHD flow.

## References

[1] XIANG, Liujin; YANG, Shuo; WANG, Qi; WU, Jian. Design and testing of a direct-current electromagnetic pump for liquid metal. *Thermal Science and Engineering Progress*. 2024, vol. 50, p. 102560. ISSN 2451-9049. Available at: https://doi.org/10.1016/j.tsep.2024.102560.

[2] POLZIN, Kurt A. *Liquid-Metal Pump Technologies for Nuclear Surface Power*. 2007. Technical report. Also available at: https://ntrs.nasa.gov/citations/20070022272.



Scan to read more:

# EXPERIMENTAL AND COMPUTATIONAL MODELING OF FUEL CLADDING UNDER LOSS OF COOLANT ACCIDENT CONDITIONS

Michaela SVATOŠOVÁ

*Czech Technical University in Prague, Czech Republic*

In this work, high-temperature creep experiments were conducted on fuel cladding samples with a chromium protective coating and reference uncoated samples. Based on the experimental data, constitutive equations were developed for describing the cladding deformation behavior, including the primary, secondary, and ballooning stage, which is associated with significant dimensional changes. These equations were subsequently implemented into the TRANSURANUS fuel performance code. Simulations reproducing the conducted high-temperature creep experiments were carried out using the modified code. The results indicate that the new model provides a reasonably accurate prediction of time to burst; however, it tends to underestimate the maximum deformation observed in the experiments.

# Experimental and Computational Modeling of Fuel Cladding under Loss of Coolant Accident Conditions

**M. Svatošová[1,2], J. Krejčí[1], M. Ševeček[2]**

[1] UJP PRAHA a.s., Nad Kamínkou 1345, 156 10 Praha – Zbraslav, Czech Republic
[2] Faculty of Nuclear Sciences and Physical Engineering, Czech Technical University in Prague, V Holešovičkách 2, 180 00 Praha 8, Czech Republic

## 1. Introduction

Loss-of-coolant accident poses a significant risk for nuclear fuel cladding in pressurized water reactors. Due to **high temperatures**, caused by the loss of heat removal, and **high fuel rod pressure**, not compensated by the coolant pressure, the fuel claddings experiences **thermal creep**. Creep, i.e. **plastic deformation** dependent on time, then causes ballooning and may lead to a burst (failure) of the cladding. Nowadays a lot of research is being done on Accident Tolerant Fuels (ATF), such as chromium coated fuel cladding. [1–3]

This work focused on modelling the **three distinct stages** of creep (primary, secondary and tertiary, shown in Fig. 1 [4]). Fuel performance codes usually calculate deformation only for the secondary stage and have limited options for calculating **ballooning** (large deformation around the center of the cladding). Therefore, a new methodology for high temperature creep experiments has been implemented for studying creep in nuclear fuel cladding samples. The data acquired from those experiments then served as the basis for **new correlations**, which were then implemented into the TRANSURANUS code. A series of calculations with this modified code was run and the results were compared with experimental data.

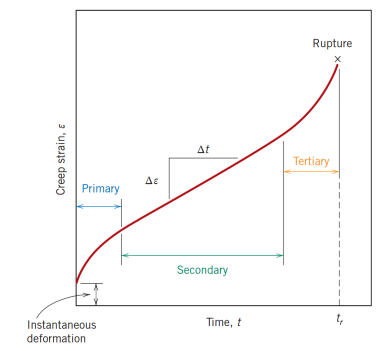


*Fig. 1: The three stages of creep [4]*

## 2. Experimental

**2.1 Materials**

- ❑ Reference uncoated Zr alloy samples
- ❑ Cr coated samples (17 μm coating layer)

**2.2 Methods – internal pressure high temperature creep tests**

- ❑ Isothermal tests at temperatures ranging from 600 °C to 1050 °C
- ❑ The samples were **heated and then pressurized** with argon
- ❑ Immediately after pressurization a valve in the proximity of the sample was closed (shown in Fig. 2)
- ❑ The amount of gas in the system was then limited and as the sample expanded (deformed), the **pressure inside decreased** (as in Fig. 3)
- ❑ Each test lasted until the failure of the sample
- ❑ After the tests, the samples were measured in diameter in different places to evaluate their deformation

*Fig. 2: Sample (left) before burst test (a valve can be seen at the top right)*

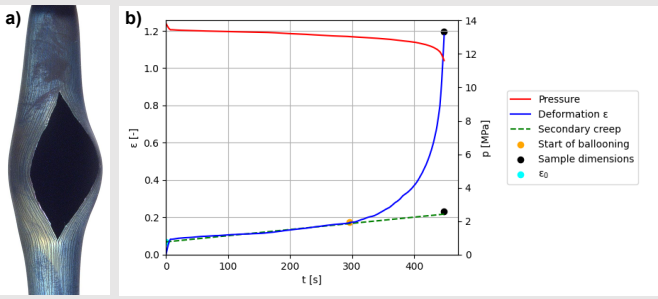


*Fig. 3: a) Cr coated sample after burst test, b) data acquired from the experiment*

**Acknowledgements:** *Financial support of this research through the grant no. TK04030168 of the Technology agency of the Czech republic is gratefully acknowledged. A portion of the samples were provided by grant IAEA CRP 2236. The author would like to thank A. Prítrský for his assistance in conducting experiments and in evaluating the data.*

## 3. Results and discussion

**3.1 Results of burst tests**

The pressure drop during the experiment (which can be seen in Fig. 3b) allowed for the calculation of the sample volume, its **deformation**, creep rate and in the tertiary stage the balloon size and shape (where it was assumed that the sample has the axial profile similar to a Gaussian bell function). The curve of deformation was divided into the three creep stages. The values for deformation at the end of primary stage ($\varepsilon_0$ in Fig. 3b), creep rate, deformation at the beginning of the tertiary stage and the shape of the balloon were processed and a **linear regression** was made for determining the dependency of these quantities on hoop stress in the cladding (for the creep rate the values were in logarithmic form, as in Fig. 4) and temperature. This way, a set of correlations was made both for Cr coated samples and for bare Zr alloy samples for the **α and β phases** of zirconium (the transition α→β occurs at around 860 °C [1]).

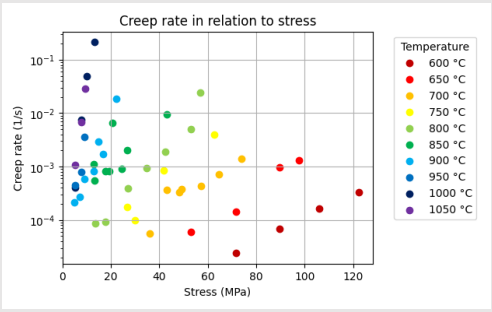


*Fig. 4: Creep rate in relation to hoop stress in the sample for different temperatures (bare Zr alloy samples)*

**3.2 Results of calculations**

The correlations were inserted into the TRANSURANUS fuel performance code and a series of calculations was done, each simulating one of the conducted experiments. The time to burst (for failure criterion no. 1 in the code – overstress) is shown in Fig. 5. **For lower temperatures there is a good match between the experiments and calculations**. However, for 850 and 900 °C the simulations lead to a much lower time to burst than experiments. This is because zirconium in the mixed α+β phase has a **different creep behavior**, is very plastic and tends to have larger deformations. For Cr coated samples, the results of calculations were most accurate in lower stresses. When comparing the maximal deformation in the balloon, the calculations are most **accurate for high temperatures**. For lower temperatures, the calculations lead to smaller deformations. This means that the ballooning deformation model needs to be improved, especially for the α and mixed α+β phase regions.

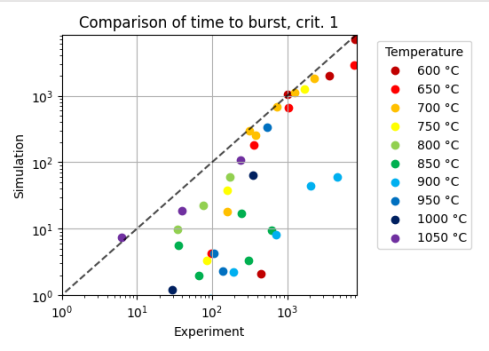


*Fig. 5: A comparison of time to burst in experiments and calculations (bare Zr alloy samples)*

## 4. Conclusions

Experiments to study the creep behavior of zirconium alloys were conducted. The deformation of the samples was determined, and the three stages of creep were identified. Based on those results a series of correlations were derived and inserted into fuel performance code. Then the code was used for simulating the experiments. Time to burst was predicted very well for lower temperatures, maximal deformation was best for high temperatures. However, the α+β phase needs further attention.

## References

[1] K. Pettersson et al., "Nuclear Fuel Behaviour in Loss-of-coolant Accident (LOCA) Conditions," OECD Nuclear Energy Agency (NEA), Paris, 2009. NEA No.6846, ISBN 978-92-64-99091-3
[2] "State-of-the-Art Report on Light Water Reactor Accident-Tolerant Fuels," Nuclear Energy Agency, Oct. 2018. doi: 10.1787/9789264308343-en.
[3] K. A. Terrani, "Accident tolerant fuel cladding development: Promise, status, and challenges," Journal of Nuclear Materials, vol. 501, pp. 13–30, Apr. 2018, doi: 10.1016/j.jnucmat.2017.12.043.
[4] CALLISTER, W. D.; RETHWISCH, D. G. Materials Science and Engineering: An Introduction, Tenth Edition. John Wiley & Sons, Incorporated, 2017. isbn 978-1-119-27856-6.

# THERMODYNAMIC CONDITIONS IN THE SAFETY DEPRESSURIZATION SYSTEM AT THE TEMELÍN NUCLEAR POWER PLANT

Petr VASTL

*University of West Bohemia in Pilsen, Czech Republic*

Today‘s nuclear renaissance relies on modern Generation III+ and SMR reactors, which place high demands on safety. As a result, there is increasing pressure to upgrade older reactors, such as the VVER-1000 at the Temelín Nuclear Power Plant. One of the planned safety improvements is a new rapid depressurization system for the primary circuit in the event of a severe core meltdown accident. This system directs steam through piping into the containment. The system is shown in Figure 1. The condensed water that fills the system is slowly cooled because of heat loss to the surroundings through the outer walls. The temperature of the water is crucial for ensuring the operability of the valves that open the system immediately at the start of a core meltdown accident. The main task is to find out the temperature in these valves and determine the thermodynamics of the designed system for four different conditions, representing four different regimes in the primary circuit (Figure 2). This study is focused on obtaining values of temperatures from thermodynamics simulations from the CFD software Ansys Fluent.

# Thermodynamic conditions in the safety depressurization system at the Temelín Nuclear Power Plant

**Author:** Petr Vastl [1,2], **Supervisor:** Doc. Ing. Petr Eret [1], Ph.D., Ing. Petr Klavík [2], Ph.D., Ing. Václav Novotný [2]

[1.] University of West Bohemia, Faculty of Mechanical Engineering, Department of Design of Power Machines and Equipment, Univerzitní 22, 301 00 Pilsen
[2.] Škoda JS a.s., Orlík 266/15, Bolevec, 31600 Plzeň

## INTRODUCTION

Today's nuclear renaissance relies on modern Generation III+ and SMR reactors, which place high demands on safety. As a result, there is increasing pressure to upgrade older reactors, such as the VVER-1000 at the Temelín Nuclear Power Plant. One of the planned safety improvements is a new rapid depressurization system for the primary circuit in the event of a severe core meltdown accident. This system directs steam through piping into the containment.

The system is shown in Figure 1. The condensed water that fills the system is slowly cooled because of heat loss to the surroundings through the outer walls. The temperature of the water is crucial for ensuring the operability of the valves that open the system immediately at the start of a core meltdown accident. The main task is to find out the temperature in these valves and determine the thermodynamics of the designed system for four different conditions, representing four different regimes in the primary circuit (Figure 2).

This study is focused on obtaining values of temperatures from thermodynamics simulations from the CFD software Ansys Fluent.

| | Operating pressure (MPa) | Operating temperature (°C) | The water level in the pressurizer (mm) |
|---|---|---|---|
| NPP1 (normal regime) | 15.7 | 345.8 | 8170 |
| NPP2 (normal regime) | 15.7 | 345.8 | 9042 |
| HP1 (immediately before the valve's opening) | 17 | 352.3 | 11555 |
| NNPP (opening of the second relief valve on the top of pressurizer) | 18.1 | 357.4 | 10780 |

*Figure 2 – Table of considered operating regimes*

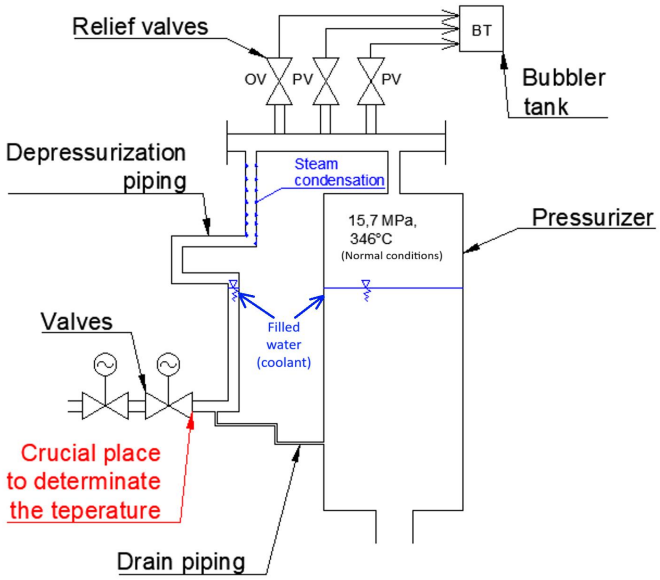


*Figure 1 – Scheme of the new rapid depressurization system connecting the pressurizer*

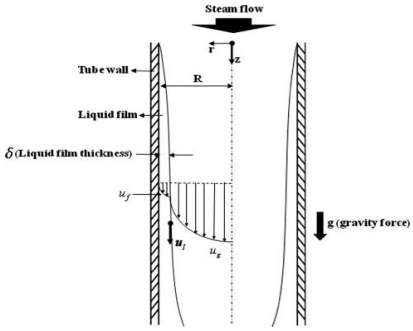


*Figure 3 – Film condensation on the inner surfaces of vertical pipes [3]*

## CONDENSATION

The amount of condensed steam on the inner surface of the depressurization piping has an impact on the difference between water (coolant) levels in the piping and in the pressurizer. The level difference ensures a slow flow of filled coolant in the depressurization piping, causing the mixing of hotter condensed steam, and it leads to a slight heating of the filled water. The coolant slowly flows through the drain piping back to the pressurizer. The temperature in the valves cannot be lower than 100 °C during normal operating regimes and lower than 120 °C before the core meltdown accident. If the temperature falls below 120°C, then the valves could fail during opening because of the thermal shock of the steam that hits the valves.

The condensation is calculated from Nusselt's theory of film condensation (Figure 3). Condensation is strongly dependent on the type of regime and on the vapor humidity conditions in the pressurizer. Based on that, it was decided to calculate more condensation conditions. The results are input conditions for the CFD simulations as a flow mass through the depressurization piping.

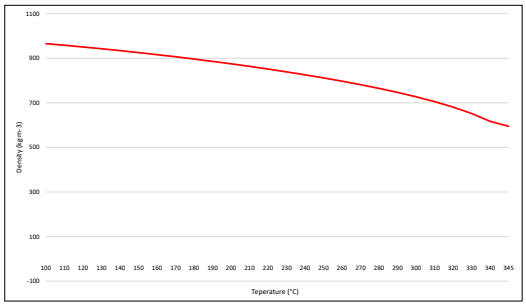


*Figure 4 – The density change depending on temperature for conditions in pressurizer*

## SIMULATIONS

Cooling has a significant effect on water properties as density (Figure 4), thermal conductivity, viscosity, and heat capacity. Simulations include the effect of gravity and these changes in the properties of water, too. Simulations run stationary.

The CFD results show slow flow and relatively significant cooling of filled water. The largest cooling occurs for the regime NPP2, which is shown in Figure 5. The valves remove a lot of heat from filled water, causing acceleration of the flow (Figures 6 and 7). Warmer water flows along the inner upper part of the pipe and, after cooling, turns and flows into the drain pipe.

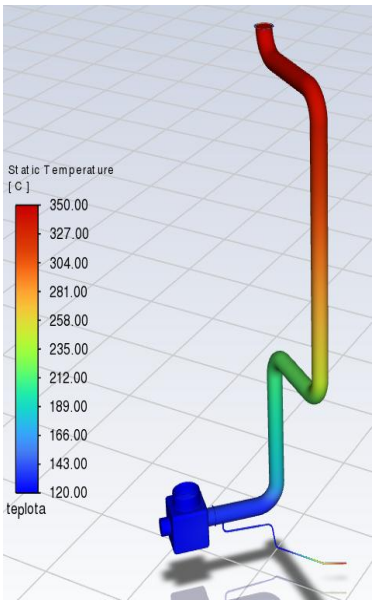


*Figure 5 – The temperature distribution by height of the depressurization pipe for the regime NPP2*

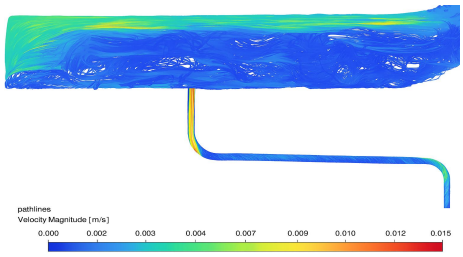


*Figure 6 – The flow velocity in front of the valves and at the entry in the drain piping*

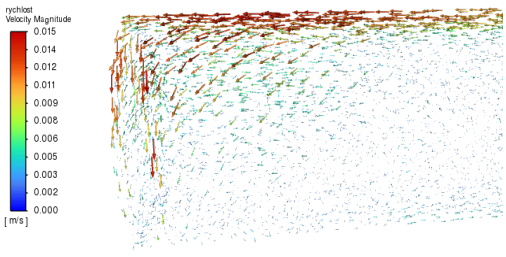


*Figure 7 – The flow velocity in front of the valves*

## RESULTS AND CONCLUSION

The temperature of each scenario for each regime is shown in Figure 8. The results of NPP1 and NPP2 regimes under normal conditions meet the temperature limit of over 120 °C that is set by rules for the primary circuit. The density difference between the coolant level and the drain piping is about 180 kg/m³ for the lowest mass flows during NPP1 and NPP2. Unfortunately, the results for the regimes NNPP, HP1 and the lowest mass flows are hard to determine. The CFD programme Ansys Fluent works with gradients of units (speed, density, ...), and for these mass flows, the gradients are probably so small that the simulations run for a very long time (weeks), and it is complicated to stabilize them. Calculations would be better to run in some different software, probably.

| NPP1 | |
|---|---|
| Mass flow (kg/s) | Temperature in the first valve (°C) |
| 0.0009 | **170** |
| 0.005 | **311.5** |
| 0.01 | **326** |
| 0.1 | **339** |

| NPP2 | |
|---|---|
| Mass flow (kg/s) | Temperature in the first valve (°C) |
| 0.0007 | **132** |
| 0.005 | **301** |
| 0.01 | **321** |
| 0.1 | **339** |

| NNPP | |
|---|---|
| Mass flow (kg/s) | Temperature in the first valve (°C) |
| 0.0004 | |
| 0.005 | **305** |
| 0.01 | **330** |
| 0.1 | **350** |

| HP1 | |
|---|---|
| Mass flow (kg/s) | Temperature in the first valve (°C) |
| 0.0003 | |
| 0.005 | **290** |
| 0.01 | **319** |
| 0.1 | **344** |

*Figure 8 – The temperature in the valves for the considered operating scenarios*

[3.] KIM, Dong Eok et al. Pure steam condensation model with laminar film in a vertical tube. *International Journal of Multiphase Flow*. 2011, roč. 37, č. 8. DOI: https://doi.org/10.1016/j.ijmultiphaseflow.2011.04.006

# CONDUCTING TECHNOLOGICAL TESTS DURING THE POWER STARTUP OF THE DUKOVANY POWER PLANT

Vít VESELÝ

*Brno University of Technology, Czech Republic*

The reactor start-up process includes process tests performed as part of the power start-up, which verify the correct functioning of all key equipment and systems. The tests include checking the stability of parameters, the correctness of control functions and verifying that the equipment is ready for real operation.

VYSOKÉ UČENÍ TECHNICKÉ V BRNĚ
FAKULTA ELEKTROTECHNIKY A KOMUNIKAČNÍCH TECHNOLOGIÍ

Nuclear Days 2025
Student Poster Competition

# CONDUCTING TECHNOLOGICAL TESTS DURING THE POWER STARTUP OF THE DUKOVANY POWER PLANT

Bc. Vít Veselý[1], Ing. Peter Mičian[1], Ing. Pavel Vrbka[2]

[1] Deptartment of Electrical Power Engineering, Faculty of Electrical Engineering and Communication, Brno University of Technology, Technicka 3058/10, Brno, 616 00, Czech Republic
[2] Dukovany Nuclear Power Plant, CEZ, a. s., Czech Republic

## Introduction

The reactor star-up process includes process tests performed as part of the power start-up, which verify the correct funcitoning of all key equipment and systems. The tests include checking the stablity of parameters, the correctness of control funcitons and verifying that the equipment is ready for real operation.

## Main goals of study

At the Dukovany Nuclear Power Plant, the EDUS program has been developed for simulations of this kind. This study verified the correct functionality of EDUS and highlighted its shortcomings. Once these are corrected, EDUS could be actively used as a support program in the testing of individual devices.

## Tested systems

1) Reactor control system (RCS)
2) Transfer station to the atmosphere (PSA)
3) Transfer station to the condenser (PSK)
4) Turbine control system (RST)

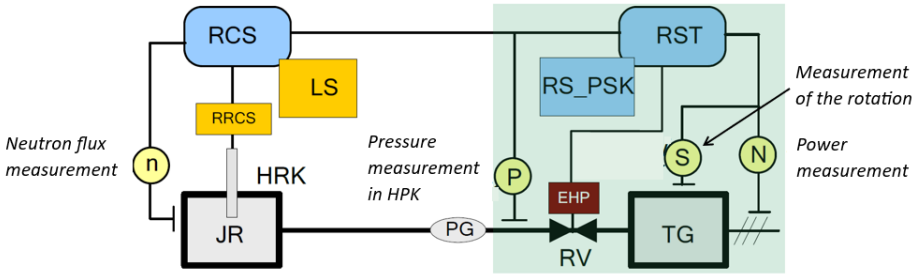


The figure shows a schematic diagram of the automatic power control system of the power unit and the links between the individual control modules.

## Example test of PSA regulation

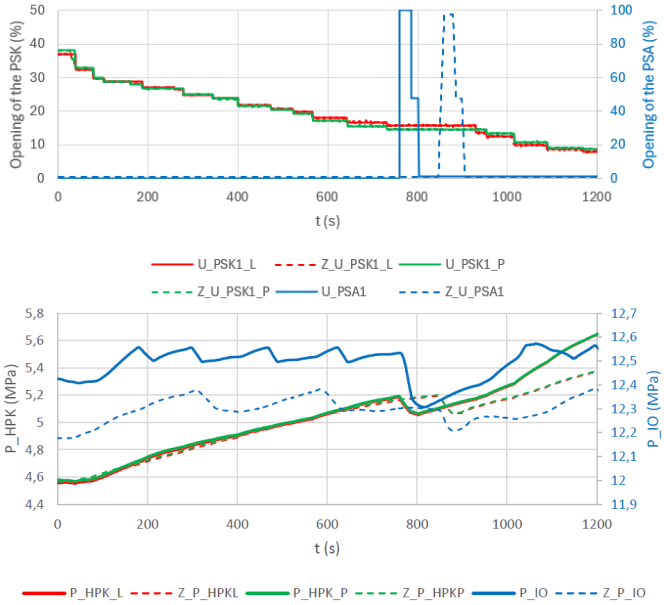


From all ten tests, that were studied and conducted, only this one is presented here as an example.

The graphs compare the results of the real and simulated PSA regulation test. In the results of this test, we can see two shortcomings of the EDUS simulator. In the bottom graph, it can be observed that the measured and simulated HPK pressure values do not match even with the same PSK opening in the top figure. The mismatch is most pronounced from about 1025 s, when the simulated values start to rise for no reason. As a result of the earlier increase in HPK pressure to 5.2 MPa, the PSA opens correctly in automatic mode about 100 s earlier. However, the second inconsistency is the lack of automatic opening of the PSA in manual mode, which can be seen in the top figure when the HPK pressure rises above 5.4 MPa, at a time of approximately 1075 s.

## Legend

- U_PSK1_L (_P) – Opening of PSK1, left (or right) side HPK
- U_PSK2_L (_P) – Opening of PSK2, left (or right) side HPK
- U_PSA1 – Opening of PSA1
- P_HPH_L (_P) – Pressure in the cooling steam collector
- P_IO – Pressure in the primary circuit
- The index „Z_" before the shortcut means the measured values

## Study results

The individual monitored parameters were described and compared in detail and the following deficiencies were found.

- The simulator automatically miscalculates the reactor power when the turbine-generator is selected to enter the initial state.
- The simulator does not take into account the input of the initial state of the controller in the initial conditions.
- In the simulator, in contrast to reality, there is no automatic 5,4 MPa (PSA opening in manual mode).
- There is no interlock in the simulator when the HPK pressure drops below 4,15 MPa (automatic PSK closure).
- Some constants in the simulator are fixed at 100 % power level and have to be adjusted at lower power level.
- The flow characteristics of some valves are not precisely tuned (set to the average between blocks).
- Δp1 and Δp2 cannot be adjusted during the simulation, they can only be adjusted for the whole simulation.
- When the controller switched from one mode to another, the previous mode had to be switched off and only then the new mode switched on.

## Conclusion

This study verified the correct functionality of EDUS and highlighted its shortcomings that could be corrected. After correction, the EDUS could verify the operating assumptions without testing in real operation and thus increase the efficiency of the tests performed during start-up and operation of the reactor. The study could serve as supporting educational material for training reactor physicists, providing an initial introduction to tests on selected equipment. This introduction would provide basic knowledge for tests that are then actually performed at EDU.

[1] BOHÚN, Pavel. *Vstupní školení do Jaderné elektrárny Dukovany.* 2016. Dukovany: ČEZ, a. s., Periodická příprava a příprava dodavatelů JE. Dostupné z: https://www.cez.cz/edee/content/file/vzdelavani/skoleni/skripta-2016.pdf. [cit. 2024-10-31].
[2] Kolektiv autorů. (2022), učební texty pro přípravu personálu JE. *PROVOZNÍ PŘEDPIS, Technologické testy vybraných zařízení bloku*. JE Dukovany.

# SIMULATION OF TEMPERATURE EVOLUTION DURING DEPARTURE FROM NUCLEATE BOILING INDUCED BY ELECTRIC ARC HEATING

Petr VNENK

*Brno University of Technology, Czech Republic*

This part of the study presents a method for simulating departure from nucleate boiling (DNB) using an electric arc heating device, with temperature measured by thermocouple sensors. The system enables fast and repeatable local heating, reaching temperatures of up to 400 °C. Both AC and DC arc modes were tested, with AC showing better stability. Temperature data were collected and processed using the MeThOp software. The method proved suitable for evaluating thermal sensor response, and comparison with reference data confirmed that the arc-based approach is effective for simplified DNB simulation.

BRNO UNIVERSITY OF TECHNOLOGY
FACULTY OF ELECTRICAL ENGINEERING AND COMMUNICATION

# Simulation of temperature evolution during departure from nucleate boiling induced by electric arc heating.

**Petr Vnenk**[a], Supervisor: **Stepan Foral**[a], Co-Supervisors: **Michal Krbal**[a], **Petr Dejdar**[b]

[a] Department of Electrical Power Engineering, Faculty of Electrical Engineering and Communication, Brno University of Technology, Czech Republic
[b] Department of Telecommunications, Faculty of Electrical Engineering and Communication, Brno University of Technology, Czech Republic

## Introduction

The simulation of Departure from Nucleate Boiling (DNB) using electric arc heating offers the advantage of high repeatability. It enables reliable testing of various types of sensors potentially used for DNB detection.

## Measurement setup

For experiments, an electric arc heating device is used which is shown in Fig. 1. It can reach temperatures of up to 400 °C within 10 seconds and is compatible with any sensor that fits into a tube with 8.5 mm inner diameter.

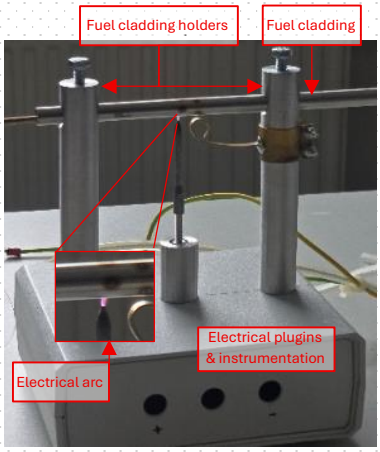


Fig. 1: Electric arc heating device

The arc device is connected to a transformer, which is linked directly to a power source, as shown in Fig. 2. The measurement is carried out using sensors inserted into the fuel cladding tube (stainless steel tube is used as a surrogate of zirconium tube to reduce the costs of experiments). The data from sensor is transferred via a measurement card to the measuring unit. All data are subsequently sent to a computer, where they are collected and processed.

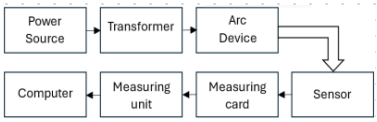


Fig. 2: Block diagram of the measurement setup

## Method assessment

The device used for arc generation is capable of operating with both altering current (AC) and direct current (DC) to ignite the electric arc. As shown in Fig. 3 and 4, DC arcs have the potential to reach higher temperatures in a shorter time. However, their ignition is less reliable compared to AC arcs.
The temperature evolution induced by the DC arc is shown in Fig. 3. The data clearly demonstrate the inconsistency of the cladding temperature induced by DC arc. Fig. 4 illustrates then the temperature evolution induced by AC arc heating, which shows significantly better stability compared to DC arc heating. Although the AC arc does not induce the same peak temperatures as DC arc, its consistency makes it more suitable for application in temperature sensor testing.

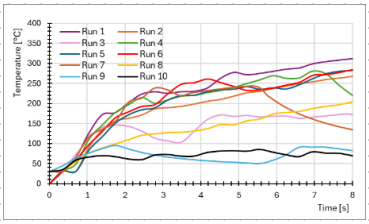


Fig. 3: Cladding temperature induced by DC arc

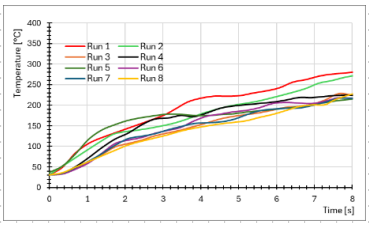


Fig. 4: Cladding temperature induced by AC arc

## Measurement program

For visualization and measurement purposes, the METHOS program (MEasurement with THermocouples and Other Sensors) is used.
The interface of the program, developed in LabVIEW, is shown in Fig. 5. It enables starting and stopping data recording as needed and selecting the number of sensors to record simultaneously. The program's structure enables easy modification and further enhancements.

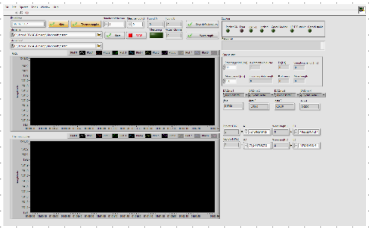

Fig. 5: Interface of METHOS program for temperature data acquisition

The measurement frequency depends on both the number and type of sensors used and a sampling time as low as 10 milliseconds can be then achieved.

## Comparison with experiments

The cladding tube temperature is compared to those presented in other studies [1, 2] as shown in Fig. 6. The temperature increase ($\Delta T=T-T_{initial}$) achieved by the arc device and stainless-steel thermocouple (ID=0.25 mm) is comparable. For reference, the blue lines represent measurements carried out in [1], where the DNB experiments were performed at electrically heated tube with internal water flow. The different positions correspond to the hottest point (position 1) and positions further from DNB occurence (positions 2 and 3). The red line represents data from [2], where a DNB experiment was performed at single pin in high-pressure loop.

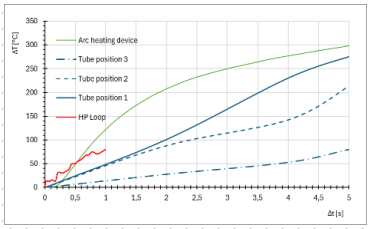


Fig. 6: Wall temperatures during DNB experiments and testing of arc device

Both reference profiles were obtained at higher initial temperatures and pressures than in the current experiment. The temperatures achieved in experiments with Arc device could potentially be even higher if a higher-voltage power source were used.

## Conclusion

Electric arc-based simulation of DNB experiments is relatively fast and allows for repeatable measurements with various sensors. After evaluating the influence of arc types, the AD arc was selected for further experiments as it is more stable and provides better repeatability. The wall temperature increase induced by arc device is comparable with that one achieved in real DNB experiments.

## References

[1] А. Молдш, К. Намыоловоки, Двухканалшыи детектор кризиса кипения и его основные измерительные характеристики, "In: Исследования критических тепловых потоков в пучках стержней, Семинар ТФ-74", Институт атомной энергии им, И.В.Курчатова, Москва 1974

[2] Augusto Moreira, Tiago; Lee, Donghwi A H. Anderson, Mark, Critical heat flux on zircaloy and accident tolerant fuel cladding under prototypical conditions of pressurized and boiling water reactors. Online. In: ScienceDirect. 2022. Available from: https://doi.org/10.1016/j.applthermaleng.2022.118740.

## Acknowledgement

Financial support of this research through the grant no. TK04030168 of the Technology agency of the Czech Republicis gratefully acknowledged.

# DOCTORAL STUDENTS

# MASS SPECTRA ANALYSIS OF IONS PRODUCED FROM NI, CA, SE AND PD OXIDE OR FLUORIDE TARGET MATERIALS BY CAESIUM SPUTTERING

Filip BABČICKÝ

*Czech Technical University in Prague, Czech Republic*

During the operation of nuclear power plants and other nuclear facilities, significant quantities of radionuclides are generated through various nuclear processes. To safeguard public health and ensure environmental protection, it is crucial to identify and quantify these radionuclides. Besides the commonly measured radionuclides like $^{137}$Cs, there exists a group known as difficult-to-measure (DTM) radionuclides, which cannot be detected effectively using standard radiometric and mass spectrometric methods alone. Determining these requires either complex chemical separation methods or advanced analytical techniques. One of them could be accelerator mass spectrometry (AMS). As well as in other mass spectrometric methods, crucial part of sample preparation and following AMS measurement is to suppress interfering isobaric nuclides. In some cases, it could be done by proper target matrix and cathode selection for caesium sputtering ion source, it is even more important for AMS with low terminal voltages. This study aims to prepare model compounds of selected elements of DTM radionuclides ($^{41}$Ca, $^{59}$Ni, $^{63}$Ni, $^{79}$Se, and $^{107}$Pd) in fluoride or oxide matrices. By mass analysis of these matrices with Tandetron 4130 MC together with background measurements on the respective cathodes, the resulting mass spectra provided insights into the possible suppression of isobaric interferences, and available chemical and ion forms.

# Mass spectra analysis of ions produced from Ni, Ca, Se and Pd oxide or fluoride target materials by caesium sputtering

Filip Babčický[1*], Mojmír Němec[1], Tomáš Prášek[1]

[1]Department of Nuclear Chemistry, Faculty of Nuclear Sciences and Physical Engineering, CTU in Prague, Czech Republi *Email: babcifil@fjfi.cvut.cz

FACULTY OF NUCLEAR SCIENCES AND PHYSICAL ENGINEERING CTU IN PRAGUE

## What is this about?

Accurate material characterization for radionuclide inventory is essential in nuclear power plant decommissioning to ensure safe waste management, environmental protection, and public safety.

A key challenge involves difficult-to-measure radionuclides like $^{41}$Ca, $^{59}$Ni, $^{63}$Ni, $^{107}$Pd, and $^{240}$Pu, which cannot be effectively analyzed with conventional radiometric methods. Advanced radioanalytical techniques, especially mass spectrometry, are required for their detection. Effective use of these methods necessitates suppressing isobaric interferences through strategies such as matrix selection and prior chemical separation.

Model target compound

Cathodes

We prepared model compounds of Ni, Co, Ca, K, Se, Br, Pd, and Ag in fluoride or oxide forms. Our goal was to find a suitable chemical matrix that would provide sufficiently high negative ion yields when sputtered by caesium ion source, while simultaneously suppressing production of the corresponding isobaric ions.

The types of ions produced for each matrix type (fluoride, oxide) were identified and the yields were subsequently estimated based on the measured ion currents.

In parallel, an initial setting was found for the determination of $^{41}$Ca by means of accelerator mass spectrometer MILEA with a maximum terminal voltage of 300 kV.

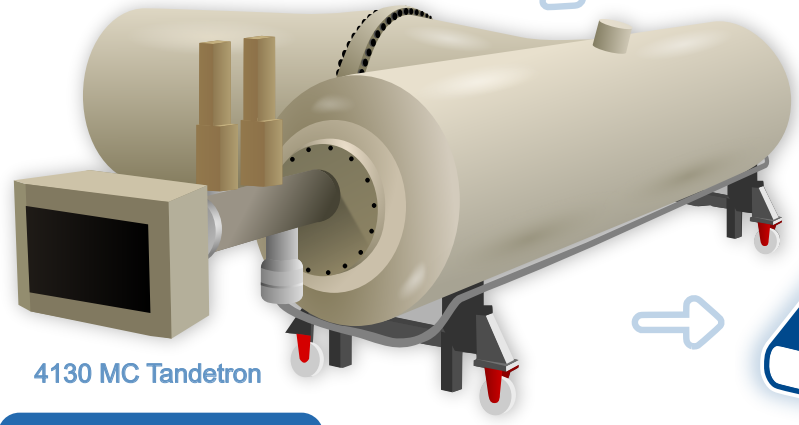

4130 MC Tandetron

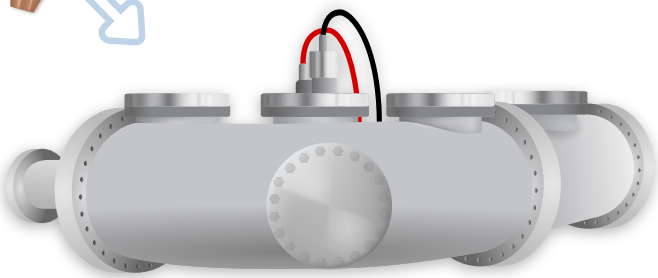

MILEA AMS


New possible analytical procedures

## What did we find out?

Based on mass spectra measurements of calcium and potassium with $PbF_2$, calcium forms relatively intense $[CaF_3]^-$ and $[CaF_4]^-$ ions as opposed to potassium. This was further utilized for finding initial beamline settings for utilizing these ions for AMS from the caesium ion source. The $^{41}$K / $^{40}$Ca ratio varies with the initial purity of reagents (ultrapure water, distilled water, tap water). For nickel and cobalt with $PbF_2$, cobalt forms similar ions to nickel but with higher intensity. Depending on the experimental conditions, it is not possible to distinguish the ionic forms of nickel from cobalt.

For selenium and bromine with $PbF_2/Eu_2O_3$, selenium peaks were less intense than bromine. In the case of measurements of palladium and its isobaric interferent silver, no significant peaks were detected as the current yields of palladium are very low. Unlike palladium, silver forms a series of intense peaks.

Dependence of isotope ratio $^{41K}/_{40Ca}$ on assumed initial purity of samples measured by MILEA AMS.

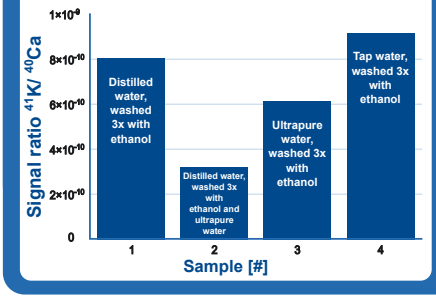


Mass spectra (current on ion mass dependence) measured via Faraday cup in low energy part of 4130 MC Tandetron. Important ionic forms are shown in green.

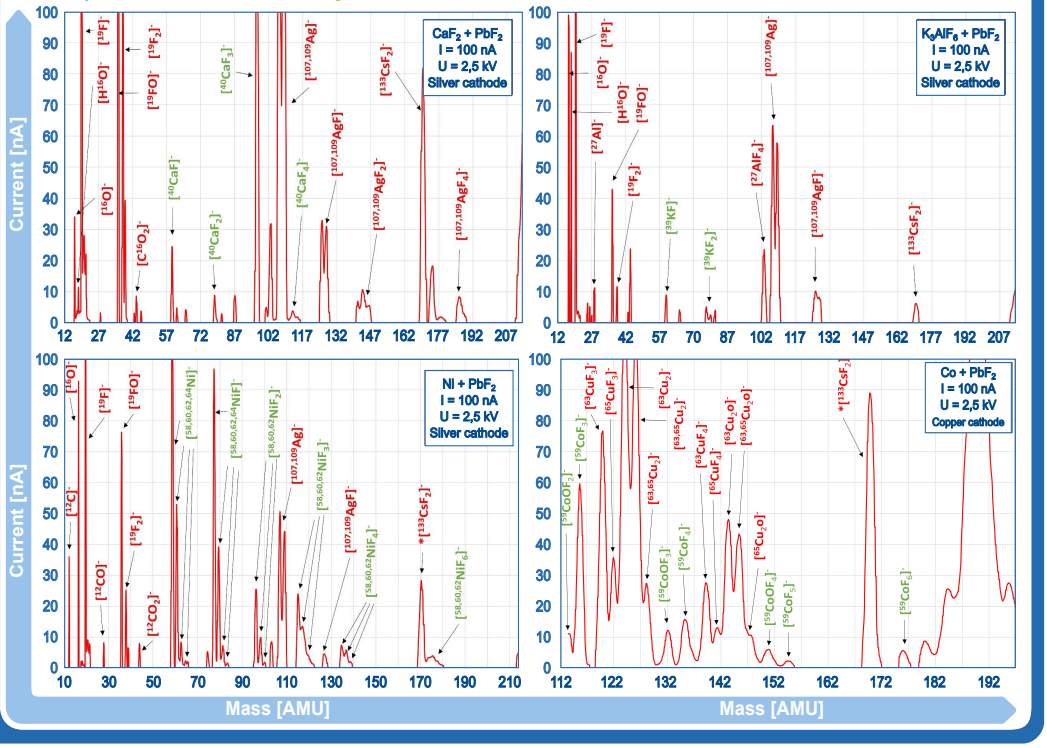


## References

Zhao, X.-L., Litherland, A. E., Eliades, J., Kieser, W. E., & Liu, Q. (2010). Studies of anions from sputtering I: Survey of. In Nuclear Instruments and Methods in Physics Research Section B: Beam Interactions with Materials and Atoms (Vol. 268, Issues 7–8, pp. 807–811). Elsevier BV. https://doi.org/10.1016/j.nimb.2009.10.036

## Acknowledgements

This work was carried out within grant project of the Predisposal management of radioactive waste (PREDIS) EU Horizon 2020 project 945098, CTU grant SGS no. SGS24/148/OHK4/3T/14 and Ultra-trace isotope research in social and environmental studies using accelerator mass spectrometry (RAMSES), No: CZ.02.1.01/0.0/0.0/16_019/0000728) supported by the Ministry of Education, Youth and Sports of the Czech Republic.

Horizon2020 European Union Funding for Research & Innovation

MINISTERSTVO ŠKOLSTVÍ, MLÁDEŽE A TĚLOVÝCHOVY

ČVUT ČESKÉ VYSOKÉ UČENÍ TECHNICKÉ V PRAZE

PREDIS

# ELECTRO- & CURRENT-LESS DEPOSITION OF NICKEL FROM LOW-CONCENTRATION AQUEOUS SOLUTIONS

Filip BABČICKÝ

*Czech Technical University in Prague, Czech Republic*

Important representatives of difficult-to-measure radionuclides include $^{59}$Ni (half-life: 7.6 × $10^4$ years, electron capture) and $^{63}$Ni (half-life: 100.2 years, $\beta^-$ decay), which are primarily produced in nuclear power plants through the (n, γ) neutron activation of stable isotopes $^{58}$Ni and $^{62}$Ni. Although the total activity of these isotopes can be high, their concentrations remain low due to their long half-lives. The aim of this work is to develop nickel separation methods from dilute aqueous solutions by means of electrodeposition combined with autocatalytic reduction using sodium phosphonate.

# Electro- & current-less deposition of nickel from low-concentration aqueous solutions

Filip Babčický[1*], Mojmír Němec[1]

[1]Department of Nuclear Chemistry, Faculty of Nuclear Sciences and Physical Engineering, CTU in Prague, Czech Republi [*]Email: babcifil@fjfi.cvut.cz

FACULTY OF NUCLEAR SCIENCES AND PHYSICAL ENGINEERING CTU IN PRAGUE

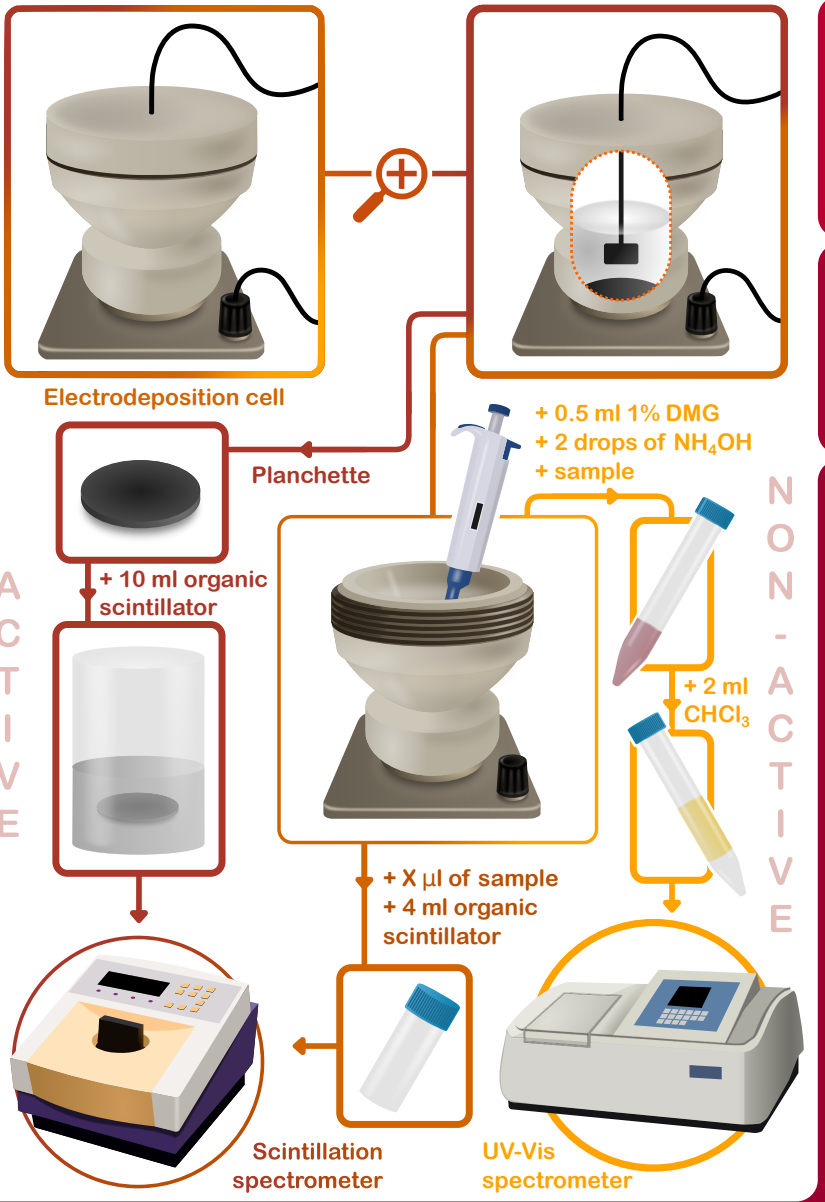


## What is this about?

Important representatives of the difficult-to-measure radionuclides are isotopes $^{59}$Ni (76 ky, EC) and $^{63}$Ni (100.2 y, -β) which are formed in nuclear power plants mainly through the neutron activation reaction (n, g) of the stable isotopes $^{58}$Ni and $^{62}$Ni. Although the total activity of these isotopes could be very high, their concentration is low due to their long half-lives. This work is therefore aimed on the development of separation procedures of nickel from low concentrated aqueous solutions by its electrodeposition together with autocatalytic reduction by sodium hypophosphite.

## What did we do?

We conducted experiments to determine how various initial parameters, such as the amount of nickel, sodium hypophosphite, applied voltage, and pH, affect the deposition yield of nickel. The electrolyte composition included boric acid (0.47 mmol·dm$^{-3}$), nickel chloride (0 to 1.03 mmol·dm$^{-3}$), and sodium hypophosphite (0.095 to 0.49 mmol·dm$^{-3}$). We optimized these parameters based on the process speed and the quality of the deposit (30 V, 0.02 to 0.06 A·cm$^{-2}$). To measure nickel concentration at different time points, we first used spectrophotometric determination with dimethylglyoxime and then confirmed our findings through an active experiment with $^{63}$Ni by liquid scintillation spectrometry.

## What did we find?

Depending on the data received, it was found that the deposition yield increases with increasing concentration of nickel cations and simultaneously with increasing concentration of sodium hypophosphite. (*see Figure 1. and 2.*)

Fig. 1: Dependence of deposition yield on different initial concentrations of added sodium hypophosphite.

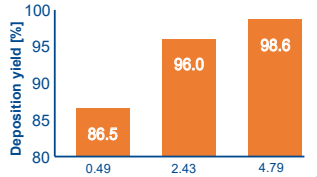


Fig. 2: Dependence of self-absorption and deposition yield on concentration of added nickel carrier after 75 minutes.

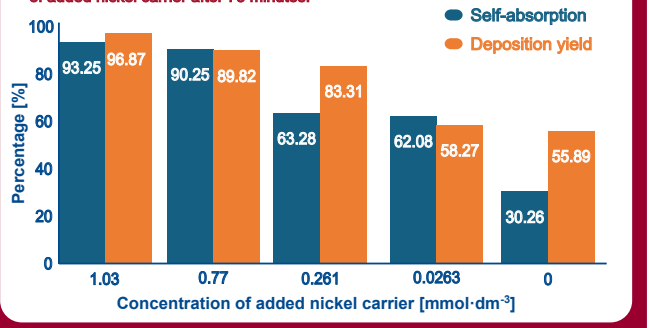


However, in the case of sodium hypophosphite a concentration of 2.43 mmol·dm$^{-3}$ was chosen for further experiments as it resulted in a better deposition on the stainless steel cathode surface.

For dependence of relative nickel concentration on time for different initial concentration of nickel carrier, a threshold can be seen at concentrations in the order of $10^{-5}$ mol·dm$^{-3}$ (*see Figure 3.*), at which saturation of the deposition yield occurs and the nickel concentration is probably no longer the controlling step.

The next task will therefore be to vary other parameters (temperature, pH, etc.) that may affect this process and increase the deposition yield.

Fig. 3: Dependence of relative amount of nickel on time for different initial concentrations of nickel carrier.

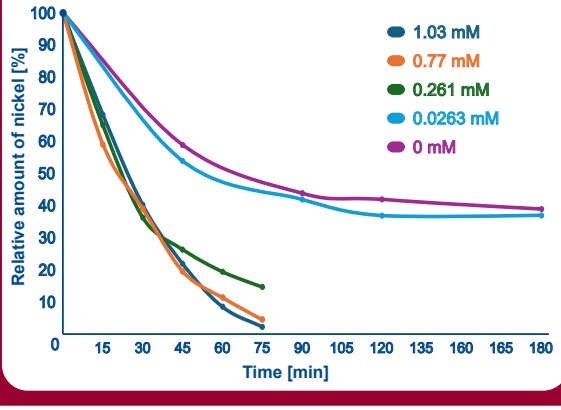


The activity of the $^{63}$Ni solution was measured by liquid scintillation spectrometer (programme $^{3}$H, 300 seconds, channel 38-400) and in the used geometry the nickel detection efficiency was determined to be 38.2 % on the planchette and 55.8 % in solution. (*see Figure 4.*)

Fig. 4: Bar chart of measured $^{63}$Ni activity in the cocktail (orange) and on the planchette (blue) and their ratio (black curve).

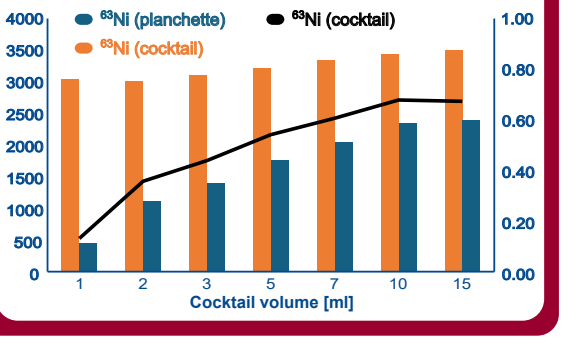


## References

W. Sha, X. Wu, a K. G. Keong, „15 - Applications of electroless nickel–phosphorus (Ni–P) plating", in Electroless Copper and Nickel–Phosphorus Plating, W. Sha, X. Wu, a K. G. Keong, Ed., in Woodhead Publishing Series in Metals and Surface Engineering, Woodhead Publishing, 2011, s. 263–274. doi: 10.1533/9780857090966.2.263.

## Acknowledgements

This work was carried out within grant project of the Predisposal management of radioactive waste (PREDIS) EU

Horizon2020 European Union Funding for Research & Innovation

ČVUT ČESKÉ VYSOKÉ UČENÍ TECHNICKÉ V PRAZE

PREDIS

# BALANCE OF PLANT DESIGN AND OPTIMIZATION FOR TOKAMAK FUSION POWER PLANTS: APPLICATIONS TO ARC-LIKE AND EU-DEMO REACTORS

Francesco COLLIVA

*Sapienza University of Rome, Italy*

This doctoral research at Sapienza University of Rome, in collaboration with ENEA and ENI MAgnetic Fusion Energy (MAFE), examines the design and performance of Balance of Plant (BoP) systems for advanced fusion reactors, particularly the ARC and EU-DEMO designs. The study supports global efforts to achieve commercially viable fusion energy. For the ARC reactor, a compact tokamak developed by MIT and Commonwealth Fusion Systems (CFS) with ENI, the research evaluates three different energy conversion cycles, supercritical Rankine, $CO_2$ Brayton, and He Brayton, using the software GateCycle and identifying the Rankine cycle as most efficient and technologically mature. It also explores a preliminary design of a Double-Wall Heat eXchanger (DWHX), analysing transient performance trade-offs between temperature stability and turbine power output by using RELAP5-3D software. In the case of the EU-DEMO reactor promoted by EUROfusion, the research focuses on the Water-Cooled Lead-Lithium (WCLL) Breeding Blanket, developing a Helical Coil Steam Generator (HCSG) and proposing strategies to manage operational fluctuations. Thermal-hydraulic modeling under steady-state, operational, and accidental scenarios confirms overall system reliability, though some localized hot-spots are noted. Ultimately, the thesis contributes significant insights into the efficiency, safety, and integration of fusion reactor BoP systems.

This work has been carried out within the framework of the EUROfusion Consortium, funded by the European Union via the Euratom Research and Training Programme (Grant Agreement No 101052200 — EUROfusion). Views and opinions expressed are however those of the author(s) only and do not necessarily reflect those of the European Union or the European Commission. Neither the European Union nor the European Commission can be held responsible for them.

# Balance of Plant Design and Optimization for Tokamak Fusion Power Plants: applications to ARC-like and EU-DEMO Reactors

Francesco Colliva*[1], Cristiano Ciurluini[1], Antonio Trotta[2], Fabio Giannetti[1]

[1] Sapienza University of Rome, Nuclear Engineering Research Group (NERG), C.so Vittorio Emanuele II 244, Rome, Italy

[2] MAFE, Eni S.p.A., Venice 30175, Italy

## ABSTRACT

This doctoral research at Sapienza University of Rome, in collaboration with ENEA and ENI MAgnetic Fusion Energy (MAFE), examines the design and performance of Balance of Plant (BoP) systems for advanced fusion reactors, particularly the ARC and EU-DEMO designs. The study supports global efforts to achieve commercially viable fusion energy. For the ARC reactor, a compact tokamak developed by MIT and Commonwealth Fusion Systems (CFS) with ENI, the research evaluates three different energy conversion cycles, supercritical Rankine, $CO_2$ Brayton, and He Brayton, using the software GateCycle and identifying the Rankine cycle as most efficient and technologically mature. It also explores a preliminary design of a Double-Wall Heat eXchanger (DWHX), analysing transient performance trade-offs between temperature stability and turbine power output by using RELAP5-3D software. In the case of the EU-DEMO reactor promoted by EUROfusion, the research focuses on the Water-Cooled Lead-Lithium (WCLL) Breeding Blanket, developing a Helical Coil Steam Generator (HCSG) and proposing strategies to manage operational fluctuations. Thermal-hydraulic modeling under steady-state, operational, and accidental scenarios confirms overall system reliability, though some localized hot-spots are noted. Ultimately, the thesis contributes significant insights into the efficiency, safety, and integration of fusion reactor BoP systems.

## Power Conversion System Analysis

Conducted with the **GateCycle** software

Proposed Configurations:
- Supercritical Rankine cycle
- Supercritical $CO_2$ Brayton cycle
- Supercritical He Brayton cycle

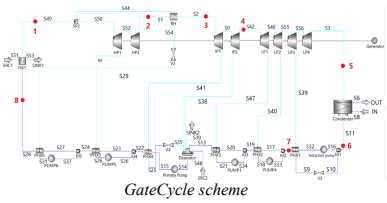

*GateCycle scheme*

| Cycle | Value [%] |
|---|---|
| Supercritical Rankine | 46 |
| Supercritical CO2 Brayton | 41 |
| Supercritical He Brayton | 32 |

*Efficiency Comparison*

- **Rankine Cycle** achieved the best efficiency among the three configurations.

## ARC-like Reactor

Proposed by Massachussetts Institute of Technology (MIT) and developed by its spin-off Commonwealth Fusion System (CFS), in collaboration with ENI S.p.A.

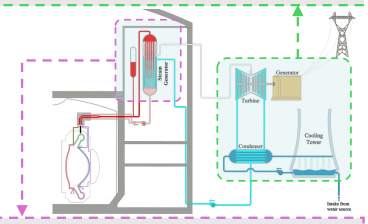

## Double Wall Heat eXchanger Proposal

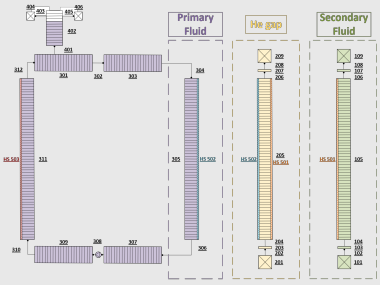


Conducted with the **RELAP5©** software

FLiBe molten salt (shell side) | Helium (gap) | Supercritical water (tube side)

| Fluid | Press. [bar] | Inlet HX Temp. [K] |
|---|---|---|
| FLiBe | 10 | 908.15 |
| Water | 250 | 593.15 |

*Boundary Conditions*

- Preliminary analysis results in an 18.3 m height DWHX and 4000 straight tubes.

### *Steady-state analysis*

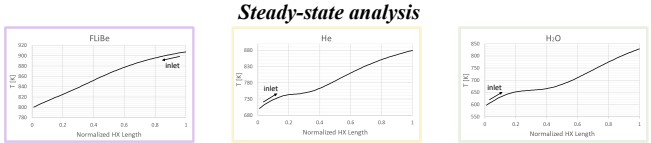


*Fluid temperature profiles along the DWXH normalized length*

### *Operational Transient analysis*

Two adopted strategies
- 1st – constant FliBe, He and water flows during transient.
- 2nd – variable water flow to accommodate power variation.

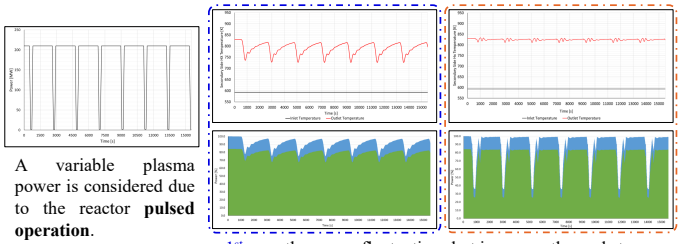

A variable plasma power is considered due to the reactor **pulsed operation**.

1st smooths power fluctuations but increases thermal stress,
2nd limits thermal stress, with higher power variation.

## Breeding Blanket Analysis

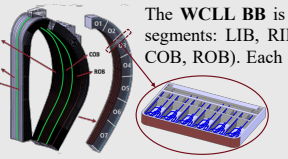

The **WCLL BB** is divided into 16 sectors, made of an **Inboard** (left/right segments: LIB, RIB) and an **Outboard** (left/central/right segments: LOB, COB, ROB). Each segment is characterized by **Breeding Elementary Cells** (BRCs) organized into 7 poloidal zones.

Cooling circuits: **FW water**, **BZ water**, **BZ PbLi**

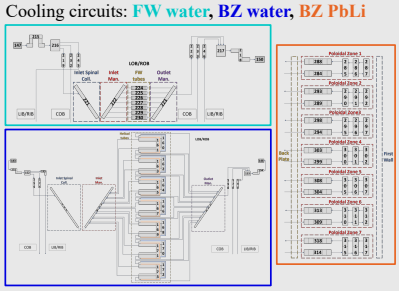

| Fluid | Press. [bar] | Inlet HX Temp. [K] |
|---|---|---|
| FW/BZ Water | 155 | 568.15 |
| PbLi | 60 | 601.15 |

*Boundary Conditions*

- The coupling between the three hydraulic models is modeled through **thermal structures**.

### *Pulse-Dwell Transient Analysis*

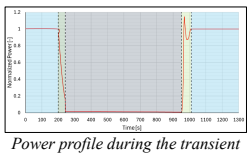

*Power profile during the transient*

- Conducted to observe **temperature variations** during the transition between operational phases.

### *Accidental Transient Analysis*

| Case ID# | Transient Type | System Involved |
|---|---|---|
| lf-FW | Complete LOFA | FW PHTS |
| lf-BZ | Complete LOFA | BZ PHTS |
| iv-FW | Inadv. Op. of Loop Isolation Valve | FW PHTS |
| iv-BZ | Inadv. Op. of Loop Isolation Valve | BZ PHTS |
| ss-FW | Shaft Seizure | FW PHTS |
| ss-BZ | Shaft Seizure | BZ PHTS |

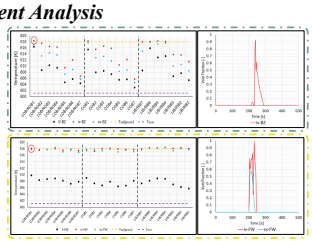

- Analyses reveal an initial **temperature increase** and **brief vapor formation** due to rapid coolant flow reduction, with **no impact on overall system safety**.

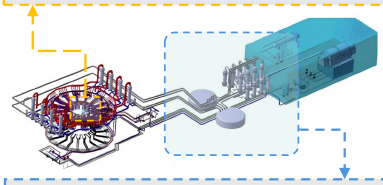

## EU-DEMO Reactor

Developed by EUROfusion consortium aiming at demonstrating fusion electricity generation by integrating key technologies into a functional power plant.

## IHTS Design and Control Strategy

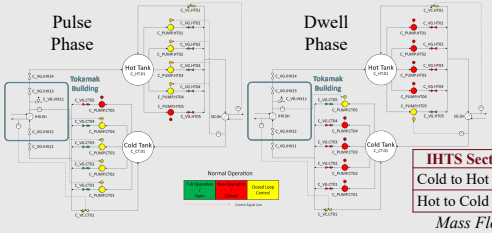


Definition of pipe layout, component selection, flow control strategy, and integration with **Helical Coil Steam Generators** (HCSG).

| IHTS Section | Unit | Pulse | Dwell |
|---|---|---|---|
| Cold to Hot Tank | kg/s | 30577.0 | 305.8 |
| Hot to Cold Tank | kg/s | 30349.5 | 3035.0 |

*Mass Flow Rate in transient phases*

### *Preliminary HCSG design*

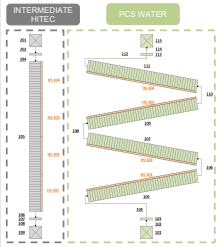


13.8 m height HX, 5217 helical tubes (79.5 m length, 10° inclination).

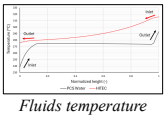

*Fluids temperature profiles along the HCSG normalized length*

| Fluid | Press. [bar] | Inlet HX Temp. [K] | Outlet HX Temp. [K] |
|---|---|---|---|
| HITEC | ~1 | 589.15 | 549.15 |
| Water | 58 | 511.15 | 566.15 |

*Boundary Conditions*

## CONCLUSIONS

- Parallel design studies on ARC and EU-DEMO focus on developing consistent and integrated BoP architectures, to support the transition from conceptual studies to feasible fusion power plant solutions.
- For ARC, two key components have been analysed: an indirect Power Conversion System and a direct DWHX, representing alternative starting points for future plant layouts.
- For EU-DEMO, the work focused on two components, the BB and the HCSG, now being integrated into full-system extended models of primary and intermediate cooling loops.

# BROOMSTICK EXPERIMENT FOR NUCLEAR DATA VALIDATION AT THE VR-1 REACTOR

Tomáš CZAKOJ

*Czech Technical University in Prague, Czech Republic*

Chromium plays a vital role in nuclear reactor systems as an additive to stainless steel improving its corrosion resistance and high-temperature strength, thus necessitating accurate knowledge of its neutron cross-section. This study presents a neutron transmission experiment—referred to as the "broomstick experiment"—conducted at the VR-1 reactor using cylindrical chromium samples and a collimated neutron beam. The experimental setup employed a pencil beam geometry designed to minimize scattered neutron contributions and increase sensitivity to total cross-section minima. Measurements of the neutron spectrum behind different layers of the chromium samples were performed with stilbene scintillation spectrometry in the 1–10 MeV energy range. The experimental spectra behind chromium cylinders of varying lengths (5, 10, and 20 cm) were compared to Monte Carlo simulations using ENDF/B-VIII.0, JEFF-3.3, JENDL-5, and INDEN evaluations. The results reveal discrepancies between simulations and measurements, particularly at low and intermediate energies, indicating the need for continued refinement of chromium nuclear data. The study highlights the importance of integral experiments for validating nuclear data and demonstrates the effectiveness of the broomstick experiment in providing valuable data for chromium cross-section validation, revealing specific areas where existing nuclear data libraries can be improved.

# Broomstick experiment for nuclear data validation at the VR-1 reactor

www.cvrez.cz

Tomáš Czakoj, Michal Košťál, Evžen Losa, Evžen Novák, Zdeněk Matěj
tomas.czakoj@cvrez.cz
Centrum výzkumu Řež, Czech Republic

## Introduction

Chromium is vital in the nuclear industry due to its exceptional properties that enhance the performance and safety of nuclear reactors; therefore; it is necessary to know chromium cross-sections properly. The best way to validate chromium cross-sections is an integral experiment in a thick slab or block neutron transport. Unfortunately, the price of chromium block is extremely high. One way to validate the cross-section of chromium cheaply is to measure the penetration of the neutron beam through the chromium cylinder.

The poster focuses on a pencil beam transmission experiment, referred to as a broomstick experiment, conducted through chromium cylinders. The broomstick-type experiment is designed to minimize the fraction of collided neutrons, making it particularly sensitive to minima in the total neutron cross-section.

## Methods

The experiment was inspired by ORNL's experiment at the Tower Shielded Reactor II in the 1960s [1]. In our case, a collimated beam from the radial channel of the VR-1 reactor was used. The spectrum of the radial channel was well-described previously [2]. It was demonstrated that the actual spectrum in the higher energy region (above ≈ 5 MeV) is nearly identical to the $^{235}U(n_{th},f)$ prompt fission neutron spectrum. Neutron flux from the radial channel was collimated by a special collimator optimized for the pencil beam formation. The beam was previously used for an initial broomstick experiment with a copper [3].

### V-1 reactor

The VR-1 reactor is a pool-type light-water reactor operated by the Czech Technical University in Prague. It uses IRT-4M low-enriched uranium fuel with thermal power of up to 5 kW. The reactor is equipped with various experimental instruments, such as horizontal, radial, and tangential channels.

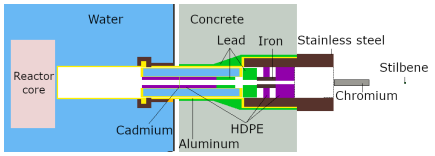


Fig. 1: Geometry of collimator.

### Collimator

The collimator consists of two main parts. The first one, next to the core, is designed for strong collimation of the reactor leakage beam. It ensures acceptable radiation in positions close to the beam and suppresses the room effect. The second part assures precise collimation to the diameter of 3 cm. The scheme is depicted in Fig. 1.

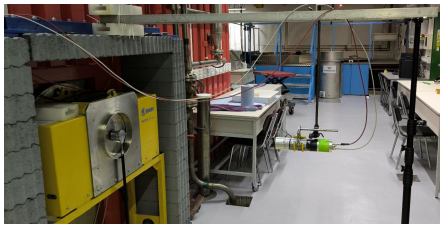

Fig. 2: Photo with 5 cm of chromium. Beam shutter is closed.

## Measurement

The primary radial channel beam was collimated into a narrow pencil beam of a diameter of 3 cm and attenuated by chromium cylinders inserted into the leakage neutron beam. Photo from measurements is in Fig. 2. Their diameter was 6 cm and lengths were 5, 10. and 20 cm. Photo of the chromium cylinders is in Fig. 3. The neutron flux (neutron spectrum) in 1.0–10.0 MeV energy interval was measured using stilbene scintillator. Measurement position was 1 m from the shutter.

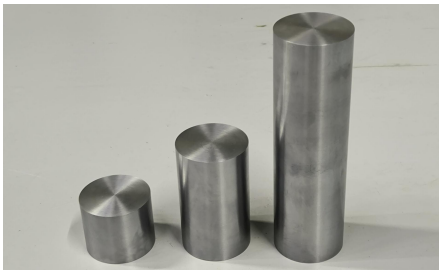

Fig. 3: Chromium cylinders used in the experiment.

### Beam characterization

Detailed characterization was performed chromium measurement. It included beam divergence, beam sharpness, and neutron spectrum. It was shown that the spectrum in the beam is stable, beam is well sharp, and beam divergence is acceptable.

### Calculations

Simulations were done using MCNP6.2 code using various neutron transport libraries as ENDF/B-VIII.0, JEFF-3.3, JENDL-5), and INDEN chromium evaluations, which will be adopted by ENDF/B-VIII.1.

## Results

The evaluated spectra behind different lengths of chromium are depicted in Fig. 4. The neutron spectra were normalized to the nominal reactor power corresponding to 130 W. The increase in the share of lower-energy neutrons (1-3 MeV) with increasing thickness of chromium is apparent. The increase is higher than in a similar experiment with copper [3].

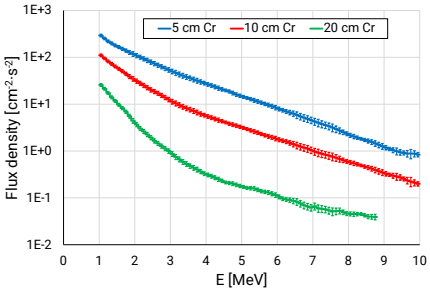


Fig. 4: Neutron spectra with inserted chromium cylinders

Comparisons of calculated and measured spectra are presented in the form of Calculation/Experiment-1 (C/E-1) in Fig. 5 and Fig. 6. Differences are mostly within uncertainties. A significantly different shape of the JEFF-3.3 disagreement can be seen in the 2.5 – 5.0 MeV energy range.

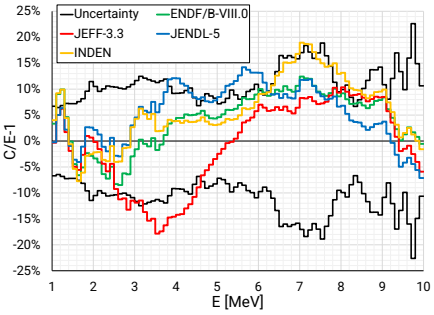


Fig. 5: C/E-1 comparison for 10 cm of chromium.

Discrepancies are more apparent in the case of 20 cm chromium. Calculations overpredict the measured spectrum at the lowest energies, 1.0-1.5 MeV. JEFF-3.3 evaluation is at energies 2.5-5.5 MeV out of the uncertainty. INDEN evaluation overpredicts the experiment at energies 6.0-8.0 MeV. Overall, no library is within uncertainty for the whole energy range.

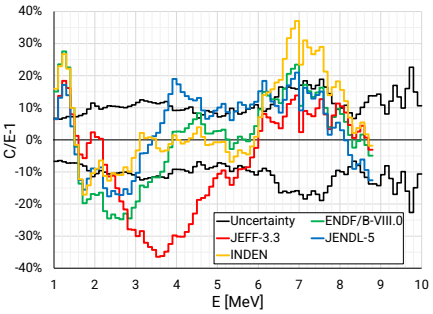


Fig. 6: C/E-1 comparison for 20 cm of chromium.

## Conclusions

A novel broomstick-type transmission experiment was successfully conducted at the VR-1 reactor using collimated neutron beams and chromium cylinders. The comparison of measured neutron spectra with MCNP6.2 simulations using different nuclear data libraries revealed discrepancies. The JEFF-3.3 evaluation showed a different shape in the 2.5-5.5 MeV range, and the INDEN evaluation overpredicted the experiment at 6.0-8.0 MeV. Overall, none of the evaluated libraries consistently agreed with the experimental results across the entire energy range. The study has shown the effectiveness of broomstick experiments as a cost-efficient and accurate method for integral data testing in modern nuclear applications, especially for very expensive materials.

### References

[1] Clifford, C. E. et al., 1967. "Measurements of the Spectra of Uncollided Fission Neutrons Transmitted Through Thick Samples of Nitrogen, Oxygen, Carbon, and Lead: Investigation of the Minima in Total Cross Sections." Nuclear Science and Engineering, 27 (2): 299–307.
[2] Košťál, M., et al., 2018. Characterization of mixed N/G beam of the VR-1 reactor. Ann Nucl Energy 122, 69–78.
[3] Košťál, M., et al., 2025. Broomstick experiment with copper in VR-1 reactor. Ann Nucl Energy 211, 110993.

### Acknowledgement

The presented results were obtained using the CICRR infrastructure, which is financially supported by the Ministry of Education, Youth and Sports - project LM2023041. The use of the VR-1 reactor infrastructure was financially supported by the Ministry of Education, Youth and Sports – project LM2023073.

**CENTRUM VÝZKUMU ŘEŽ S.R.O.**

Hlavní 130, Řež, 250 68 Husinec, Czech Republic
T: +420 266 173 181, F: +420 266 172 398
E: cvrez@cvrez.cz, W: www.cvrez.cz

CVŘ Research Centre Řež

# MULTISCALE THERMAL-HYDRAULIC ANALYSIS OF EXPERIMENTAL FACILITIES IN SUPPORT OF THE LEAD-COOLED FAST REACTORS DEVELOPMENT

Tommaso DEL MORO

*Sapienza University of Rome, Italy*

Nuclear energy plays a key role in reducing carbon emissions and enabling a sustainable energy transition. Among advanced reactor designs, Lead-cooled Fast Reactors (LFRs) stand out as a promising Generation IV technology due to their improved safety, fuel efficiency, and waste reduction capabilities. By using Heavy Liquid Metals (HLMs) as coolants and MOX fuel from reprocessed spent fuel, LFRs help close the fuel cycle and minimize long-lived radioactive waste.

# Multiscale Thermal-Hydraulic Analysis of Experimental Facilities in Support of the Lead-Cooled Fast Reactors Development

Tommaso Del Moro, Sapienza University of Rome, tommaso.delmoro@uniroma1.it

## Background

Gen-IV nuclear reactors pose new challenges from the simulation and modeling perspectives

### System scale analysis

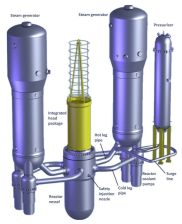

### Component scale analysis

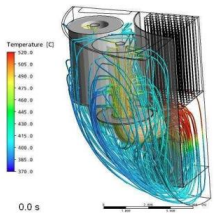


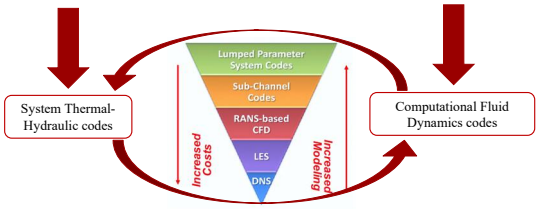


## Methodology

A coupling tool between the STH code RELAP5/Mod3.3 and the CFD code Ansys CFX has been developed

### Time advancing scheme

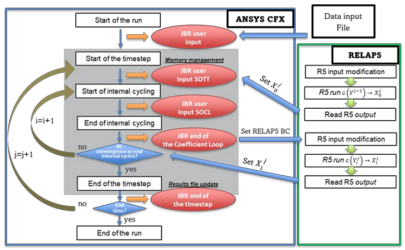


### Spatial domain discretization

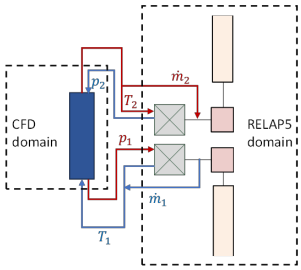


The figures refer to the semi-implicit time advancing scheme and the separate domain discretization approach, but in the thesis work, also the explicit scheme and the domain overlapping approaches have been developed

## Main objective

Perform multiscale thermal-hydraulic analyses in support to the Lead-cooled Fast Reactors (LFRs)

## Correlated objective

Design a facility capable of reproducing the main thermal-hydraulic phenomena of LFRs

## VERIFICATION & VALIDATION

### SIRIO

- Testing of a prototype of an innovative DHR for LFRs/ADSs and LWRs.
- System codes validation.

*This work has been performed within the PIACE project. This project has received funding from the European Union's Horizon 2020 research and innovation program under the Grant Agreement No. 847715.*

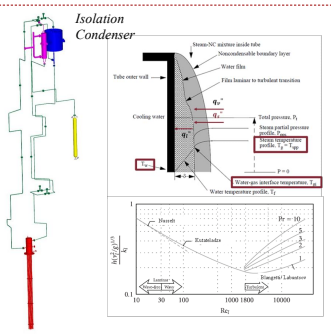


**Code modifications**

- Cooper correlation for pool boiling
- Kutateladze correlation for laminar-wavy film condensation
- Blangetti and Labuntsov correlations for turbulent film condensation
- Inclusion of the sensible heat contribution when dealing with condensation in presence of non-condensable gases.

$$q''_l = q''_v + q''_s \rightarrow h_c(T_{vi} - T_w) = h_m h_{fgb} \rho_{vb} \ln\left(\frac{1-\frac{P_{gi}}{P}}{1-\frac{P_{gb}}{P}}\right) + h_s(T_{vb} - T_{vi})$$

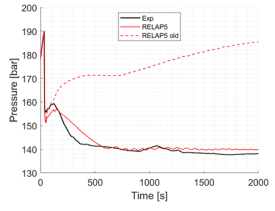


✓ Loop pressure well predicted with the new version of the code because of the higher condensation heat transfer coefficient calculated by the code

### NACIE-UP

- Component testing.
- Transition from forced to natural circulation experiments in Heavy Liquid Metal (HLM) systems.
- Codes validation.

*The data and information presented in the paper are part of an ongoing IAEA coordinated research project on "Transition from Forced to Natural Circulation Experiment with Heavy Liquid Metal Loop – CRP- I31038".*

#### NUMERICAL MODELS

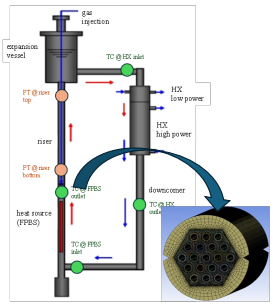


#### RESULTS

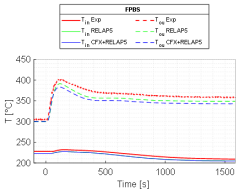


✓ Loop temperatures well predicted both with the RELAP5 stand-alone code and with the coupled code since NACIE is almost a 1D loop

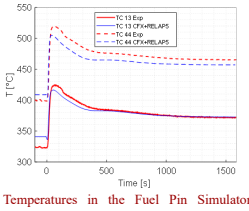


✓ Temperatures in the Fuel Pin Simulator well predicted by the coupled code. These temperatures cannot be calculated through RELAP5 stand-alone as they are local temperatures

### TALL-3D

- Transition from forced to natural circulation experiments in HLM systems.
- Experimental and numerical investigation of pool behavior.
- Codes validation.

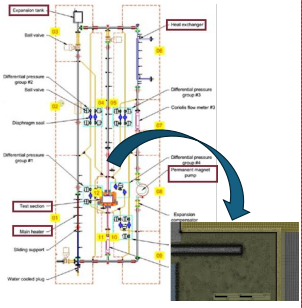

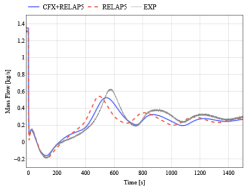


✓ Mass flow rate oscillations following a forced to natural circulation transition better predicted by the coupled code

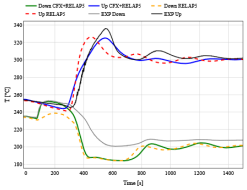


✓ Inlet and outlet temperatures peaks are better predicted by the coupled code than the RELAP5 stand-alone

### ATHENA

- Large scale facility (3.2 diameter and 10 m height, 800 tons of lead) representative of a LFR layout, and capable to test full scale components
- Definition and pre-test analysis of Loss of Heat Sink (LOHS) and Loss of Flow Accident (LOFA) through the coupled tool preliminary validated through the comparison between numerical results with experimental data from LFR-relevant experimental facilities
- After the ATHENA experimental campaign and a further validation of the coupled tool, it can be used to support the design and safety anaylsis on a reactor scale

#### NUMERICAL MODELS

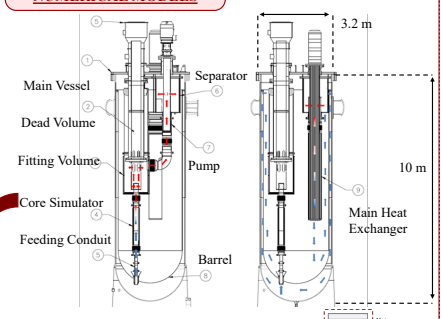


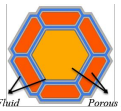


*Core Simulator CFD model*

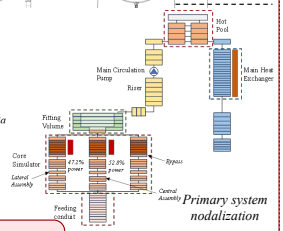


*Primary system nodalization*

#### RESULTS

Reference transient: Loss Of Flow Accident

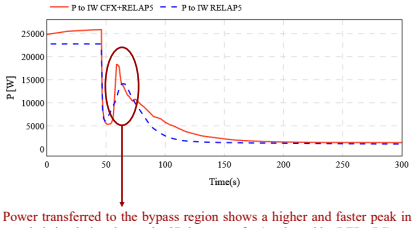


Power transferred to the bypass region shows a higher and faster peak in the coupled simulation due to the 3D heat transfer (neglected by RELAP5).
The proper evaluation of this quantity is relevant for a LFR core since the bypass allows to reduce the coolant (and the cladding) temperature

# UNDERGROUND STORAGE OF SPENT NUCLEAR FUEL: TECHNOLOGIES AND PROSPECTS

Yuliia HADAIEVA

*National Technical University Kharkiv Polytechnic Institute, Ukraine*

This article examines modern approaches to the long-term storage of spent nuclear fuel (SNF) using deep geological disposal technologies. Key international projects, technological solutions, and the main challenges associated with implementing such repositories are analyzed. Special attention is given to the prospects for the development of this technology in the next decade.

# Underground Storage of Spent Nuclear Fuel: Technologies and Prospects


## Abstract

This article examines modern approaches to the long-term storage of spent nuclear fuel (SNF) using deep geological disposal technologies. Key international projects, technological solutions, and the main challenges associated with implementing such repositories are analyzed. Special attention is given to the prospects for the development of this technology in the next decade.


## Introduction

Modern deep geological disposal (DGD) systems are complex engineering and geological structures based on the principle of multi-barrier protection. The design of such repositories includes: metallic containers (copper, special alloys), buffer materials (bentonite clay), and natural geological barriers (granite, clay, or salt formations).

International experience in implementing DGD projects demonstrates various technological approaches. Finland (Onkalo project) and Sweden have chosen granite massifs as the primary natural barrier. France (Cigéo project) is developing a repository in clay formations, emphasizing the advantages of their low permeability. The United States employs a combined approach, integrating temporary storage at nuclear power plant sites with permanent solutions in salt formations.

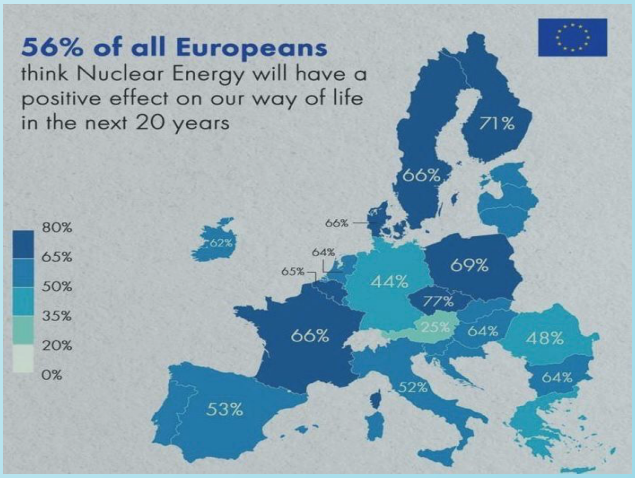


The main technological challenges include:

– Ensuring long-term corrosion resistance of containers

– Developing reliable monitoring systems

– Predicting geological stability over millennia

– Reducing construction and operation costs

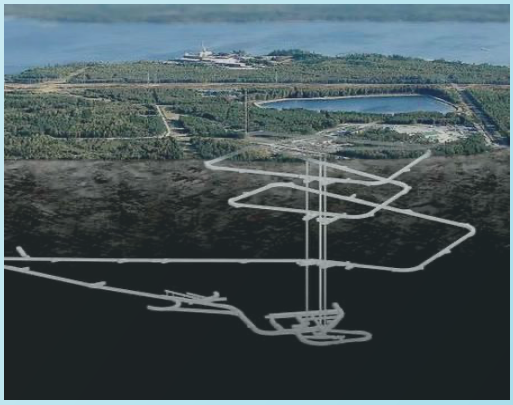

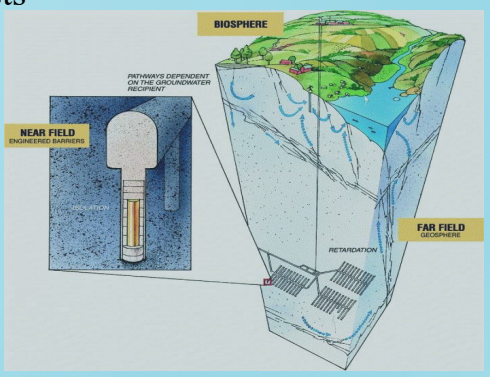


## Conclusion

The analysis of modern DGD projects shows that this technology is becoming the standard solution for the long-term storage of SNF. The successful implementation of Finland's Onkalo project confirms the technical feasibility of the concept. The prospects for industry development are linked to the improvement of container materials, the creation of intelligent monitoring systems, and cost optimization. International cooperation and experience sharing will play a key role in the further advancement of technologies for the safe storage of nuclear waste.


**Yuliia.Hadaieva@mit.khpi.edu.ua**

# ISOTHERMAL FLOW PAST MIXING GRID WITH PARABOLIC VANES

Vojtěch JÁNSKÝ

*University of West Bohemia in Pilsen, Czech Republic*

Heat is produced by nuclear fission of Uranium fuel in the form of pellets organized in "fuel rods". The produced heat in the nuclear reactor's fuel has to be transported to the turbine. This is realized by using water (or other coolant) flowing between the fuel rods. Nuclear fuel grids are designed to keep the fuel rod in position and to enhance the heat transfer by mixing of the coolant flow. The mixing grid can aim to mix the hot boundary layer with the faster but cooler fluid at the centers of the inter-rod channels and to mix the fluid between neighboring channels to achieve the heat transfer enhancement. The present experiment maps the flow past such a grid in the wind tunnel under isothermal flow conditions and visualise the turbulences using the Particle Image Velocimetry.

ZÁPADOČESKÁ UNIVERZITA V PLZNI

# ISOTHERMAL FLOW PAST MIXING GRID WITH PARABOLIC VANES

NUCLEAR DAYS

Vojtěch Janský, Daniel Duda, Václav Marek, Matěj Dolejš, Anna Mrázová, Vitalii Yanovych & Václav Uruba

## Wind tunnel measurement of isothermal flow through a short nuclear fuel assembly model

- Test section 0.3 × 0.2 × 0.7 m, mixing grid 2×
- Rod diameter D = 5 cm, Mesh M = 6.7 cm
- Two mixing grids in distance 30 cm
- Stereo Particle Image Velocimetry (SPIV) at the outlet

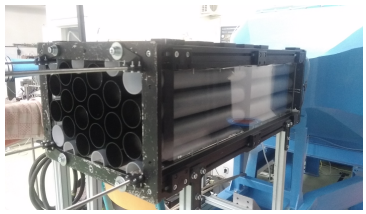

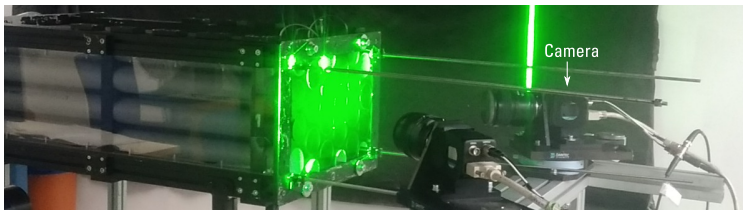


## Abstract & introduction

- Nuclear energy is stable and ecologic energy source
- Heat is produced by nuclear fision of Uranium fuel in the form of pellets organized in "fuel rods"
- The produced heat has to be transported into turbine. This is realized by using water (or other coolant) flowing between the fuel rods
- Therefore, the grid has two main functions:
  1. it keeps the fuel rods in positions
  2. it enhances the mixing and thus the heat transfer
- The mixing grid can aim to achieve two goals:
  1. to mix the hot boundary layer with the faster but cooler fluid at the centers of the inter-rod channels
  2. to mix the fluid between neighboring channels
- The present experiment maps the flow past such a grid
- Wind tunnel velocity 24 m/s (Re = $3.3 \cdot 10^4$)
- Isothermal flow conditions
- "Half-cut" geometry, only in short test section

## Mixing grid with parabolic vanes

Single cell | Vane | Fixation to thread rod

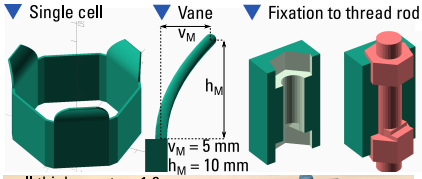


wall thickness $t_w$ = 1.2 mm

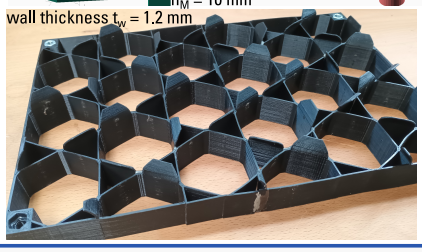

## Mean streamwise velocity

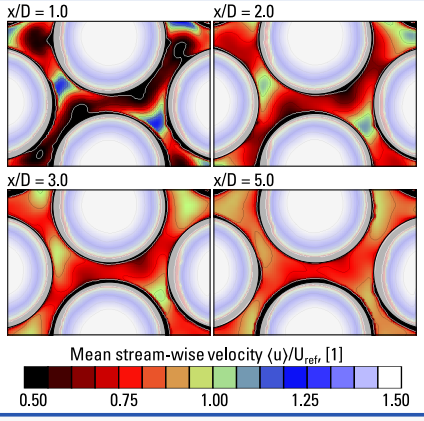


## Turbulence intensity

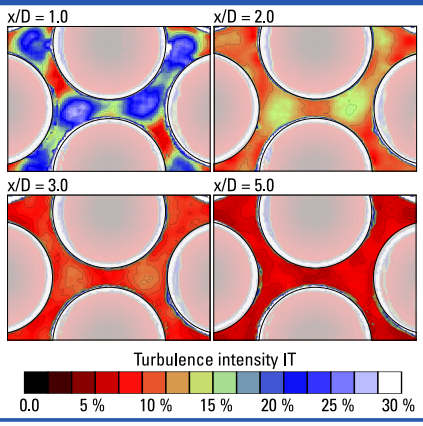


## Fluctuations along main axes

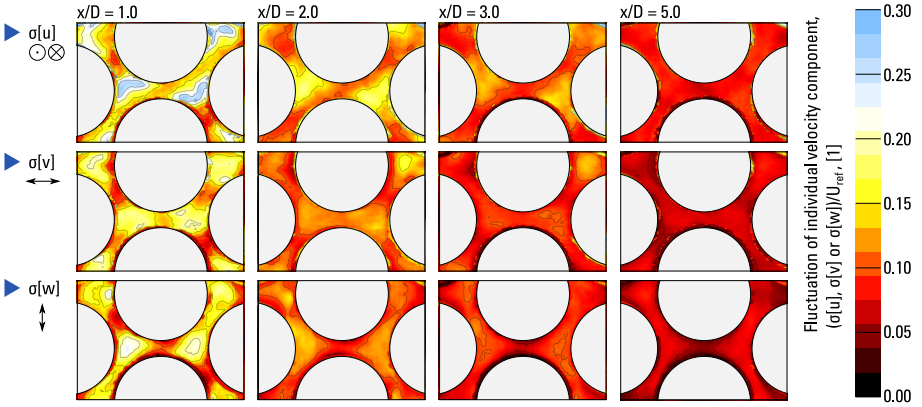


## Autocorrelation function of the stream-wise velocity

$$R_{ww}(\vec{x},\vec{y}) = \frac{\left\langle \left(w(\vec{x},t_i) - \langle w(\vec{x})\rangle\right) \cdot \left(w(\vec{y},t_i) - \langle w(\vec{y})\rangle\right)\right\rangle}{\sigma[w(\vec{x})] \cdot \sigma[w(\vec{y})]}$$

Reference point | Any other point | Standard deviation at given point | Average over all frames

▼ Autocorrelation with a point in wide channel (between 3 rods)

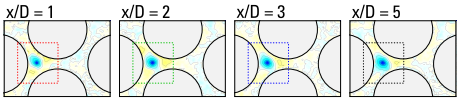


▼ Autocorrelation with a point in narrowest part of the channel

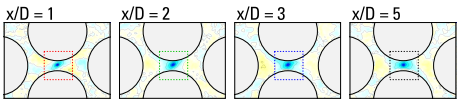



- Comparison of isolines of stream-wise autocorrelation function with reference point in the center of the widest part of the channel

x/D = 1
x/D = 2
x/D = 3
x/D = 5

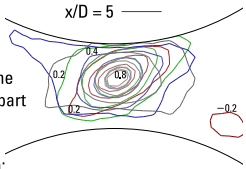


- with reference point in the center of the narrowest part of the channel
- Blue: positive correlation; yellow: anticorrelation

## Estimation of Taylor microscale

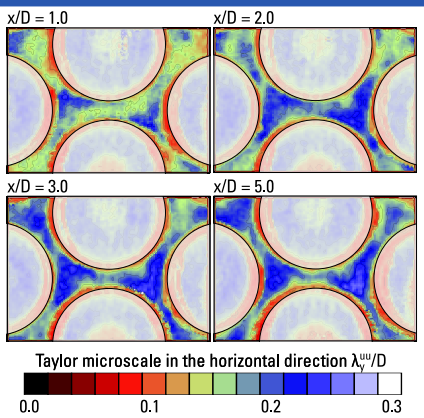

# MEASUREMENT OF SPECTRUM AVERAGED CROSS SECTIONS IN THE BENCHMARK LR-0 REFERENCE FIELD

Alena KRECHLEROVÁ

*Czech Technical University in Prague, Czech Republic*

A reactor pressure vessel (RPV) is a critical component that determines the lifetime of a power plant and plays a key role in nuclear safety. Consequently, both the inner and outer surfaces of the RPV are monitored by a set of activation detectors to ensure the nuclear power plant's safe operation. Data from these activation detectors is used to determine the neutron fluence and neutron spectrum. Achieving high precision in these measurements requires input parameters to be as accurate as possible. One of the essential input parameters is the microscopic cross-section, specifically the spectrum averaged cross section (SACS). Furthermore, the SACS is a preferred tool for validating cross section, especially in a standard or reference neutron field. A large set of measurements was performed at Research Centre Řež using the LR-0 reactor, which provides a benchmarked reference neutron field. The SACS of threshold reactions such as $^{54}$Fe(n,p) $^{55}$Mn(n,2n), and $^{75}$As(n,2n) were investigated. All experimentally derived SACS were compared with calculated SACS obtained via MCNP6.2 code employing cross sections from IRDFF-II nuclear data library.

CICRR | Czech International Centre of Research Reactors

www.cicrr.cz

# Measurement of spectrum averaged cross sections in the benchmark LR-0 reference field

Alena Krechlerová[1,2], Martin Schulc[1], Michal Košťál[1], alena.krechlerova@cvrez.cz
[1]Research Centre Řež, CZ; [2]Faculty of Nuclear Sciences and Physical Engineering, CTU, CZ

## Introduction

The safe and reliable operation of nuclear power plants is critical, as accidents can have severe consequences for both the environment and human health. One key parameter in ensuring nuclear safety is neutron fluence, which is essential for evaluating the structural integrity of the reactor pressure vessel. Over time, exposure to fast neutrons can degrade the vessel material, potentially leading to brittle fracture if not properly monitored. Therefore, accurate and regular measurement of neutron fluence is crucial for maintaining reactor safety and estimating the plant's operational lifespan.

An essential aspect of accurately determining neutron fluence is the precise knowledge of neutron reaction cross sections. Any uncertainty in cross section values directly affects the reliability of fluence rate estimations. As a result, continuous efforts in cross section evaluation, experimental validation, and nuclear data refinement are vital for reactor dosimetry, spectrum unfolding, and ensuring the overall accuracy of safety assessments in nuclear power plants.

## Research Reactor LVR-0

The LR-0 research reactor is light-water, zero-power, pool-type reactor. It serves as an experimental reactor for measuring neutron physics characteristics of VVER type power reactors.

It provides a scientific and technological facility for experiments in the area of validations and biological shielding of VVER reactors (Temelín, Dukovany, etc.), related to the storage of spent fuel from nuclear power plants and providing advice for the nuclear power industry.

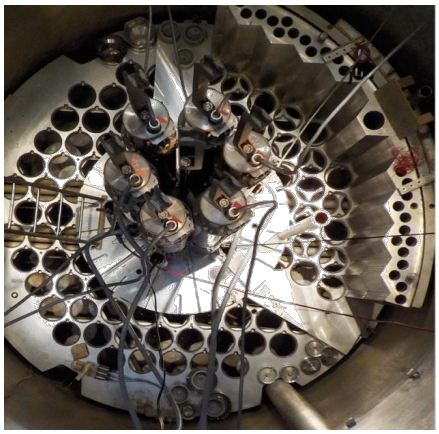

LR-0 benchmark core

## LR-0 reactor benchmark core

Reference neutron benchmark field is permanent and reproducible neutron field with well-defined spatial distribution of the neutron field, well-defined energy spectrum and characterized gamma spectrum. It was established to perform high quality reactor physics experiments, benchmarking and dosimetry studies, with a focus on Spectrum averaged cross section (SACS) measurements. The benchmark configuration contains 6 fuel shortened VVER-1000 assemblies with dry central irradiation cavity (cylinder D=20 cm, H=20 cm). For the neutron energies above 1 MeV, the flux is approximately $3\times10^{7}$ $cm^{-2}s^{-1}$.

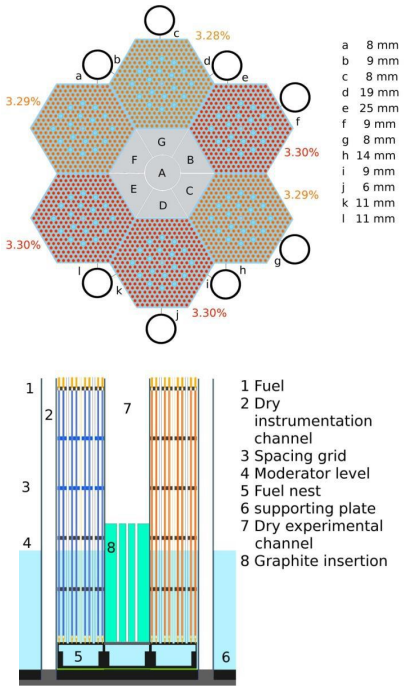


LR-0 benchmark core

## HPGe detector

The HPGe detector located at CVŘ is well characterized due to development of Monte Carlo calculational model. Dimensions of the detector were established from the radiography. Insensitive layer was determined using $^{241}$Am soure. The developed model was validated using various point and volume etalon sources.

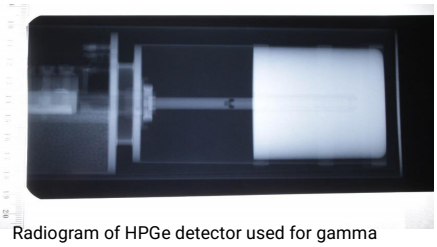

Radiogram of HPGe detector used for gamma spectroscopy

## Methods of evaluation

Activation detectors of different materials were prepared and attached to the aluminium holder. Together with the investigated detectors, monitors with well-known cross sections were also attached to the aluminium holder. Furthermore, the aluminium holder with the activation foils was irradiated in the LR-0 reference benchmark field. After irradiation, the foils were subsequently measured on the HPGe detector, and the experimental reaction rate is then inferred.

To compare the experimental SACS from LR-0 with SACS in $^{235}U(n_{th},f)$ prompt fission neutron spectrum (PFNS), the SACS from LR-0 need to be corrected to the SACS values in $^{235}U(n_{th},f)$ PFNS. The MCNP6 calculated SACS are using $^{235}U(n_{th},f)$ PFNS from ENDF/B-VIII.0 library and IRDFF-II cross sections. Correction factor was determined using calculations in MCNP6, accounting for self-shielding and flux loss. The table lists SACS in $^{235}U(n_{th},f)$ PFNS of various reactions measured over the years during various experiments, their relative uncertainty, then the SACS and their relative uncertainties obtained from IRDFF-II nuclear data library and the difference between the experimental and IRDFF-II SACS (Eval/E-1).

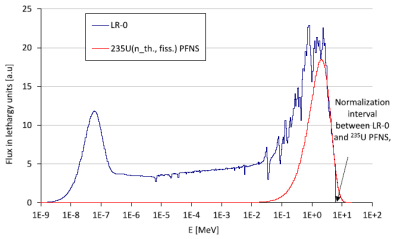


Comparison of measured and calculated neutron spectrum in the dry experimental channel

## Results

| | LR-0 measurement | | IRDFF-II data | | |
|---|---|---|---|---|---|
| | Mean [mb] | Rel. unc. | Mean [mb] | Rel. unc. | Eval / E-1 |
| $^{63}$Cu(n,α) | 0.5050 | 3.7% | 0.5146 | 2.2% | 1.9% |
| $^{54}$Fe(n,α) | 0.7963 | 6.3% | 0.8156 | 4.0% | 2.4% |
| $^{56}$Fe(n,p) | 1.069 | 3.4% | 1.058 | 3.6% | -1.0% |
| $^{48}$Ti(n,p) | 0.2901 | 3.4% | 0.2935 | 2.8% | 1.2% |
| $^{27}$Al(n,α) | 0.6730 | 3.8% | 0.6872 | 3.2% | 2.1% |
| $^{51}$V(n,α) | 0.0228 | 3.5% | 0.0239 | 5.5% | 4.9% |
| $^{197}$Au(n,2n) | 3.372 | 4.2% | 3.297 | 6.1% | -2.2% |
| $^{93}$Nb(n,2n) | 0.4307 | 3.5% | 0.4519 | 6.7% | 4.9% |
| $^{127}$I(n,2n) | 1.192 | 4.8% | 1.186 | 6.6% | -0.5% |
| $^{55}$Mn(n,2n) | 0.2324 | 3.8% | 0.2485 | 6.8% | 6.9% |
| $^{75}$As(n,2n) | 0.3205 | 3.1% | 0.3256 | 6.1% | 1.6% |
| $^{89}$Y(n,2n) | 0.1708 | 3.2% | 0.1727 | 7.9% | 1.1% |
| $^{19}$F(n,2n) | 0.0079 | 4.1% | 0.0081 | 7.9% | 2.7% |
| $^{90}$Zr(n,2n) | 0.1071 | 4.0% | 0.1061 | 0.9% | -1.0% |
| $^{23}$Na(n,2n) | 0.00384 | 4.9% | 0.00396 | 11.7% | 3.1% |

## Conclusions

A large set of experiments at the LR-0 reactor were performed. Various SACS in $^{235}U(n_{th},f)$ PFNS of reactions were investigated and were published in [1,2]. The striking agreement with MCNP calculations was achieved with experiment using ENDF/B-VIII.0 $^{235}U(n_{th},f)$ PFNS and IRDFF-II dosimetric cross sections for all reactions under study.

## References

[1] Physical Review C - 109(5) (May 2024),

[2] Annals of Nuclear Energy - Volume 206 110616 (October 2024)

### Acknowledgement

This work was supported by the Ministry of Education, Youth and Sports of the Czech Republic by project LM2023041.

**CENTRUM VÝZKUMU ŘEŽ S.R.O.**

Hlavní 130, Řež, 250 68 Husinec, Czech Republic
T: +420 266 173 181, F: +420 266 172 398
E: cvrez@cvrez.cz, W: www.cvrez.cz

ÚJF | CVŘ Research Centre Řež

# CHARACTERIZATION AND DEVELOPMENT OF CEMENTITIOUS MATERIALS USED IN STORAGE FACILITIES FOR IMMOBILIZATION OF ILW RADIOACTIVE WASTE

Francesco RIZZO

*Sapienza University of Rome, Italy*

The research activity focused on the design and experimental validation of cement-based matrices for the immobilization of intermediate level radioactive waste, with particular attention to mechanical performance, durability, and radionuclide retention, also through accelerated aging and leaching tests. All the results are according the Technical Guide N°33, that is the Italian Law for the acceptance criteria for matrices and waste (from LLW to HLW).

# Characterization and Development of Cementitious Materials Used in Storage Facilities for Immobilization of ILW Radioactive Waste


Ph.D. in Energy and Environment at Sapienza University of Rome, XXXVII ciclo, 2021-2024
Ph.D. Thesis defended on 27th January 2025

Candidate: **F. Rizzo**; Thesis Advisor: Prof. F. Giannetti; Co-Supervisor: PhD A. Tonti


## Activity Framework

My Ph.D. was carried out at **Sapienza University of Rome** within the **Ph.D. program in Energy and Environment**, **Department of Astronautical, Electrical and Energy Engineering** (**DIAEE**), in the **Nuclear Engineering Research Group**, and was **financially supported by INAIL** (**Italian National Institute for Insurance against Accidents at Work**). The research was conducted as part of the **BRiC ID47/2022 project**, focused on radioactive waste management and decommissioning strategies.

The research activity focused on the **design and experimental validation of cement-based matrices** for the **immobilization of intermediate level radioactive waste**, with particular attention to **mechanical performance**, **durability**, and **radionuclide retention**, also through **accelerated aging and leaching tests.**

The matrix, poured into a metallic container, becomes the **first barrier** of the **Italian National Repository**, a **Near-Surface Repository** composed of **waste packages (1), modules (2), cells (3), and a multilayer waterproof hill (4)**, following the **Defence-in-Depth (DID)** principle.

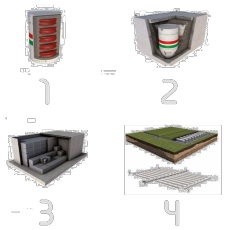


The images were granted by SOGIN www.depositonazionale.it

**Main topics**: Intermediate level waste; Waste immobilization; Decommissioning; Leaching tests; Durability assessment; Cementitious materials engineering; Wasteform qualification.

## Matrix Development Approach

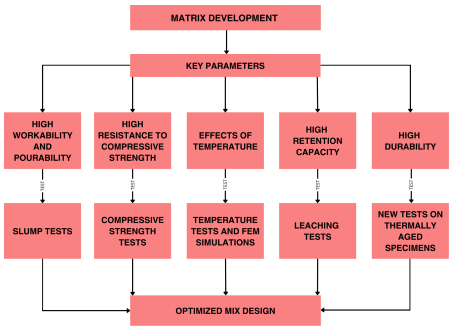


Matrix development approach systematically evaluates **key material parameters**—like **workability**, **resistance to compressive strength**, and **durability**—through rigorous testing. This comprehensive assessment leads to an optimized mix design, according with Italian Law, **Technical Guide N°33 (TG33) criteria.**

## Materials Used

### Matrix Raw Materials

| Cement | Aggregate | Mixing Water | Superplasticizer |
|---|---|---|---|
| CEM IV/A (P) 42.5R-SR | Alluvial sand Ø 0-4 mm | Demineralized water | Polynapthalene sulphonate (PNS) |

### Surrogate Radionuclides (SRs) as Waste

SRs are **tracers dissolved** in **mixing water** that **simulate** chemical-physical **behavior** of **radionuclides**, as **Li** (high ionic mobility), **Co** (that replaces $^{60}$Co), **Cs** (that replaces $^{137}$Cs) and **Pb** (low ionic mobility, it represents heavy elements)

## Before Starting: Aggregate Characterization

Aggregate enhances **matrix stability** and **durability**. Characterization involves **drying** and **sieving** sand (ASTM E11; 5.6 mm, 4 mm, 2.36 mm, 2 mm, 1 mm, 0.6 mm, 0.25 mm, 0.125 mm, and 0.063 mm) to determine its natural particle size distribution. This is compared with **theoretical models** (**Fuller**, **Andreasen**, **Funk&Dinger**) to optimize performance. Modifying this size yields a refined distribution closely fitting the **Andreasen** curve, further **maximizing material stability and durability**.

$$\%P_{Fuller} = \left(\frac{d}{D_{MAX}}\right)^{q} \cdot 100 \qquad q = 0.5$$

$$\%P_{Andreasen} = \left(\frac{d}{D_{MAX}}\right)^{q} \cdot 100 \qquad q = 0.37$$

$$\%P_{Funk\&Dinger} = \frac{d^q - d_{min}^q}{D_{MAX}^q - d_{min}^q} \cdot 100 \qquad q = 0.37$$

%P = Cumulative percentage passing through the sieve with opening "d"
$D_{MAX}$ = Maximum particle size required
$d_{min}$ = Minimum particle size required
d = Particle size
q = Distribution modulus

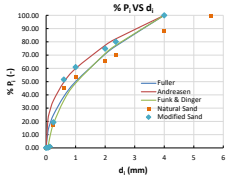


## Matrix Development and Ph.D. Thesis Outcomes

### Specimens Preparation

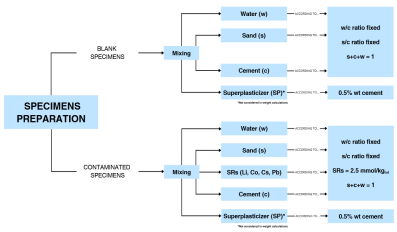


### Step 1 - Workability

**Workability** is a mix parameter intrinsically **linked to** the water-to-cement ***w/c*** and sand-to-cement ***s/c*** ratios. Although **low *w/c*** ratios are targeted for **high mechanical strength**, the **superplasticizer helps** maintain adequate workability. Tests use a reduced Abram's Cone to evaluate the **spreading diameter Δd,** the difference between the diameter reached by the mix on the surface and the diameter of the cone. Two optimal values of Δd are fixed (5.0 cm and 10.0 cm) , and for each one are fixed three different values of *s/c*, that are 0, 0.5 and 1. In this way, it is possible to explore different values of *w/c*, obtaining 6 mixes. Only "blank mixes" are tested (SRs quantities don't significantly affect workability).

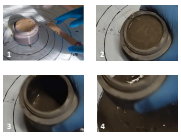

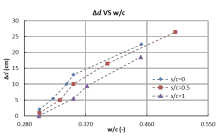


**Workability test**: the fresh mix is poured into the cone (1) and compacted (2), then the cone is removed (3) and after the mix spreads on the surface (4). After that, the Δd is measured.

| s/c = 0 | | s/c = 0.5 | | s/c = 1 | |
|---|---|---|---|---|---|
| $\Delta d_{MIN}$ 5.5 cm | $\Delta d_{MAX}$ 10.0 cm | $\Delta d_{MIN}$ 5.0 cm | $\Delta d_{MAX}$ 10.0 cm | $\Delta d_{MIN}$ 5.5 cm | $\Delta d_{MAX}$ 9.5 cm |
| w/c | w/c | w/c | w/c | w/c | w/c |
| 0.32 | 0.34 | 0.33 | 0.35 | 0.35 | 0.37 |

### Step 2 – Preliminary Compression Tests

After workability test, the 6 **mixes are poured** into various **molds** to obtain **cubic specimens** with dimension of 3 cm x 3 cm x 3 cm. After 28 days of curing, all the specimens are compressed to measure the **compression strength $f_c$**. All the results fits well with TG33, that **requests 10 Mpa at minimum.** During this step, **Formulate 1, 3 and 5 are chosen** for higher compressive strengths.

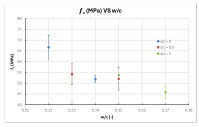


| Formulate | s/c | w/c | $f_c$ (MPa) |
|---|---|---|---|
| 1 | 0 | 0.32 | 66.47 ± 5.56 |
| 2 | 0 | 0.34 | 51.85 ± 1.69 |
| 3 | 0.5 | 0.33 | 56.17 ± 4.61 |
| 4 | 0.5 | 0.35 | 52.08 ± 5.26 |
| 5 | 1 | 0.35 | 55.70 ± 5.21 |
| 6 | 1 | 0.37 | 45.81 ± 2.78 |

### Step 3 – Temperature Tests

To **prevent thermal cracking** in nuclear waste containers, the **temperature** must be **controlled** during first phases of **cement hydration**. **NTC2018** guidelines specify a maximum matrix temperature of 70°C and a maximum thermal difference of around 20°C, verifiable through **FEM analyses** using **ANSYS© Mechanical**. A **2D axisymmetric model** is used to simulate a **CC-440 304L steel container** (d = 700 mm, h = 1300 mm, t = 3 mm) and its **internal cementitious matrix**. The model analyzes key thermal phenomena, including **internal heat generation** (**q '''** ), **measured** with a **Differential Scanning Calorimeter** (**DSC**), and **external convection effects** (air, 22°C). Simulation uses a 5 mm mesh (with a mesh quality factor of 0.8614) to evaluate the thermal performance of three different mixes, M1, M2, and M3, that are respectively Formulate 1, 3 and 5.

**M1** shows **highest results**, that are **all above** the values suggested by NTC2018. Based on these findings, **Formulation 1 is excluded** from further testing. While **Formulation 5** yielded the **lowest results**, **Formulation 3** showed **intermediate values**. Therefore, taking into account both these results and preliminary compression tests, **Formulation 3 has been selected** for more in-depth analysis.

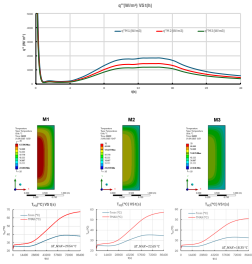


### Step 4 – Compression Tests, Leaching Tests and Durability on Formulation 3

Following successful preliminary tests, Formulation 3 is a candidate mix with ***w/c*** of **0.33** and ***s/c*** of **0.5** and it is selected for **new standard compliance tests**. New standardized samples, measuring **10 cm x 10 cm x 10 cm**, were prepared and subjected to compression and leaching tests both before and after an accelerated aging process.

This aging was achieved through **freeze-thaw cycles**, designed to simulate the rapid expansion and contraction of water within the mixture. According to TG33, the samples underwent at least **30 cycles of 24 hours each**, with temperatures ranging from **−40°C to +40°C**, in order to meet nuclear-grade requirements.

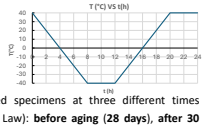


**Compression tests** were performed on both blank and contaminated specimens at three different times requested by TG33 (in addition to the first points not required by the Law): **before aging** (**28 days**), **after 30 freeze-thaw cycles** (**58 days**, the n**uclear-grade** requirement), and **after an additional 60 days of cycles** (**118 days**, not requested by TG33). Data shown that **all the results meet the criteria of TG33**.

| Day | fc_b (MPa) | fc_c (MPa) |
|---|---|---|
| 0 | 0.0 | 0.0 |
| 7 | 45.2 | 46.5 |
| 14 | 47.6 | 49.0 |
| 28 | 56.8 | 57.7 |
| 58 | 69.0 - 45.2 | 76.1 – 69.7 |
| 118 | 75.1 – 47.6 | 72.5 – 66.6 |

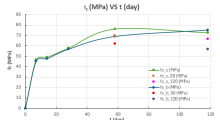


$$CFL = \frac{\Sigma a_n}{A_0} \qquad CFL \propto \sqrt{D_{eff}} \qquad LI = \log\left(\frac{1}{D_{eff}}\right)$$

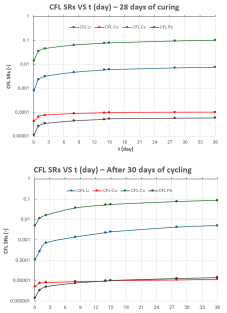


**Leaching tests** were performed on both blank and contaminated specimens, the first one type for removing the background during the analyses. These tests consist in immersing in distilled water the specimens. At specific time intervals, a portion of the liquid is collected and analyzed using **Atomic Absorption Spectroscopy (AAS)**, and the entire solution is replaced.

The main objective is to calculate the **Leachability Index (Li)**, as required by TG33 and defined by the **ANSI/ANS-16.1-2019** standard, that should be **> 7**. This index is derived from the **effective diffusion coefficient (De)**, which is calculated based on the **cumulative leached mass fraction CFL** (ratio between $\Sigma a_n$, the cumulative mass fraction leached during the period $n\ (mg)$, and $A_0$, the total quantity of the contaminant in the matrix) and the geometric properties of the specimen. Test are performed at **28 days of curing** and **after 30 days of cycling**, and, as requested by TG33, all the results meet its criteria.

| SR | Cured - LI (-) | Aged - LI (-) |
|---|---|---|
| Li | 10.71 | 10.46 |
| Co | 14.26 | 16.71 |
| Cs | 8.46 | 8.26 |
| Pb | 15.06 | 15.06 |


This work was promoted by INAIL (Italian National Institute for Insurance against Accidents at Work) with the National Project: *BRiC ID47/2022 - Procedure innovative per la qualifica di attrezzature di lavoro utilizzate per le attività di decommissioning - Studio di modelli matematici e di procedure di validazione*

# PHYSICS-INFORMED NUCLEAR IMAGING FOR GLIOMA LOCALIZATION AND RECURRENCE PREDICTION

Carlos Andres SEPULVEDA LEON

*Heidelberg University*

Tumor recurrence in high-grade gliomas remains one of the major challenges in neuro-oncology. This work presents a hybrid model combining multimodal MRI and physics-informed equations based on nuclear energy transport, implemented using PINNs (Physics-Informed Neural Networks). Using the BraTS 2021 dataset, the model learns tumor morphology and infers recurrence-prone regions based on the assumption of non-uniform energy deposition similar to that of radionuclide-based therapies in nuclear medicine. This approach aims to bridge medical imaging, nuclear transport modeling, and deep learning to move toward personalized dosimetry and recurrence prediction.

# Physics-Informed Nuclear Imaging for Glioma Localization and Recurrence Prediction

Carlos A. Sepulveda Leon

## Problem

Conventional medical imaging fails to capture the full extent of tumor cell distribution, as low-density regions remain undetected. This limitation, compounded by scarce clinical data, hinders personalized radiotherapy planning and necessitates models that integrate physical knowledge with observed imaging information.

## Solution

Physics Regularization Framework: Soft constraints are applied to guide learning toward spatiotemporal consistency with known physical models, such as tissue elasticity and tumor progression, enabling smooth integration of diverse imaging modalities.

## Physics-Constrained Modeling of Tumor and Tissue Dynamics

**Advection-reaction of tumor cell field $c$:**

$$\frac{\delta c}{\delta t} = \underbrace{\mathcal{D}_c}_{\text{cell migration through diffusion}} + \underbrace{\mathcal{S}_c}_{\text{cell proliferation}} - \underbrace{\nabla \cdot (\boldsymbol{v} c)}_{\text{tissue displacements through advection}} \tag{1}$$

**Tumor induced tissue stress. $\sigma$: stress tensor, $F$: deformation tensor**

$$\nabla \cdot \boldsymbol{\sigma}(\boldsymbol{u}) + \gamma \nabla c = 0 \quad \boldsymbol{\sigma} = \frac{\bar{\mu}}{J}\left(\mathbf{F}\mathbf{F}^T - \mathbf{I}\right) + \bar{\lambda} \ln(J)\mathbf{I} \tag{2}$$

**Continuity equation for brain tissue vector $m$:**

$$\delta_t \boldsymbol{m} + \operatorname{div}(\boldsymbol{m} \otimes \boldsymbol{v}) = 0 \tag{3}$$

**Loss terms for deformable mesh cells:**

$$\begin{aligned} L_{\text{Tissue Elasticity PDE}} &= \textstyle\sum_{n=0}^{N_t} \sum_{i=0}^{N_x} \left(\nabla \cdot \sigma_i^n + \gamma \nabla c_i^n\right)^2 \\ L_{\text{Tumor Growth PDE}} &= \textstyle\sum_{n=1}^{N_t} \sum_{i=0}^{N_x} \left(\frac{|\Omega_i^n|}{\Delta t}\left(c_i^n - c_i^{n-1}\right) - \mathcal{D}\left[c_i^n, D_i^n\right] - \mathcal{S}\left[c_i^n\right]\right)^2 \end{aligned} \tag{4}$$

$$\mathcal{D}\left[c_i^n, D_i^n\right] = \sum_{j \in N_i} \left|\Gamma_{ij}\right| D_{ij}^n \frac{c_j^n - c_i^n}{\left\|\boldsymbol{x}_j^n - \boldsymbol{x}_i^n\right\|}, \quad \mathcal{S}\left[c_i^n\right] = \left|\Omega_i^n\right| \rho c_i^n \left(1 - c_i^n\right) \tag{5}$$

Initial condition assumptions: The healthy brain appears symmetrical when projected onto a regular grid, while tumor cells are represented as Gaussian-shaped blobs ($\mathcal{F}^G$ grid projection).

$$L_{\text{Tumor starts from a Gaussian}} = \sum_{i=0}^{N_x} \left(\mathcal{F}^G(c)_i^0 - D_1 \exp\left(-\frac{(x_i - x_0)^2}{D_2}\right)\right)^2 \tag{6}$$

## Spatiotemporal Tumor Evolution Estimation

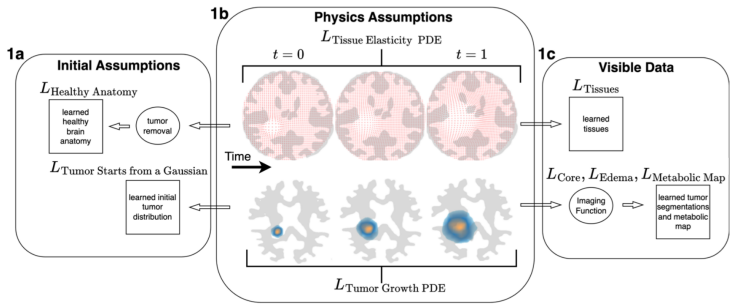


## Inference Beyond Visible Imaging

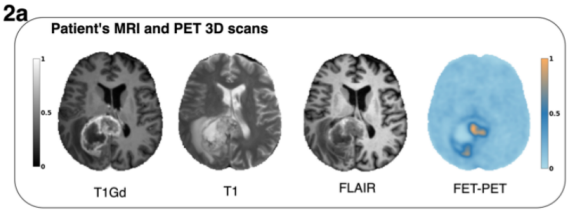


## Physics-Constrained Loss Function

Physics-constrained learning of dynamic tumor and tissue distributions.

$$\begin{aligned} \mathcal{L}_{\text{Total}} = & \underbrace{\alpha_1 L_{\text{Tumor Growth PDE}} + \alpha_2 L_{\text{Tissue Elasticity PDE}}}_{\text{Physical Assumptions}} + \\ & \underbrace{\alpha_3 L_{\text{Tumor Starts From a Gaussian}} + \alpha_4 L_{\text{Healthy Anatomy}}}_{\text{Initial Assumptions}} + \\ & \underbrace{\alpha_6 L_{\text{Core}} + \alpha_7 L_{\text{Edema}} + \alpha_8 L_{\text{Metabolic Map}} + \alpha_9 L_{\text{Tissues}}}_{\text{Visible Data}} \end{aligned} \tag{7}$$

## Forecasting Tumor Recurrence

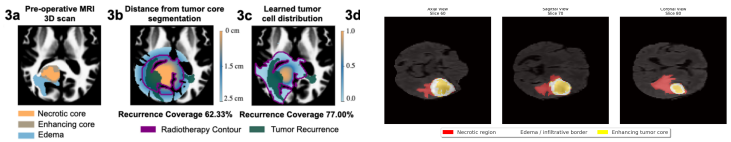


## Results

| Model | Recurrence Coverage% (Any) | Recurrence Coverage% (Enhancing Core) | Dynamical Tissues | Inferable Healthy Anatomy | Population-Based Data-Driven | Physics-Constrained |
|---|---|---|---|---|---|---|
| NN (Unconstrained) | 59.0 ± 4.3 | 66.8 ± 4.9 | -- | -- | -- | -- |
| NN (Physics-Constrained) | 70.4 ± 3.7 | 84.6 ± 3.3 | -- | -- | ✓ | Hard |
| Numerical Physics Simulations | 67.1 ± 3.8 | 86.4 ± 3.3 | ✓ | -- | -- | Hard |
| Standard Plan | 70.0 ± 3.8 | 87.3 ± 3.6 | -- | -- | ✓ | -- |
| Static Grid Discretization | 72.9 ± 3.5 | 89.5 ± 3.4 | -- | ✓ | ✓ | Soft |
| Ours (w/o inferable anatomy) | 73.4 ± 3.2 | 89.3 ± 3.9 | -- | ✓ | ✓ | Soft |
| Ours | **74.7 ± 3.1** | **89.9 ± 2.7** | ✓ | ✓ | ✓ | Soft |

**Delivers higher recurrence coverage than either data-only or physics-only strategies.**

## References


- C. A. Sepulveda Leon, "Optimization of Radiotherapy Dosimetry using Machine Learning and Monte Carlo Simulations for Personalized Brain Cancer Treatment", Master's thesis, 2025. [Online]. https://doi.org/10.5281/zenodo.16636244
- Chandra, Ravi A. et al. (2021). "Contemporary radiotherapy: present and future." In: "The Lancet", Vol. 398, No. 10295, pp. 171–184.
- Liu, Z., Feng, S., and Wang, X. et al. (2020). "Improving dose calculation accuracy in radiotherapy with deep learning." In: "Journal of Radiation Research", Vol. 61, No. 4, pp. 650–657. https://arxiv.org/abs/2005.03065

# NEURAL NETWORKS FOR PREDICTIVE CONTROL OF SMRS IN INDUSTRIAL ENERGY SYSTEMS

Jan ULLMANN

*University of West Bohemia in Pilsen, Czech Republic*

Decarbonizing energy production and industrial processes is a major global challenge in the effort to mitigate climate change. Nuclear energy, especially in the form of Small Modular Reactors (SMRs), is increasingly considered as a flexible and low-carbon source of both electricity and process heat. Modern power grids with high shares of renewable energy require energy producers to provide not only stable output but also operational flexibility and ancillary services such as frequency regulation. The operation of SMRs in hybrid systems supplying both electricity and heat presents a complex control problem, as the thermal output must be dynamically split to satisfy variable electricity grid demands and industrial heat requirements. Accurate forecasting and adaptive control strategies are needed to optimize this multi-objective operation while maintaining safety and efficiency. In our work we show a neural-network-based predictive control framework for SMRs that integrates real grid and weather data to optimize the joint production of electricity and heat. Our tools and results demonstrate that advanced neural network models (LSTM, GRU, Transformer), optimized via multi-objective hyperparameter tuning and supported by attention mechanisms for interpretability, significantly improve forecast accuracy and operational flexibility compared to traditional control methods. This work expands previous knowledge by enabling anticipatory control of SMRs based on real-time system dynamics, thus facilitating their participation in electricity markets and grid ancillary services without compromising thermal supply reliability. The developed software tools and methodology provide a flexible foundation for adapting SMR control to various industrial and grid environments. Overall, this approach supports the integration of nuclear energy into decarbonized, hybrid energy systems and highlights the potential for AI-driven control to enhance the role of SMRs in future sustainable energy infrastructures.

# Neural Networks for Predictive Control of SMRs in Industrial Energy Systems

FACULTY OF ELECTRICAL ENGINEERING
UNIVERSITY OF WEST BOHEMIA

Jan Ullmann [1], Jiří Závorka [1], Radek Škoda [1]

[1]Faculty of Electrical Engineering, University of West Bohemia, Univerzitni 26, Pilsen, 30614, Czech Republic

NUCLEAR DAYS

## Introduction & Motivation

The decarbonization of energy-intensive industrial processes is one of the most urgent priorities in the global effort to mitigate climate change. In this context, small modular reactors (SMRs) are gaining increasing attention as promising sources of both electricity and process heat. Industrial deployment of SMRs, however, introduces a new operational challenge: the need to dynamically balance the production of electricity and heat, while simultaneously responding to the demands of modern power grids. These grids—characterized by high shares of intermittent renewables—require nuclear units to not only act as stable producers but also provide flexibility and even ancillary services, such as frequency regulation or load-following.

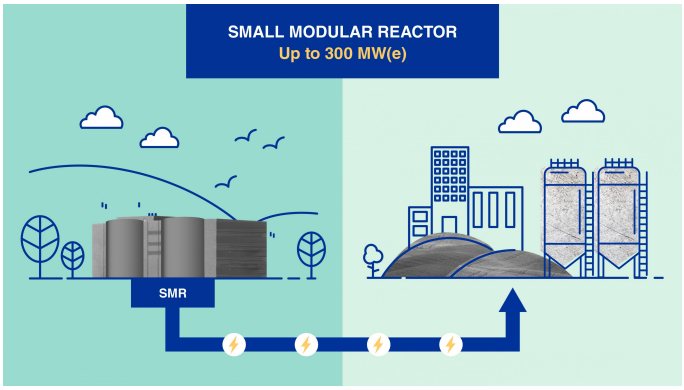


Figure 1. IAEA illustration: The use of nuclear power beyond generating electricity [1]

## Objectives and Goals

**Goal of this work:** To present a neural-network-based predictive control framework for optimizing SMR operation in hybrid electricity and heat supply systems.

To achieve this, we focused on:

- Developing a **flexible methodology for neural network (NN) prediction and control,**
- Creating tools for **forecasting and optimizing SMR operation for heat and electricity,**
- Integrating **predictive control with real data and NNs.**

## Flexible methodology for NN prediction and control

The deployment of NNs in energy systems requires more than just choosing the right architecture—it begins with building high-quality, validated datasets. In our work, we focused intensively on the methodology of dataset construction, ensuring that inputs to the models are accurate, reliable, and generalizable.

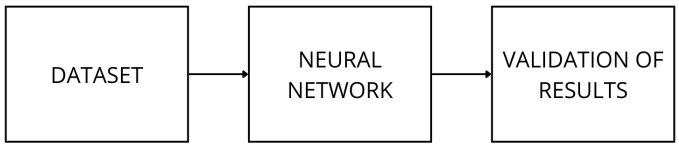


Figure 2. Methodology of the developed tools for the use of NNs

We have developed a comprehensive software framework for:

1. Data ingestion and preprocessing, integrating historical grid data (e.g., from Czech Transmission System Operator ČEPS), weather forecasts, and operational data,
2. Validation and verification tools, allowing automated quality control of time series inputs,
3. Modular implementation, enabling use across various sectors (nuclear, district heating, renewables integration).

NeuroPrep

Learn DataPrep

DataGridExtractor

Figure 3. Developed tools for dataset preparation, validation, and visualization

Once the data foundation is established, we employ advanced optimization techniques to fine-tune model performance. Specifically, we utilize the Optuna optimization framework to perform:

- Hyperparameter tuning of Recurrent Neural Networks (RNN) such as LSTM and GRU, as well as Transformer models,
- Multi-objective search to maximize forecasting accuracy and model generalizability,
- Efficient evaluation of large neural network configuration spaces using cross-validation and parallel computing.
- Feature Attention Mechanisms - highlight the contribution of each input variable, improving model transparency and supporting safe deployment in nuclear applications.

## Forecasting and optimizing SMR operation for heat and electricity

SMRs offer a unique capability to serve both the electricity grid and industrial thermal loads. However, operating a nuclear system in such a dual-role introduces significant complexity. At any given moment, operators must decide how to split the reactor's thermal output between:

- Electricity production, which can be sold to the grid or used locally,
- Heat delivery, required by industrial processes, district heating, or cooling systems.

This dual-role operation creates a multi-objective optimization problem:

- Ensure reliable heat supply for industrial consumers,
- Maximize economic return via electricity sales or ancillary services,
- Respond to real-time grid signals and forecasts.

Achieving such coordination requires advanced control strategies that go far beyond traditional set-point. It demands forecasting capability, fast adaptation, and the ability to learn complex dependencies between external variables (e.g., weather, market prices, industrial schedules).

## Predictive Control with Real Data and NNs

We present a neural-network-based control framework for SMRs in hybrid electricity-heat systems. The toolset enables:

- Forecasting key variables (e.g., grid imbalance, weather effects, generation of NPPs - see Figure 4),
- Optimizing SMR dispatch for electricity and heat,
- Supporting ancillary services (aFRR, mFRR) and thermal storage management.

By anticipating system dynamics, the controller adjusts SMR output in advance—improving flexibility, reducing unit stress, and enhancing market participation.

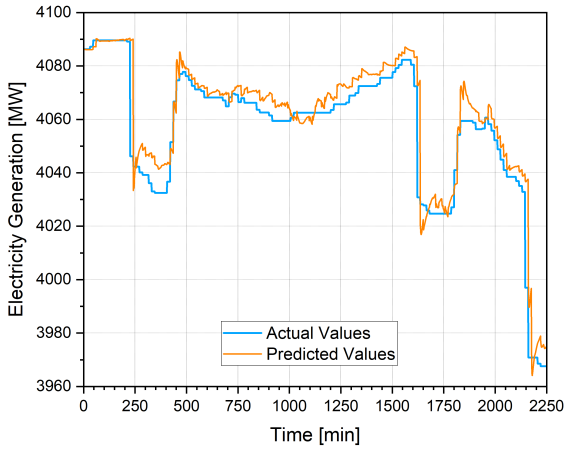


Figure 4. 15-minute ahead predictions of NPP generation in the Czech Republic [2].

## Conclusion & Future Work

This work presents a novel methodology for integrating SMRs into hybrid energy systems by leveraging neural network-based predictive control. We developed a robust data infrastructure, including custom software tools for dataset validation, transformation, and neural network optimization using *Optuna*. These tools are designed to be flexible across multiple industrial sectors [3].

Our results demonstrate that accurate forecasting of electricity grid dynamics and thermal demand can significantly enhance the operational flexibility of SMRs.

**Future work** will focus on expanding predictive capabilities toward industrial heat demand modeling and techno-economic optimization under market scenarios, further increasing the applicability of intelligent SMR operation in real-world conditions. In collaboration with **industry partners**, we will continue efforts to implement our tools in real applications—both for **TSOs** and for **operating nuclear/thermal power plants**. Particular emphasis will be placed on deployment and testing of our predictive control framework in the **state of Texas (USA)**, where diverse market conditions and industrial clusters provide a valuable testbed for SMR integration.

## References

[1] Jeffrey Donovan and Paula Calle Vives. *Accelerating SMR Deployment: New IAEA Initiative on Regulatory and Industrial Harmonization*. International Atomic Energy Agency. Apr. 2022. URL: `https://www.iaea.org/newscenter/news/accelerating-smr-deployment-new-iaea-initiative-on-regulatory-and-industrial-harmonization` (visited on 07/29/2025).

[2] J. Ullmann et al. "Neural Network Optimization of Nuclear Energy Integration for Industrial Applications and Grid Stability". In: *Proceedings of the European Young Generation Forum (ENYGF'25)*. June 2–6, 2025. Zagreb, Croatia, June 2025.

[3] Jan Ullmann et al. "Neural Networks and AI-Decision Making for a More Flexible Nuclear Industry". In: *11th European Commission Conference on EURATOM Research and Training in Reactor Safety & Radioactive Waste Management*. 12–16 May 2025. European Commission. Warsaw, Poland, May 2025.

# THERMAL-HYDRAULIC DESIGN AND ANALYSIS OF THE STEAM AND WATER LOOP FACILITIES TO SUPPORT THE DEVELOPMENT OF THE EU-DEMO TOKAMAK FUSION REACTOR

Alessandra VANNONI

*Sapienza University of Rome, Italy*

This PhD research supports the development of the EU-DEMO fusion power plant by addressing the thermal-hydraulic challenges related to pulsed operation, especially for the Water-Cooled Lithium-Lead (WCLL) breeding blanket system. A dedicated experimental platform, W-HYDRA, was developed, integrating two complementary facilities: STEAM, for the investigation of a mock-up steam generator under pulsed conditions, and the Water Loop, designed to test components under a wide range of thermal-hydraulic conditions. The main objective was the conceptual design and assessment of the steam generator test section based on the Once-Through Steam Generator (OTSG) configuration, chosen for its low thermal inertia and proven reliability in fission applications. Thermal-hydraulic analyses using the RELAP5 code supported the experimental campaign definition and control strategy development. The design of the STEAM facility ensured adequate power dynamics and included safety-oriented evaluations of key components such as air coolers and low-pressure heat exchangers. The Water Loop was designed to test multiple component configurations, including plasma-facing units, by enabling precise control of operating conditions. Sensitivity analyses helped optimize the integration between STEAM and Water Loop, minimizing component redundancy and facility costs. While STEAM focuses on component-level performance validation under pulsed conditions, the Water Loop allows system-level assessments, including transient and safety analyses. The project culminated in the definition of experimental activities and the preparation of technical specifications for component procurement. This work significantly contributes to the qualification of fusion reactor components, providing a unique infrastructure to validate technologies for ITER and DEMO.

# Thermal-Hydraulic Design and Analysis of the STEAM and Water Loop Facilities to support the development of the EU-DEMO tokamak fusion reactor

Alessandra Vannoni, alessandra.vannoni@uniroma1.it

## Open Issue: unconventional operation of magnetic confinement fusion reactors

### - Pulsed operation

Magnetic confinement fusion reactors operate in pulsed mode due to the intrinsic limitation in sustaining the plasma current induced by the central solenoid. This leads to repetitive thermal and hydraulic transients in components and systems, which are very far from fission standard practice.

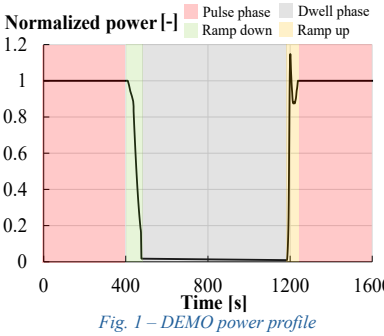


*Fig. 1 – DEMO power profile*

### -Plasma irradiation

Plasma-facing components are directly exposed to energy deposition in vacuum and irradiation by 14 MeV neutrons. This contrasts with fission systems, where components are submerged in coolant, shielded, and subjected to a softer neutron spectrum (~2 MeV).

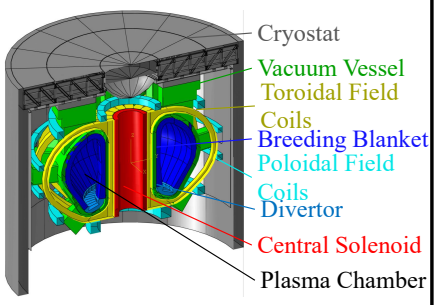


*Fig. 2 – Tokamak main components*

## Main Objective: study the T/H behaviour of proven nuclear equipment in fusion-like environment

DEMO reactor adopts components commonly used in fission power plants, leveraging their proven technological maturity. However, these systems were not designed for fusion-specific conditions. Since fission reactors cannot reproduce such environments, dedicated design and validation under representative fusion conditions are essential to assess their functional feasibility and ensure reliable operation in DEMO.

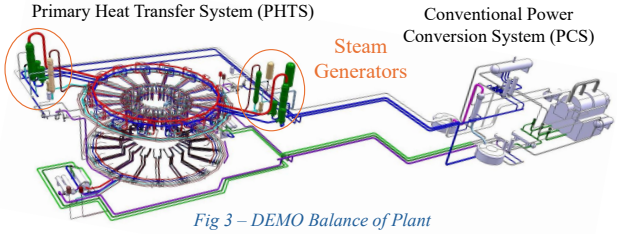


*Fig 3 – DEMO Balance of Plant*

## Methodology: design experimental facilities for investigating systems and components in fusion-like environment supported by analyses with SYST-T/H code RELAP5/Mod3.3

### STEAM facility: Characterize the DEMO Steam Generator (SG) scaled down mock-up in pulsed operation

- SG design (scaling from DEMO SG and analysis of distortions)

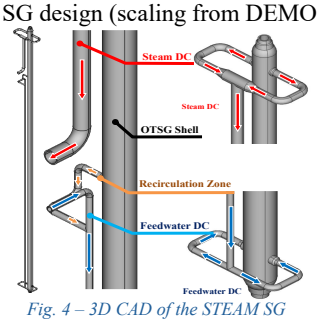


*Fig. 4 – 3D CAD of the STEAM SG*

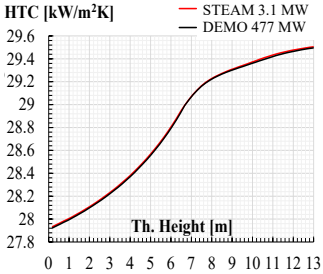


*Fig. 5 – HTC along the thermal length*

- Pre-test analysis in pulsed mode testing proportional(P)-integral(I) controllers

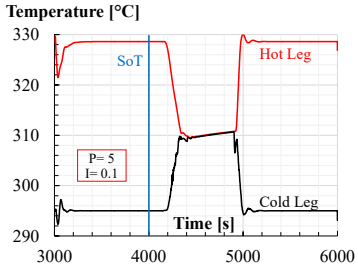


*Fig. 6 – Temperature evolution in pulsed mode*

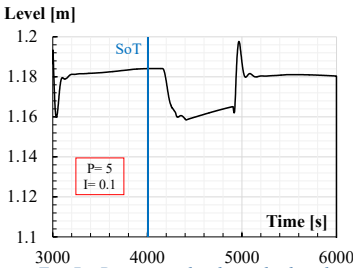


*Fig. 7 – Pressurizer level in pulsed mode*

### Water Loop facility: Testing components inside a Vacuum Chamber irradiated by an 800kW-Electron Beam Gun

- Design: ensure versatility to investigate many Test Sections (different p, T, power)

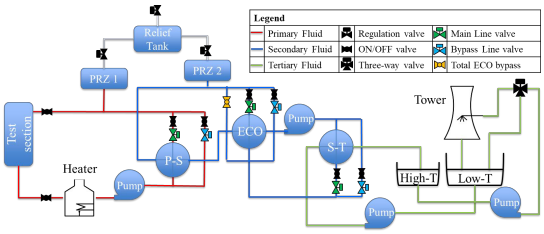


*Fig. 8 – Water Loop conceptual design*

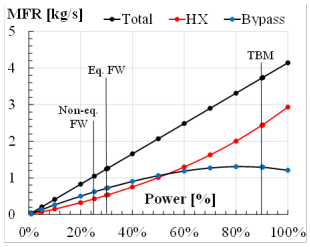


*Fig. 9 – WL regulation at different powers*

- Sensitivity analyses to optimize the design for pulsed mode

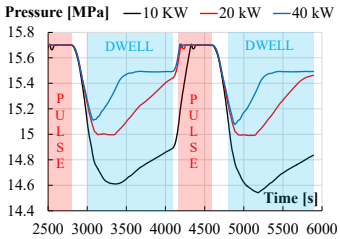


*Fig. 10 – Pressurizer pressure in pulsed mode*

Study the effect of pressurizer electric heaters on primary loop pressure to keep a constant pressure during the pulsed operation

## Conclusions

✓ Facility conceptual design, ✓ Design of the experimental campaign, ✓ Pre-test analyses, ✓ Feedback on regulation strategies

This work has been carried out within the framework of the EUROfusion Consortium, funded by the European Union via the Euratom Research and Training Programme (Grant Agreement No 101052200 — EUROfusion). Views and opinions expressed are however those of the author(s) only and do not necessarily reflect those of the European Union or the European Commission. Neither the European Union nor the European Commission can be held responsible for them.

**STUDENTS POSTERS**
**NUCLEAR DAYS 2025**

Editor:
David Mašata

Published by:
University of West Bohemia in Pilsen
Univerzitní 8, 301 00 Plzeň

1st Edition, 69 Pages
Pilsen 2025

ISBN 978-80-261-1307-2
ISBN 978-80-261-1308-9 (printed)